Fetuin-A-based theranostics in ectopic calcification

Von der Medizinischen Fakultät
der Rheinisch-Westfälischen Technischen Hochschule Aachen
zur Erlangung des akademischen Grades eines Doktors der
Theoretischen Medizin genehmigte Dissertation

vorgelegt von

Dr. med. Robert Dzhanaev

aus Wladikawkas (Russland)

Berichter: Herr Univ.-Prof. Dr. rer. nat. Wilhelm Jahnen-Dechent
Herr Univ.-Prof. Dr. med. Felix Mottaghy

Tag der mündlichen Prüfung: 8.9.2023

BIOINTERFACE LABORATORY, HELMHOLTZ-INSTITUTE
FOR BIOMEDICAL ENGINEERING
RWTH Aachen University, Aachen, Germany

&

CARDIOVASCULAR RESEARCH INSTITUTE MAASTRICHT,
DEPARTMENT OF BIOCHEMISTRY
Maastricht University, Maastricht, The Netherlands

FETUIN-A-BASED THERANOSTICS IN ECTOPIC CALCIFICATION

Robert Dzhanaev

2023

Mæ zynarh fydy fydæn, iugændzon myn dæncæg či uyd,
æmæ mæ razængard či kodta.

To my dear grandfather, who has always been an example
and encouragement to me.

Teile dieser Dissertation wurden vorveröffentlicht in:

- Dzhanaev R, Hasberg C, Gorgels A, Schmitz C, Winkler CF, Malyaran H, Gräber S, Gentier A, Jaminon A, Agten S, Hackeng T, Akbulut AC, Schurgers L, Mottaghy FM, Goettsch C, Jahnen-Dechent W. Application of the mineral-binding protein fetuin-A for the detection of calcified lesions. Theranostics. 2023 Jan 1;13(2):659-672.

CONTENTS

LIST OF ABBREVIATIONS

Abbreviation	Meaning
6xHis	polyhistidine tag
ACP	amorphous calcium phosphate
ANOVA	analysis of variance
AR	average requirement
Arg	arginine
Asp	aspartic acid
ATCC	American Type Culture Collection
ATP	adenosine triphosphate
bFA	bovine fetuin-A
bOPN	bovine osteopontin
CAC	coronary artery calcium
CHO	Chinese hamster ovary
CKD	chronic kidney disease
CM	calcification medium
CPM	calciprotein monomer
CPP	calciprotein particle
CSF-1R	colony-stimulating factor-1 receptor
CT	computed tomography
CTR	C-terminal region
CY	cystatin-like domain
DAPI	4′,6-diamidino-2-phenylindole
ddH_2O	double-distilled water
DEX	dexamethasone
DIC	differential interference contrast
DMEM	Dulbecco's Modified Eagle's Medium
DNA	deoxyribonucleic acid
DTPA	diethylenetriamine-pentaacetic acid
EBT	electron beam tomography
EDTA	ethylenediaminetetraacetic acid

EDX	energy-dispersive X-ray spectroscopy
EFSA	European Food Safety Authority
FBS	fetal bovine serum
FDA	fluorescein diacetate
FGF23	fibroblast growth factor 23
Glu	glutamic acid
Gly	glycine
HAP	hydroxyapatite
HEK293	human embryonic kidney 293 cells
HEPES	4-(2-hydroxyethyl)-1-piperazineethanesulfonic acid
HO	heterotopic ossification
HRP	horseradish peroxidase
IC_{50}	half maximal inhibitory concentration
IMAC	immobilized metal affinity chromatography
ITS	insulin, transferrin, selenic acid
iVSMC	immortalized vascular smooth muscle cells
IVUS	intravascular ultrasound
KCM	kidney calcification medium
LAA2P	L-ascorbic-acid-2-phosphate
LANUV	Landesamt für Natur-, Umwelt- und Verbraucherschutz
M-CSF	macrophage colony-stimulating factor
MAC	medial artery calcification
MALDI-TOF	matrix-assisted laser desorption/ionization-time of flight mass spectrometry
MDCT	multidetector computed tomography
mFA	murine fetuin-A
MGP	matrix Gla protein
MRI	magnetic resonance imaging
MSC	mesenchymal stromal cells
MUMC	Maastricht University Medical Center
NEB	New England Biolabs®
NFATc1	nuclear factor of activated T cells c1
OCT	optical coherence tomography

ODI	osteoclast differentiation index
OM	osteogenic medium
OPG	osteoprotegerin
PET	positron emission tomography
PFA	paraformaldehyde
pm-mFA	phosphomimetic murine fetuin-A
PRI	population reference intake
PTH	parathyroid hormone
PTM	post-translational modification
RANK	receptor activator of nuclear factor κB
RANKL	receptor activator of nuclear factor κB ligand
S-DCM	serum-depleted calcification medium
scRANKL	single-chain RANKL
SDS-PAGE	sodium dodecyl sulfate-polyacrylamide gel electrophoresis
SEM	scanning electron microscopy
sRANKL	soluble RANKL
T2DM	type 2 diabetes mellitus
TNF	tumor necrosis factor
TNFSFR	tumor necrosis factor superfamily receptor
UKA	University Hospital Aachen
VC	vascular calcification
VSMC	vascular smooth muscle cells
β-GP	β-glycerophosphate

LIST OF FIGURES

LIST OF TABLES

1. INTRODUCTION

1.1 Calcium homeostasis in the physiology and pathology

In the human body, calcium is the most prevalent metallic element. Hydroxyapatite (HAP) ($Ca_{10}[PO_4]_6[OH]_2$) of the collagenous matrices of bones and teeth accounts for approximately 98% of 1200 g of total body calcium. The remaining amount is dispersed throughout tissues and extracellular fluid, with plasma levels ranging from 8.5 to 10.5 mg/dL [1]. Of this amount, about half is physiologically active ionized calcium, and the remainder is represented by the protein-bound and complexed fractions [2]. Ionized calcium is essential for a variety of physiological processes, including signal transduction, muscle contraction, blood coagulation, and others [3-7]. The average requirement (AR) for calcium is 750 mg/day for adults, and the population reference intake (PRI) values range from 950 mg/day for adults to 1000 mg/day for young adults (18-24 years), as proposed by the European Food Safety Authority (EFSA) Panel on Dietic Products, Nutrition and Allergies [8]. Insufficient dietary calcium intake contributes to the development of rickets, a skeletal disorder characterized by decreased bone mass and resulting deformities and fractures [9].

Calcium metabolism is tightly regulated by a network of hormones and regulatory molecules. Calcium is absorbed in the mammalian small intestine via two main mechanisms: a transcellular active transport that occurs mostly in the duodenum and upper jejunum, and a paracellular, passive diffusion that occurs across the mucosal layer [10]. ATP-dependent calcium transport is regulated by the active form of vitamin D, 1,25-dihydroxycholecalciferol, which is synthesized from a precursor molecule by enzymatic hydroxylation [11]. Vitamin D increases calcium diffusion primarily by inducing calbindins, a class of Ca^{2+}-binding molecules mediating the intestinal absorption of calcium [12]. Expression of the specific 1α-hydroxylase is upregulated by parathyroid hormone (PTH) and calcitonin secreted by parafollicular cells of the thyroid gland and downregulated by bone-derived fibroblast growth factor 23 (FGF23) [13-15]. PTH further increases the serum calcium concentration by promoting bone catabolism and renal calcium reabsorption [16, 17]. Contrary to PTH, calcitonin inhibits bone degradation and moderately increases urinary calcium excretion [18, 19].

Once evolved as a mechanism to protect the vulnerable bodies of primitive Cambrian-era animals, biomineralization became the cornerstone of the skeletal systems of modern species [20]. The essence of the biomineralization process is the intake of a mineral from the external environment, followed by its redistribution and incorporation into body tissues. This is inevitably associated with the risk of local supersaturation of inorganic salts at critical points such as the vasculature or excretory system. As physiological mineralization in humans is restricted to bones and teeth, a number of systemic and tissue-resident inhibitors of calcification emerged in the course of evolution to prevent extraosseous precipitation of calcium salts in a process known as ectopic calcification [21, 22]. Deviations in either system, caused by genetic defects or external factors, lead to severe dysregulation of mineral metabolism [23-25]. However, ectopic calcification does not always pose a health risk and often arises as an organism's adaptive response that delineates a pathological process (Figure 1). Such protective reactions can be exemplified by nodal calcifications in tuberculosis, plaque-stabilizing macrocalcifications in atherosclerosis, and more rare phenomena such as lithopedion formation in vestigial miscarriages. On the other hand, certain calcification patterns, such as pro-inflammatory microcalcifications of atherosclerotic plaques or medial artery calcification (MAC) accompanying CKD and diabetes, are thought to be detrimental as they aggravate the course of the underlying condition [26-28]. Micrometer-sized calcium deposits within atherosclerotic plaques are of particular clinical importance, as they destabilize the fibrous cap, leading to the formation of vulnerable plaques and consequent cardiovascular events such as the myocardial infarction and stroke [29, 30]. Vascular calcification (VC) is an ancient disease, as demonstrated by a radiological examination of a 5300-year-old mummy preserved in permafrost [31]. Calcifying atherosclerosis is a common feature of uremic cardiovascular disease, and patients with advanced CKD, especially those on dialysis or refusing therapy, develop some of the most pronounced forms of ectopic calcifications [32, 33]. The high susceptibility of the cardiovascular system to calcification may be due to the fact that the vessel wall constitutes the primary interface between calcium-rich blood and body tissues, rendering the vasculature one of the most calcification-prone structures after the skeletal matrix [34].

Recent research suggests that VC may develop from dystrophic deposition of calcium salts onto dead or dying cells and remnants to a cell-autonomous process driving heterotopic ossification (HO), similar to bone formation [35-37]. While HO is associated with several late-stage degenerative pathologies including peripheral arterial disease or severe trauma,

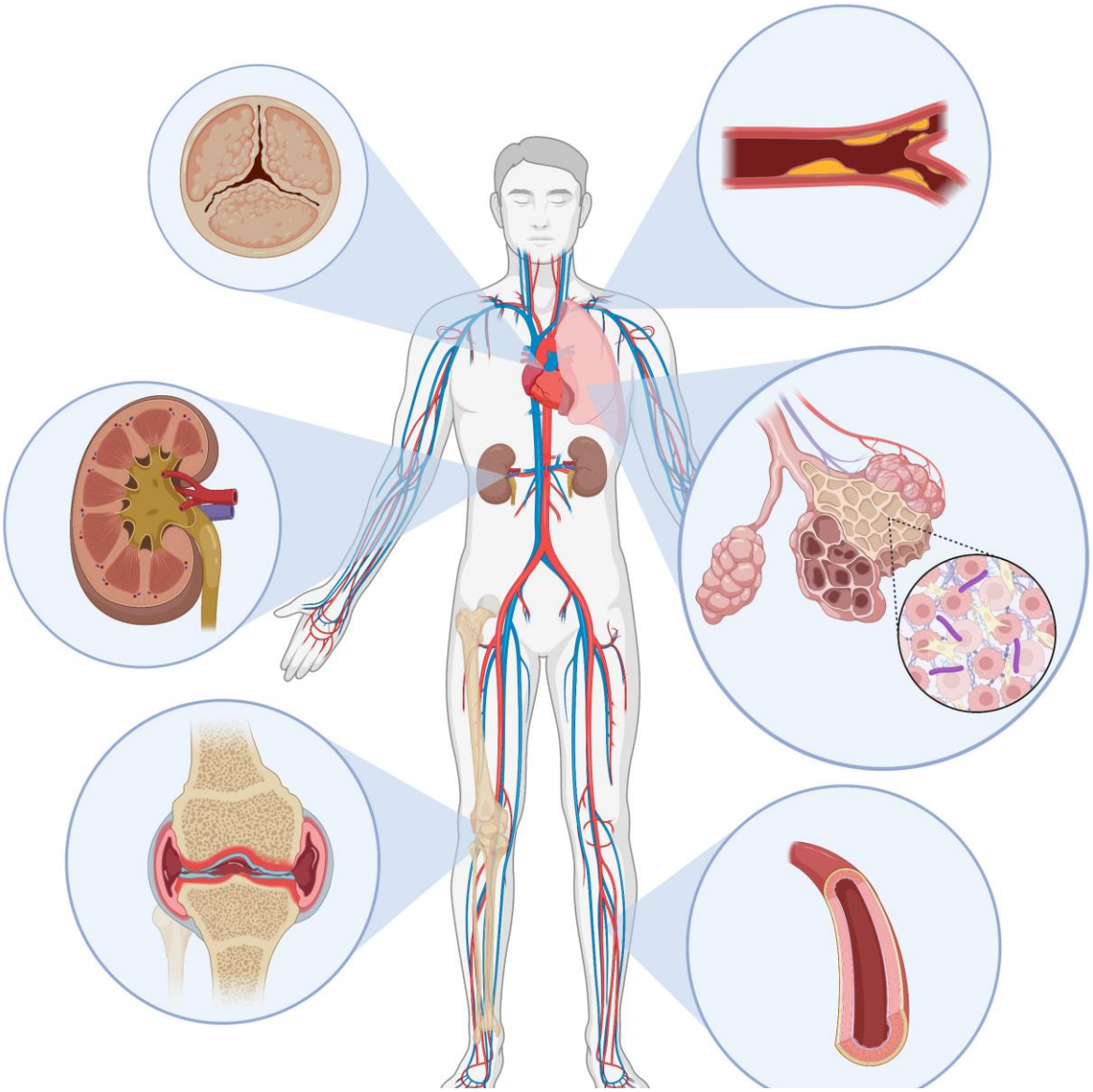

Figure 1. Common sites of ectopic calcification. Being in direct contact with calcium-rich blood, the cardiovascular system is often affected by the pathological mineral deposition. Inflammatory diseases of joints and chronic lung infections such as tuberculosis render target organs vulnerable to soft tissue calcification. Nephrocalcinosis is associated with hyperparathyroidism and chronic vitamin D intoxication.

most soft tissue calcifications nevertheless develop in the absence of osteogenic differentiation, as demonstrated in one of the most affected genetic models of ectopic calcification – the fetuin-A deficient DBA/2 mouse strain [23, 38]. Overall, the much-debated theory of vascular ossification needs to be reconsidered in the light of current views on the pathogenesis of ectopic calcification.

1.2 Diagnostic approaches to ectopic calcification

A multitude of various methods for diagnosing ectopic calcifications have emerged over the past few decades. Histopathological assessment of mineralization relies on the use of different staining methods aimed to highlight the calcified matter in a specimen. Numerous stains were tested for their ability to detect calcium phosphate deposits, and many were found to be unspecific and, therefore, inapplicable [39]. For instance, one of the oldest staining techniques for calcium described by von Kossa in 1901, did not prove to be a specific test for calcium or phosphate but stained a variety of salts such as carbonates and phosphates of calcium, strontium, barium, iron, and copper as well as calcium oxalate and oleate [40]. Nevertheless, this method remains widely used for histological detection of VC [41]. Another decades-old method for identifying calcium deposits in tissues is based on the madder plant pigment alizarin [39]. While believed to be effective for localizing calcium-rich minerals at a certain pH, this dye is not well suited for the detection of microcalcifications and also binds cations other than calcium [42]. Application of a polyanionic fluorescein derivative calcein and a fluorescent bisphosphonate probe OsteoSense™ represents a relatively new fluorescence-based approach that enables live imaging of mineralization [43, 44], although the development of toxic effects related to the chemical nature of the compounds cannot be excluded [45, 46]. The major drawback of most histological methods is the processing of samples using harsh reagents and fixatives, which virtually eliminates the possibility of in vivo detection of calcification. A significant step in intravital imaging of microcalcifications was the development of serum protein fetuin-A-based fluorescent probes that provide a good safety profile and high detection sensitivity [38, 47].

Clinical evaluation of ectopic calcification mostly relies on radiological techniques [32]. Coronary artery calcium (CAC) score measured using electron beam tomography (EBT) or more modern multidetector computed tomography (MDCT) is a guideline-endorsed tool for assessing risk for major cardiovascular outcomes in patients with atherosclerotic cardiovascular disease [48]. Screening results are normally expressed as a single number produced by an algorithm, with the one proposed by Agatston et al. considered to be the international standard [49]. Such data processing imposes certain limitations on the sensitivity of the method, for instance, by setting the size threshold for individual calcified lesions above 1 mm^2 [50]. Thus, proinflammatory pathological microcalcifications are automatically excluded from the analysis. However, it is worth noting that CAC is used to

evaluate the extent of atherosclerosis and does not address ectopic calcification *per se*, which partially justifies the limitations of this approach. Multislice spiral CT represents an accurate method for the assessment of VC, including that affecting peripheral arteries, although it is associated with significant radiation exposure and is not used in routine clinical practice [51]. A plain X-ray is superior to a CT scan in terms of radiation dose per examination, but loses much in image resolution and therefore is of no interest as a means for evaluating small calcifications. Breast calcification imaging is another widely used, cost-effective, and fast radiographic method for the identification of pathological mineral deposits [52]. The diagnostic value of this approach arises from the possibility of detecting certain calcification patterns consistent with malignancy. Again, in this case, calcium deposits serve as a marker for the underlying disease.

Alternative common non-invasive imaging modalities for detecting ectopic calcifications are magnetic resonance imaging (MRI) and transcutaneous sonography. As the calcific lesions are diamagnetic, standard MRI modalities are insensitive to ectopic calcification. To enhance the imaging capacity of this method, special high-field sequences are used [53]. However, the low temporal resolution inherent in MRI results in artifacts caused by cardiac contractions and respiration [54]. High-frequency transcutaneous ultrasonography is used to detect superficial ectopic microcalcifications, while lower frequencies allow deeper tissue penetration but provide poor resolution [55, 56]. On the other hand, intravascular ultrasound (IVUS) can be used to directly image the vessel wall, enabling the identification of hyperechoic calcific plaques [54]. Low axial resolution due to the physical properties of calcified matter is a common limitation of both transcutaneous and intravascular sonography [57]. Optical coherence tomography (OCT) is a method that utilizes the principle of low-coherence interferometry for cross-sectional tissue imaging [58]. Invasive OCT was reported to be an effective tool for assessing atherosclerotic calcification that surpasses IVUS in terms of tissue penetration [59]. However, differentiating between lipid and calcified plaques remains challenging when using this imaging modality [54].

Integrated positron emission tomography and X-ray computed tomography (PET/CT) imaging using ^{18}F-NaF tracer is a highly sensitive method for detecting calcified atherosclerotic plaques that allows distinguishing between macro- and microcalcifications [60, 61]. Accumulation of the radiotracer indicates an active calcification process, whereas heavily calcified stable plaques show low uptake [62]. NaF PET/CT-derived values were reported to be more sensitive and have more prognostic value than traditional tools such as

the Framingham risk score [63]. Importantly, the application of the method is not restricted to assessing cardiovascular calcification as it can be used for detecting bone metastases or areas of ectopic bone formation in pseudoxanthoma elasticum [64-66]. Drawbacks of the technique include radiation exposure and modest spatial resolution of PET scans.

Several candidate biomarkers of VC have been identified, but none of them possesses enough specificity to allow an unambiguous diagnosis of the disease [67]. However, the study of specific molecules involved in the pathogenesis of ectopic calcification may shed light on the molecular pathways orchestrating VC and potentially lead to the discovery of novel therapeutic options.

To summarize, current imaging approaches lack sensitivity toward microcalcifications reflecting the early stages of a pathological process [41]. More research is required to generate sensitive probes suitable for *in vivo* imaging of VC.

1.3 Therapeutic approaches to ectopic calcification

Despite the known causative relationship between atherosclerotic calcification and cardiovascular complications, virtually no conservative treatment options for vascular calcification in the context of atherosclerosis are discussed in current clinical guidelines. However, recent advances in calcification pathophysiology have enabled the identification of several promising pharmacological approaches aimed to reduce the ectopic calcification burden. Reagents regulating the chemical milieu, which determines calcification propensity, have in fact been most successful in reducing calcification.

CKD-associated hyperphosphatemia is a major risk factor for VC [68]. Several groups of phosphate binders were developed to address this issue. Calcium-containing phosphate binders such as calcium carbonate are the most commonly prescribed drugs in this class. At first glance, calcium-based binders appear to be a good choice because they not only reduce phosphate levels but also correct hypocalcemia, which develops due to diminished renal production of 1,25-dihydroxycholecalciferol in CKD patients. However, there is a risk of hypercalcemia and accelerated vascular calcification upon administration of such drugs, especially when used in combination with vitamin D [69-71]. This risk has been reduced with the advent of Mg^{2+}-based phosphate binders [72]. Aluminium hydroxide is a highly effective phosphate binder. Although this drug does not disturb the calcium balance, recent KDIGO clinical practice guideline recommends avoiding the long-term use of aluminum-containing

phosphate binders to prevent aluminum intoxication [73]. Finally, some newer drugs, such as the polymer sevelamer and lanthanum carbonate, have been reported to attenuate HC and improve outcomes in patients with CKD [70, 74], while causing less pronounced side effects than traditionally used medications.

Unlike metastatic calcification, which is partly reversible [33], most progressed soft tissue calcifications are not. Atherosclerosis and diabetes associated peripheral arterial disease historically progressed until limb amputations became inevitable [75]. Meanwhile atherosclerosis prevention and treatment have undoubtedly much improved [76], but advanced stage extracranial and intracranial carotid disease, as well as coronary disease still ultimately require surgical intervention or stenting to remove live-threatening occlusive lesions in vessels or valves [77]. Chelation therapy is a conservative approach to treat peripheral arterial occlusive disease and arterial stiffness [78, 79]

Chelation therapy aims at reducing soft tissue calcifications with chelating agents ethylenediaminetetraacetic acid (EDTA) or diethylenetriamine-pentaacetic acid (DTPA). These compounds were reported to remove calcium from the calcified human aorta [80]. Although intravenous administration of EDTA can cause kidney damage and bone loss [81, 82], the generation of a slow-release drug product based on nanoparticle-EDTA conjugates was shown to retain calcium-chelating properties without triggering systemic side effects [83]. Furthermore, EDTA-loaded nanoparticles were reported to reverse arterial calcification in an animal model [84]. Although EDTA-based chelation therapy has been used for decades, there is still no agreement on its effectiveness in treating cardiovascular disease [85-87].

Research on the calcium receptor (CaR) function paved the way for the development of new drugs that correct elevated serum calcium levels. The CaR is expressed mainly in organs that regulate calcium metabolism and also in the vasculature, where its loss of function was reported to promote calcification [88]. In parathyroid cells, CaR activation results in the inhibition of PTH secretion, while in the thyroid C cells it increases calcitonin production, cumulatively leading to a decrease in serum calcium concentration. Positive allosteric CaR modulators named calcimimetics were designed to interact with the receptor either by mimicking the action of extracellular calcium or by increasing the sensitivity of CaR toward calcium ions [89]. Although such compounds were shown to inhibit the progression of vascular calcification [90], it remains unclear whether calcimimetics are a better alternative to the standard of care.

Magnesium, a biologically active bivalent ion present in all body fluids, was shown to inhibit the initial stages of VSMC calcification *in vitro* [91] and in animal trials [23]. Several mechanisms explaining the protective role of magnesium were discussed. First, the administration of Mg^{2+}-based phosphate binders was shown to decrease serum phosphate levels by disrupting the intestinal phosphorus absorption while assuring a better safety profile than other metal salt-based absorption inhibitors [92]. Another pathway underlying Mg^{2+}-mediated calcification inhibition is its direct interaction with amorphous calcium phosphate (ACP), resulting in decreased conversion of ACP towards hydroxyapatite [93], which is the main crystalline structure of a calcified matter. This was further supported by the observation that magnesium-enriched serum had lower calcification propensity, measured by changes in the maturation rate of primary calciprotein particles, colloidal nanoparticles formed in serum upon supersaturation with calcium and phosphate [94]. In the clinical setting, oral magnesium oxide administration was reported to slow down carotid artery calcification progression compared to oral carbon adsorbent [95]. However, due caution should be taken when prescribing magnesium salts as they are effective osmotic laxatives that can potentially cause electrolyte imbalance [96]. All calcification treatment options relying on Mg^{2+}-based substances are predominantly of physicochemical nature, and therefore a continuous intake of a drug is required to maintain a beneficial effect. Further attempts to develop a safe HAP crystals growth inhibitor resulted in the production of SNF472, a fully phosphorylated myo-inositol that was shown to effectively bind HAP crystals [97]. Administration of SNF472 was reported to attenuate cardiovascular calcification in a phase 2b trial. However, more data is required to estimate its effects on cardiovascular events [98].

Bisphosphonates, or pyrophosphates, are commonly prescribed antiresorptive drugs that affect osteoclast resorptive function [99]. Some authors reported the application of bisphosphonates for the treatment of soft tissue calcification, including VC in pre- and dialysis CKD patients [100-102]. This approach largely relies on maintaining hypocalcemia upon reduced bone degradation. However, the insufficient safety profile and severe side effects such as osteomalacia often lead to discontinuation of bisphosphonates [103]. Overall, bisphosphonates can be considered a more aggressive intervention aimed at alleviating vascular calcium burden in dialysis patients.

Bone morphogenetic protein antagonists inhibiting the widely proposed osteogenic origin of vascular calcification largely failed to inhibit vascular calcification. This casts serious doubt on the hypothesis that calcification is caused by osteogenic differentiation of

vascular cells. The induction of Runx2 transcription factor, long believed to be bone-specific, was recently shown to be part of a DNA damage response triggered by cellular damage [104], which further detracts from the osteogenic origin of calcification and returns to the front aging, cell damage and death and the ensuing dystrophic calcification of cell debris [105].

Another promising approach to the management of vascular calcification alludes the induction of naturally occurring calcification inhibitors. Matrix Gla protein (MGP) is an active tissue-bound calcification inhibitor that depends on vitamin K-mediated carboxylation to exert its function [25, 106, 107]. Notably, vitamin K antagonists such as warfarin are widely prescribed due to their potent anticoagulant action, with a common side effect being vascular calcification as a result of compromised MGP activity [108-110], and dietary vitamin K was shown to counteract the progression of calcification [107]. Being a natural nutritional compound, vitamin K displays a good safety profile, and its intake can be effortlessly adjusted. Combined with the absence of pronounced side effects, this ensures high compliance in patients receiving vitamin K supplementation. Patients with advanced CKD, who are already at high risk for vascular calcification, follow dietary restrictions that unintentionally reduce vitamin K intake, causing vitamin K deficiency and associated unfavorable effects [111-113]; therefore, vitamin K should be considered as a prophylactic of ectopic calcification in this group of patients.

Direct inhibition of osteoclast maturation represents another strategy for reducing serum calcium levels. Anti-osteoporotic monoclonal antibody denosumab targeting the nuclear factor κB ligand (RANKL), the key driver of osteoclastogenesis, was shown to reverse aortic arch calcification in CKD patients [114]. However, other groups reported no direct evidence of denosumab-related effects on VC progression [115-117]. It is uncertain whether this was related to insufficient treatment duration, given the effect of denosumab on VC was shown to be evident 30 months following therapy initiation [114].

Enhancing osteoclastic activity strictly at calcified lesions should theoretically reduce calcification without unduly increasing serum calcium. Thus, local stimulation of osteoclasts was studied here as a novel cellular calcification therapy addressing the lack of effective pharmacological methods for the treatment of ectopic calcification.

1.4 Bone resorption

Bone-producing osteoblasts and bone-degrading osteoclasts represent the cell forces that interact intimately to maintain bone mass [118, 119]. The osteoclast is a giant multinucleated cell of a monocyte/macrophage lineage that exerts the unique function of breaking down biological hydroxyapatite in a process known as bone resorption. Osteoclasts act by attaching to the bone matrix and creating an acidic resorptive microenvironment upon recognizing the specific Arg-Gly-Asp integrin-binding motifs of bone proteins [120, 121]. A circumferential actin-rich sealing zone, the marker of ongoing bone resorption, is formed due to various cytoskeleton rearrangements that the resorbing cell goes through to create an isolated microenvironment [122, 123]. The portion of the plasma membrane directly opposed to the bone surface extends into a highly convoluted ruffled border that serves to deliver acidified vesicles, the product of vacuolar proton pumps, and cathepsin K, a protease [124, 125]. Thus, after hydroxyapatite mobilization, the enzyme degrades the matrix proteins constituting the organic component of bone. The resorption products are then endocytosed by the osteoclast and released into the extracellular environment through the functional secretory domain [126].

Osteoclast activity is precisely regulated in order to prevent uncontrolled bone resorption. Several hormones and cytokines orchestrate the differentiation and activation of osteoclasts. Two molecules, macrophage colony-stimulating factor (M-CSF), produced by stromal cells, and RANKL, a cytokine primarily expressed by osteoblasts, were shown to be critically important for osteoclastogenesis [127, 128]. M-CSF binds to the colony-stimulating factor-1 receptor (CSF-1R) exposed on the membranes of mononuclear osteoclast precursors and renders them sensitive toward stimulation with RANKL by inducing the expression of receptor activator of NF-κB (RANK), the tumor necrosis factor superfamily receptor (TNFSFR) 11A [129]. In turn, RANK-RANKL binding launches downstream signaling pathways resulting in the metabolic reprogramming and induction of the nuclear factor of activated T cells c1 (NFATc1), a major regulator of the osteoclast differentiation program [130]. RANKL is initially expressed as a type II transmembrane protein that is susceptible to cleavage by certain shedding enzymes [131, 132]. The product of this reaction, termed soluble RANKL (sRANKL), possesses full biological activity [133]. Similar to other members of TNF family cytokines, sRANKL forms a homotrimer with each monomer

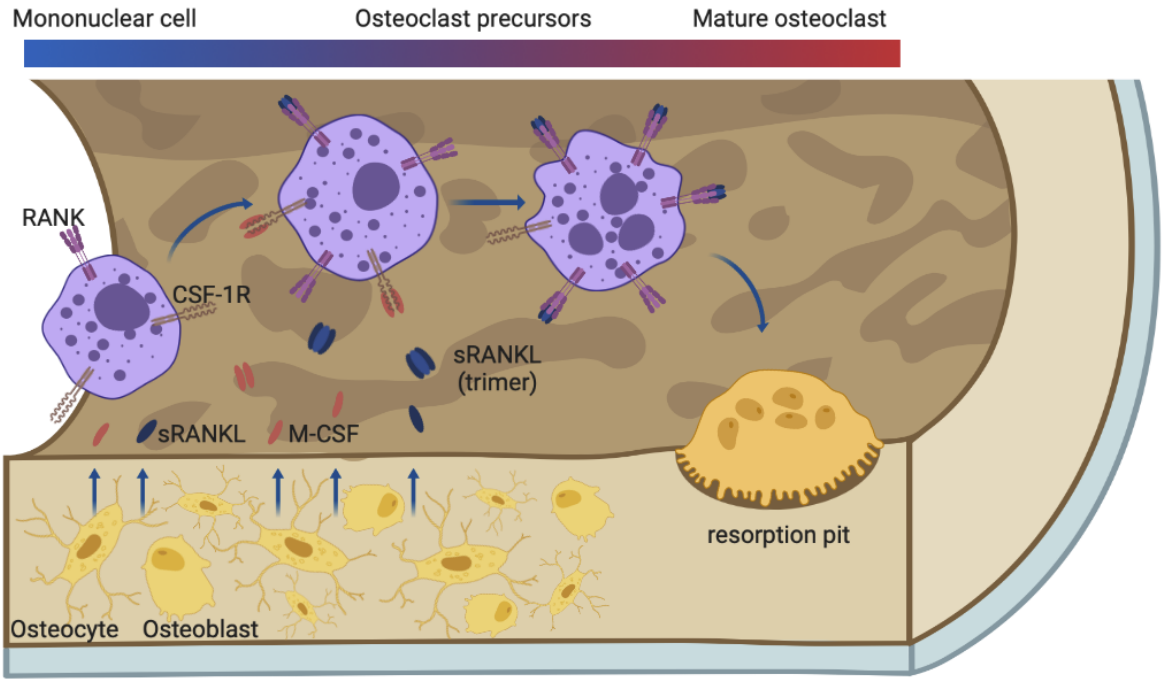

Figure 13. Bone resorption by osteoclasts. Mononuclear cells are rendered sensitive toward RANKL upon stimulation with M-CSF. RANKL produced by bone cells binds to RANK on the surface of precursor cells and thus triggers their metabolic reprogramming and differentiation to mature multinucleated osteoclasts capable of resorbing bone.

recognizing a single RANK molecule [134, 135]. Figure 2 illustrates a schematic representation of the bone resorption process.

The activating effect of the RANK-RANKL interaction is effectively counterbalanced by osteoblast-derived osteoprotegerin (OPG), a soluble decoy receptor for RANKL [136]. Thus, the RANKL/RANK/OPG axis constitutes the major effector system that governs osteoclastogenesis. Upstream signaling involves calcium-regulating hormones that either directly affect osteoclasts through specific receptors, as in the case of osteoclast-inhibiting calcitonin, or modulate the expression of RANKL/RANK/OPG as exemplified by the pro-resorptive action of PTH [137, 138]. The impact of vitamin D on bone resorption is controversial, as the vitamin was shown to have completely opposite effects on osteoclast function when tested in vivo and in vitro [139].

The osteoclast, being the sole cell type capable of breaking down otherwise insoluble hydroxyapatite, identical to that constituting ectopic calcifications, is thus a promising pharmacological target for the treatment of vascular calcification.

1.5 Fetuin-A, a systemic inhibitor of calcification

Fetuin-A, also referred to as α_2-Heremans-Schmid glycoprotein, is a liver-derived mineral chaperone that effectively prevents the spontaneous precipitation of calcium salts in soft tissues [140]. The 55-kDa protein consists of two cystatin-like domains, CY1 and CY2, and a C-terminal region (CTR). The monomeric form of the protein binds nascent clusters of calcium and phosphate, resulting in the formation of calciprotein monomers (CPM) that further consolidate into larger and more crystalline mineral-protein complexes termed calciprotein particles (CPP). DBA/2 mice lacking the functional fetuin-A gene develop severe soft-tissue mineralization associated with multiple organ dysfunction and increased mortality [141]. The potent inhibitory effect of fetuin-A on ectopic calcification is explained by its structural features. Extended beta-sheet of the domain CY1 of fetuin-A bears a negative charge due to the high content of aspartic acid (Asp) and glutamic acid (Glu) residues and therefore shows high affinity for positively charged calcium-phosphate mineral precursors [142]. Furthermore, the CTR consists of a flexible, intrinsically disordered amino acid sequence, which is believed to be an important structural characteristic of mineral-binding proteins [143-145]. The CTR also contains several phosphorylation sites, a feature long considered important for proteins involved in calcium binding [146]. Fetuin-A, chemically labeled with fluorescent tags, was shown to effectively detect early-stage microcalcifications ex vivo and in vivo [38, 47]. A bioengineering approach can further expand the theranostic potential of fetuin-A. For instance, the incorporation of a polyhistidine tag into the original amino acid sequence to aid protein purification concomitantly creates a structural prerequisite for site-specific radiolabeling, which, in turn, enables in vivo imaging of calcification using emission tomography techniques.

Taken together, the unique property of fetuin-A to preferentially bind to freshly formed mineral can be utilized to generate novel molecular agents that address imaging and treatment of ectopic calcification.

1.6 Alternative molecules with theranostic potential in ectopic calcification

Although significant progress has been made in understanding calcium biology, there are still large gaps in knowledge regarding the specific molecular mechanisms involved in calcium binding and mobilization. Proteins involved in mineral binding and stabilization

have collectively been addressed as mineral chaperones [147], a concept well known in milk components [148], which was recently extended to cell and tissue chaperoning [145]. I selected several mineral chaperones active in calcium-rich tissues and body fluids for screening as candidate agents for imaging and therapy of ectopic calcification.

Albumin is the most abundant serum protein that acts as a key modulator of plasma oncotic pressure and one of the main transport proteins. It is known for its ability to sequestrate calcium in a pH-dependent manner, with the ion binding being controlled by the pK of imidazole and amino groups [149]. However, it is unclear whether albumin binds to mature calcium deposits. Binding to established hydroxyapatite crystals is generally believed to be dependent upon the protein's ability to assume multiple conformational states, a feature common to many intrinsically disordered proteins such as osteopontin (OPN). Osteopontin, also known as bone sialoprotein I, is a highly phosphorylated multifunctional glycoprotein found in mineralized tissues and ectopic calcifications. Apart from its involvement in inflammation pathways, cell survival, and wound healing, this protein is considered a modulator of hydroxyapatite formation [150, 151]. Therefore, it is of particular interest whether labeled OPN can be used to detect calcified lesions.

Like blood, milk is a physiological fluid rich in calcium. As milk is the primary source of nutrition for mammalian young, it is naturally formulated to contain all macro- and micronutrients required for the development of the neonate. Certain molecular mechanisms have emerged to stabilize the complex mixture of proteins, carbohydrates, fats, and microelements. To avoid the precipitation of excess calcium phosphate, mammals secrete a group of milk phosphoproteins termed caseins that can bind and thereby solubilize calcium salts [152]. The milk fat globule membrane (MFGM) is a complex tri-layer membrane that stabilizes fat globules emulsified in the aqueous phase of milk [153]. Although this structure was described decades ago, the full range of its functions has yet to be revealed. The MFGM contains numerous bioactive components, including glycosylated proteins, which justifies a more detailed study of the structure for its potential calcium-binding properties.

Casein, the major micelle forming carrier protein in milk, may be considered the most potent mineral chaperone of all [154]. As casein has its function outside the blood in milk, it was not considered here. Nevertheless, important lessons regarding mineral stabilization and macromolecular assembly of supramolecular complexes can be gleaned from casein [155].

2. AIM AND OBJECTIVES

Certain patterns of ectopic calcification, including microcalcification of atherosclerotic plaques, pose serious health risks. Most current imaging approaches lack sensitivity toward nascent mineral deposits reflecting early stages of ectopic calcification, and those capable of resolving micrometer-sized lesions are costly and labor-intensive, which limits their use in clinical practice. Moreover, there are no effective conservative methods for the treatment of soft tissue calcification to date. Thus, there is an urgent need to fundamentally reconsider the management of ectopic calcifications.

An ideal diagnostic and therapeutic tool should be non-toxic, sensitive toward microcalcifications and capable of reversing ectopic calcification by clearing the established mineral deposits. I hypothesized that an intrinsically fluorescent protein probe targeting nascent mineral deposits would provide new prospects in intravital and reporter-based imaging of both physiological and pathological calcification. I further conjectured that natural bone-resorbing osteoclasts may be used in the management of ectopic calcification if their directed activation at the sites of pathological mineral deposition can be achieved, considering the significant similarity of the pathways involved in the processes of physiological bone mineralization and pathological calcification of soft tissues. Figure 3 shows a cartoon demonstrating the theranostic potential of fetuin-A-based fusion proteins in vascular calcification.

To address the study's objectives, I attempted to design and produce a set of fusion proteins with the desired parameters. Fetuin-A, a plasma-derived calcium phosphate-binding glycoprotein, was the main structural unit of all fusion proteins due to its unique ability to target the freshly formed mineral. To generate imaging probes, the fetuin-A molecule was intended to be coupled to either a green or red fluorescent protein variant with a flexible linker, and to produce a targetable osteoclast activator, the mineral chaperone was meant to be fused to the extracellular domain of the osteoclast-inducing cytokine RANKL. Further objectives included the amplification of plasmid DNAs in *E. coli* cultures and their introduction into suspension-adapted Chinese hamster ovary (CHO) cells by lipofection. Finally, the expressed fusion proteins were intended to be evaluated in a series of experiments.

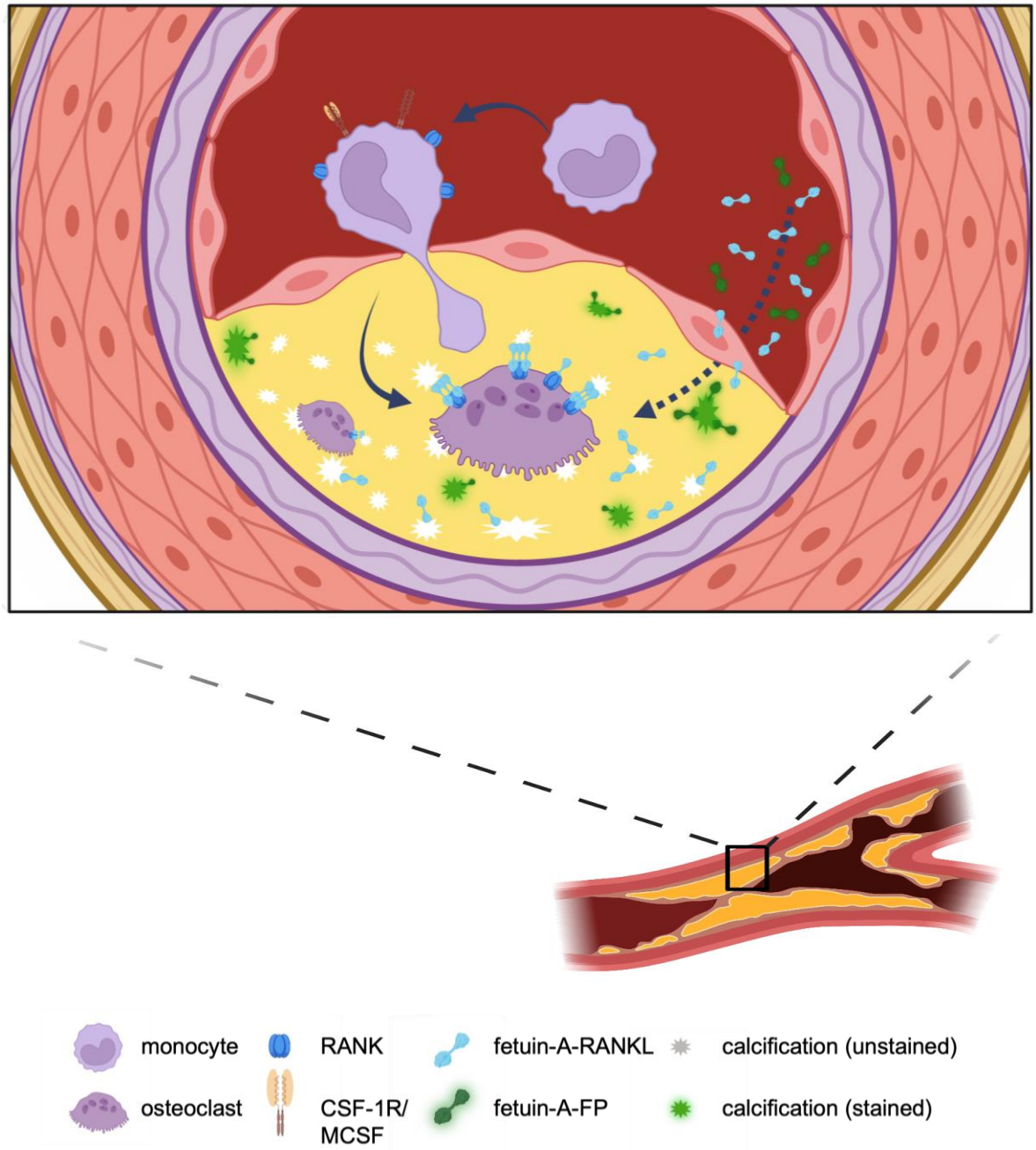

Figure 3. Application of the fetuin-A-based fusion proteins in vascular calcification. Microcalcifications occurring in an atherosclerotic plaque are targeted by fetuin-A coupled to a fluorescent protein (fetuin-A-FP) or the osteoclastogenic cytokine RANKL (fetuin-A-RANKL). Fetuin-A-FP decorates nascent calcifications enabling their detection. Fetuin-A-RANKL also binds microcalcifications yet triggers local differentiation of myeloid cells toward osteoclasts capable of dissolving the calcified matter.

3. MATERIALS AND METHODS

3.1 Cell cultures

All human cells were isolated in accordance with local, state, and federal laws and regulations. Human tissue banking was approved by ethical review boards for research and diagnostic procedures at UKA (EK 300/13) or MUMC. Collection, storage, and use of tissue and patient data were performed in agreement with the Dutch Code for Proper Secondary Use of Human Tissue (https://www.federa.org/codes-conduct accessed on July 30, 2021). All parts of this study complied with the Declaration of Helsinki.

3.1.1 ExpiCHO-S cells

The ExpiCHO-S™ cell line represents a subclone of the suspension-adapted CHO-S cell line [156] optimized for a high-yield protein production that is supplied as a part of the ExpiCHO™ Expression System Kit (Life Technologies Corporation, Carlsbad, USA, Cat. # A29133). Following thawing, the cells were maintained in ExpiCHO™ Expression Medium in a humidified atmosphere of 8% CO_2 at 37 °C upon constant agitation. Subculturing was performed when the cell density was reaching 5×10^6 viable cells/ml, typically every 3 days. The seeding density was 0.2×10^6 viable cells/ml. Cells were counted using FastRead 102 disposable cell counting slides (3H Biomedical AB, Uppsala, Sweden, Cat. # 3HBVS100), and the cell viability was estimated by trypan blue exclusion assay.

3.1.2 Mesenchymal stromal cells

Primary human mesenchymal stromal cells (MSC) were obtained with written consent from patients undergoing total hip arthroplasty in the Clinic of Orthopedics, Trauma and Reconstructive Surgery of University Hospital Aachen. MSC harvesting was performed according to the published protocols [157, 158]. Following isolation, MSC were maintained in Mesenpan medium containing 2% fetal bovine serum (FBS), 1% ITS-plus (insulin, transferrin, selenic and linoleic acids, bovine serum albumin), 1 nM dexamethasone (DEX), 100 µM L-ascorbic-acid-2-phosphate (LAA2P), 10 ng/ml epidermal growth factor (all from

Pan-Biotech, Germany), 80 U/ml penicillin, 80 µg/ml streptomycin, and 1.6 mM L-glutamine (all from Gibco, Germany). The culture medium was exchanged every 3-4 days. Following expansion and characterization by flow cytometry, the cells were seeded on 8-well Ibidi µslides (Ibidi GmbH, Germany) at a density of $1x10^4$ cells/cm^2 and cultured for 72 h in low-glucose Dulbecco's Modified Eagle's Medium (DMEM, glucose content 1 g/L) (Thermo Scientific, Germany) supplemented with 10% FBS, 100 U/ml penicillin, 100 µg/ml streptomycin, and 2 mM L-glutamine.

3.1.3 Immortalized vascular smooth muscle cells

Immortalized vascular smooth muscle cells (iVSMC) were derived from primary commercial cell lines. iVSMC were immortalized by transduction using the SV40LT and HTERT systems. Clone IM1 was isolated and maintained at 37 °C and 5% CO_2 in a M199 medium (Thermo Scientific), 10% FBS, 100 U/ml penicillin, 100 µg/ml streptomycin, and 2 mM L-glutamine. Prior to experiments, iVSMC were seeded on 8-well Ibidi µslides (Ibidi GmbH, Gräfelfing, Germany, Cat. # 80826) at a density of $2x10^4$ cells/cm^2 and left to attach for 24 hours.

3.1.4 Primary human vascular smooth muscle cells

Primary human vascular smooth muscle cells (VSMC) were isolated from healthy aortic tissue biopsies at Maastricht University Medical Center [47]. VSMC were cultured in DMEM supplemented with 20% FBS, 100 U/ml penicillin, 100 µg/ml streptomycin, and 2 mM L-glutamine at 37 °C and 5% CO_2. For calcification experiments, the cells between passages 5 and 9 were seeded into a 48-well plate at a density of $1x10^4$ cells/cm^2.

3.1.5 Human atherosclerotic cells

Human atherosclerotic smooth muscle cells HASMC66 were cultured in a M199 medium (Thermo Scientific) supplemented with 10% FBS, 100 U/ml penicillin, 100 µg/ml streptomycin, and 2 mM L-glutamine. The cells were maintained at 37 °C and 5% CO_2. Prior to experiments, iVSMC were seeded on 8-well Ibidi µslides (Ibidi GmbH, Gräfelfing, Germany, Cat. # 80826) at a density of $1.5x10^4$ cells/cm^2.

3.1.6 Human embryonic kidney cells

Human embryonic kidney 293 cells (HEK293) (CRL-1573, ATCC, Manassas, USA) were cultured in DMEM containing 100 U/ml penicillin, 100 µg/ml streptomycin, and 2 mM L-glutamine at 37 °C in a humidified atmosphere of 5% CO_2. The cells were maintained in base medium for three passages prior to transfection and induction of calcification.

3.1.7 RAW 264.7 cells

The murine macrophage/monocyte-like Abelson leukemia virus-transformed cell line RAW 264.7 was obtained from ATCC. Unlike other osteoclast precursor cells, RAW 264.7 monocytes readily differentiate to osteoclasts upon stimulation with RANKL regardless of added M-CSF. Following thawing, the cells were cultured in antibiotic-free DMEM supplemented with 10% FBS. Cell splitting was performed every 3-4 days by scraping off the adherent culture using a cell scraper.

3.2 Animal experiments

All experiments involving animals were conducted in agreement with the recommendations of the Federation for Laboratory Animal Science Associations FELASA and were approved by the animal welfare committee of the Landesamt für Natur-, Umwelt- und Verbraucherschutz (LANUV) of the state of North Rhine-Westphalia. All mice were maintained on a 12:12 light-dark cycle. Animals received food and water *ad libitum*. Tissue samples were taken from 24-25 week old DBA/2-*Ahsg*$^{-/-}$ mice. Animals were euthanized by an overdose of isoflurane and exsanguinated prior to organ harvesting.

3.3. Production of proteins

Bioengineering of chimeric proteins is a complex task that requires careful analysis of the amino acid sequences of the proteins selected for fusion. Furthermore, the secondary and tertiary structures of the proteins should be taken into account, as combining proteins may result in impaired folding or the inability of the protein to be secreted. The intended application of the protein, as well as the preferred expression system and purification method,

should also be considered during the protein design. Finally, the development of appropriate assays is often required in order to evaluate the function of the engineered proteins.

3.3.1 Protein design

Fusion fluorescent proteins consisted of the N-terminal full-size murine fetuin-A (mFA, accession number P29699 of UniProtKB) with its native signal peptide coupled to either a green or red fluorescent protein variant, mEmerald (fluorescent protein database ID AD4BK) or mRuby3 (fluorescent protein database ID MZMFB), with a flexible $(GGGGS)_3$ linker. Additionally, the C-terminal mRuby3 was coupled to a hydroxyapatite-binding protein bovine osteopontin (bOPN, accession number P31096 of UniProtKB). To facilitate protein purification using immobilized metal affinity chromatography (IMAC), a C-terminal polyhistidine tag (6xHis) preceded by a factor Xa preferred cleavage site (IEGR) was included in all sequences. Figure 4A contains data on the fetuin-A-based fluorescent fusion protein sequences and their 3D structures generated using the neural-network-based algorithm for protein structure prediction AlphaFold [159].

Three variants of the fetuin-A-RANKL fusion protein were designed. All three proteins had the same signal peptide of mFA, flexible $(GGSG)_5$ linker connecting the N-terminal fetuin-A and C-terminal RANKL subunits, and a C-terminal factor Xa cleavage site followed by a 6xHis purification tag. mFA-sRANKL contained the full-size mFA coupled to sRANKL (amino acid residues 162-316, accession number O35235 of UniProtKB), mFA-scRANKL comprised the full-size mFA coupled to a single-chain RANKL (three sRANKL sequences connected with a $(GGSG)_3$ linker [135]), and CY1_mFA-sRANKL consisted of domain CY1 of mFA (C32S) fused to sRANKL. Point mutation C32S was introduced to eliminate the unpaired cysteine of the mFA domain CY1. Figure 4B shows amino acid sequences and ribbon diagrams of the fetuin-A-RANKL variants.

3.3.2 Plasmid vector design

Vectors encoding the fusion proteins were designed using GeneArt Gene Synthesis Portal. The Kozak consensus sequence and the *Hin*dIII restriction site were introduced 5'-terminally in each case, followed by the codon optimization to enhance protein expression

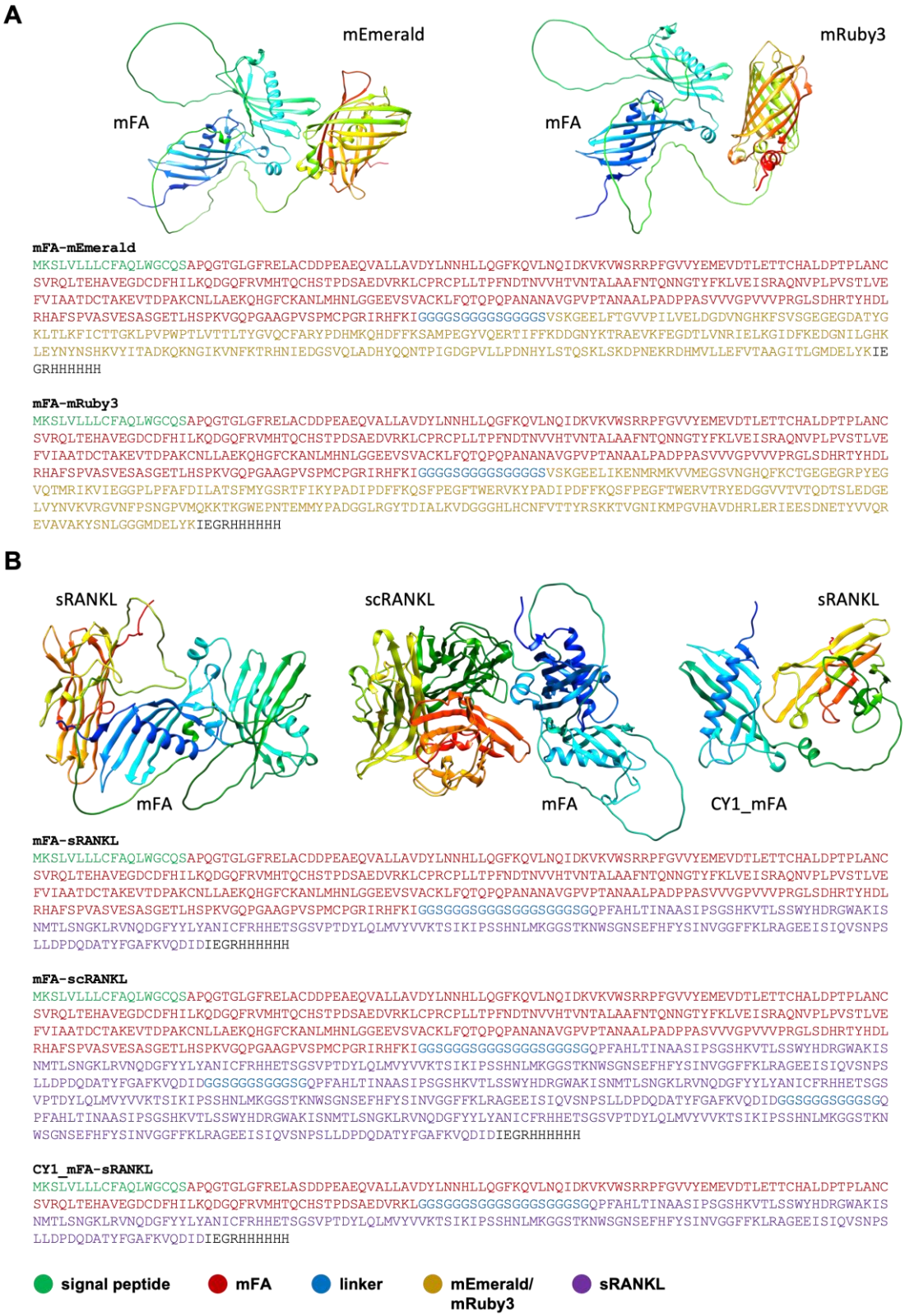

Figure 4. AlphaFold-generated 3D models of fusion proteins and corresponding amino acid sequences. The rainbow depiction mode (blue-to-red) of ribbon diagrams indicates the N- to C-terminal arrangement of amino acid residues. **(A)** Structures and peptide chains of fluorescent fusion proteins mFA-mEmerald and mFA-mRuby3. **(B)** Structures and peptide chains of fetuin-A-RANKL fusion proteins mFA-sRANKL, mFA-scRANKL and CY1_mFA-sRANKL.

in the target cell line ExpiCHO-S™ (*Cricetulus griseus*). The constructs were cloned into the pcDNA™ 3.4 TOPO mammalian expression vectors by Life Technologies GmbH (Darmstadt, Germany).

3.3.3 Plasmid preparation

Eukaryotic cell transfection relies crucially on the quality and amount of the genetic material intended to be introduced into host cells. In order to obtain the transfection-grade plasmid DNA, small amounts of plasmids were propagated in a chemically competent endonuclease I-deficient NEB Turbo *E. coli* strain. Purification of the amplified plasmids was carried out using the PureYield™ Plasmid Midiprep System (Promega, Madison, USA) according to instructions of the manufacturer. The purified plasmid DNA concentration was measured at 260 nm using NanoDrop 1000 Spectrophotometer (Thermo Scientific, Waltham, USA) and its purity was assessed by the A260/A280 ratio. Plasmid DNA was snap-frozen in liquid nitrogen and stored at -20°C until required for further experiments.

3.3.4 Protein expression

The biological activity of many proteins depends on post-translational modifications (PTMs). Murine fetuin-A is known to undergo several PTMs, including N-linked glycosylation and phosphorylation, and the latter was shown to be associated with the formation of mineral complexes, the major function of fetuin-A [160]. Mammalian expression platforms are believed to possess the necessary molecular machinery to provide a broad spectrum of PTMs that ensure structural and functional similarity of the expressed proteins to their natural counterparts [161]. For the recombinant fusion protein expression, a commercially available eukaryotic ExpiCHO-S™ cell line (Section 3.1.1) was selected as a suitable expression system.

The transfection-grade plasmid DNA was introduced into the CHO cells by lipofection using the ExpiFectamine™ transfection reagent. On the next day, ExpiCHO™ Feed and ExpiCHO™ Enhancer were added to the transfected cell cultures, and the flasks were transferred to the 32°C incubator with a humidified atmosphere of 5% CO_2. Cultivating CHO cells at lower temperatures was reported to increase the overall protein yield and induce phosphorylation of the expressed proteins [162].

Culture sampling was performed daily to assess cell viability. To this end, 10 µl of cell suspension was gently mixed with 10 µl 0.4% trypan blue solution (Gibco, Grand Island, USA) on Parafilm M™ film (Bemis, Oshkosh, USA, Cat. # P0201), and the cells were counted using FastRead 102™ cell counting chamber at ×100 magnification. In the case of fluorescent protein-expressing cultures, sampled cells were additionally imaged using fluorescence microscopy to detect the fusion proteins.

Protein harvesting was carried out on days 8–12 post-transfection when cell viability decreased to 80%. The expressed proteins were purified using HisTrap™ HP column (GE Healthcare, Boston, USA, Cat. # 17-5248), and the elution fractions were analyzed by sodium dodecyl sulfate-polyacrylamide gel electrophoresis (SDS-PAGE). The chemicals used for SDS-PAGE are listed in table 1.

Elution fractions containing target proteins, as revealed by gel electrophoresis, were rebuffered into an imidazole-free 4-(2-hydroxyethyl)-1-piperazineethanesulfonic acid (HEPES) buffer using Zeba™ spin desalting columns (Thermo Scientific, Rockford, USA, Cat. # 89894) with a molecular weight cut-off of 7 kDa.

Immunodetection of expressed proteins was performed by western blotting (Owl™ HEP-1 semi-dry electroblotter) using either rabbit anti-mouse fetuin-A antiserum from institute stocks or the HisProbe™-HRP nickel-activated conjugate (Thermo Scientific, Waltham, USA, Cat. # 15165) following the manufacturer's instructions. Additionally, the primary anti-RANKL antibody (R&D Systems, Minneapolis, USA, Cat. # AF462) was used for detecting mFA-sRANKL fusion proteins.

3.3.5 Phosphomimetic fetuin-A proteins

Serine or threonine residues at positions 135, 138, 305, 309, 312, and 314 of mFA were replaced with glutamic acid in order to mimic constitutive phosphorylation of residues listed in UniProt P29699 as putative phosphorylation sites. Phosphomimetic versions of the recombinant (fusion) proteins are denoted with the prefix "pm-", i.e., pm-mFA, pm-mFA-mEmerald, and pm-mFA-mRuby3. Modified proteins were expressed as described above.

3.4 Mass spectrometry

The presence of contaminants in protein preparations purified using affinity purification methods such as IMAC depends on the target protein yield. A low amount of the tagged protein in the supernatant subjected to affinity chromatography leaves many binding sites of a purification column unoccupied, creating a prerequisite for the binding of unspecific contaminants. Given that cytokines are generally expressed in smaller amounts than other secreted proteins, matrix-assisted laser desorption/ionization-time of flight (MALDI-TOF) mass spectrometry was applied to confirm the purity of the expressed fetuin-A-sRANKL fusion protein variant. The elution fraction containing the protein of interest was subjected to SDS-PAGE, and a square fragment at the position corresponding to the fusion protein band was cut out of the gel. The protein was recovered from the gel and subjected to MALDI-TOF mass spectrometry.

Table 1. Reagents for gel electrophoresis.

Buffer	***Chemical***	***Final concentration***
1x Laemmli buffer	Tris base	25 mM
	Glycine	192 mM
	SDS	3.5 mM
2x SDS sample buffer	Tris-HCl, pH 6.8	0.125 M
	Glycerol	20% (v/v)
	SDS	4% (w/v)
	Bromophenol blue	0.01%
4x stacking gel buffer	Tris-HCl, pH 6.8	0.5 M
	SDS	0.4% (w/v)
4x resolving gel buffer	Tris-HCl, pH 8.8	1.5 M
	SDS	0.4% (w/v)

3.5 Purification and chemical labeling of fetuin-A

Serum-derived bovine fetuin (Sigma, Taufkirchen, Germany, Cat. # F2379) was subjected to gel filtration, and the monomeric protein was collected as described [163]. The purity of the obtained fractions was confirmed by SDS-PAGE. Bovine fetuin-A was labeled

with Alexa Fluor™ 488 NHS ester fluorescent dye (Life Technologies Corporation, Carlsbad, USA, Cat. # A20000) according to the manufacturer's protocol and aliquoted into screw cap vials. The labeled protein was frozen in liquid nitrogen and stored at -20°C.

For SPECT imaging, recombinant mFA bearing an N-terminal hexahistidine tag was concentrated to 13 mg/ml and labeled with ^{99m}Tc radionuclide using the tricarbonyl moiety $[^{99m}Tc(CO)_3(H_2O)_3]^+$.

3.6 Toxicity testing of fluorescent fetuin-A proteins

As the fluorescent proteins were intended to be applied for live imaging, it was important to verify their lack of toxicity. To assess toxicity, MSC were exposed to 12 µM fluorescent fetuin-A probes, corresponding to twice the amount used for short live cell staining and 50-fold the amount used for one-week extended live staining. The cells were seeded in 24-well plates at $5x10^3$ cells/cm^2 density and cultured in low-glucose DMEM supplemented with 10% FBS. After 1 week of culture, the medium was exchanged, and 12 µM fluorescent fetuin-A protein was added for two hours. MSC were washed and cultured for further three days. Cells were detached by trypsinization, and their viability was assessed by trypan blue dye exclusion as described above.

3.7 Calcium phosphate precipitation inhibition assay

Protein fusion can lead to serious structural rearrangements of its constituent domains, which can adversely affect the functionality of such chimeric proteins. The activity of the produced fetuin-A fusion proteins was tested employing the calcium phosphate precipitation inhibition assay. The assay investigates the capacity of fetuin-A to prevent the growth of calcium phosphate crystallization nuclei in a supersaturated solution by forming colloidal mineral-protein complexes. Test proteins were added in concentrations from 0 to 8 µM in 1 µM increments to the assay buffer (50 mM Tris, 140 mM NaCl, pH 7.4 at 37 °C). All stock salt solutions were sterile-filtered (pore size 0.2 µm). Phosphate and calcium were added to 3 mM Na_2HPO_4/NaH_2PO_4 and 5 mM $CaCl_2$, respectively, in a total volume of 200 µl assay buffer. After each addition, the solution was thoroughly mixed to avoid local supersaturation, and until incubation, all mixtures were stored on ice. Following 1 h of incubation at 37 °C, the precipitate was obtained by centrifugation (10 min, 20000 × g, 4°C). Next, 50 µl of 0.6

M HCl and then 50 µl of a basic ammonium buffer (45 mM NH_4Cl pH 10.5, 5% v/v NH_4OH) were stepwise added to half of the supernatant (100 µl) and mixed thoroughly. Similarly, 50 µl 0.6 M HCl and 50µl ammonium buffer (45 mM NH_4Cl pH 10.5, 5% v/v NH_4OH) were successively added to the remaining 100 µl supernatant with pellet. The resulting solution was mixed thoroughly to dissolve the pellet. Calcium content in the supernatant and the corresponding precipitate was determined photometrically using Randox Calcium Reagent™ (Randox Laboratories, Crumlin, UK, Cat. # CA590) according to the manual.

3.8 Induction of mineralization and calcification in cell cultures

To mimic physiological mineralization, the osteoblastic differentiation of MSC (Section 3.1.2) was induced by switching base medium to osteogenic medium (OM), consisting of the low-glucose DMEM supplemented with 10% FBS, 100 U/ml penicillin, 100 µg/ml streptomycin, 2 mM L-glutamine, 100 nM DEX, 10 mM β-glycerophosphate (β-GP), and 50 µM L-ascorbic acid-2-phosphate (LAA2P) (all from Sigma Aldrich, Germany). The OM was exchanged twice a week.

To imitate pathological calcification, iVSMC (Section 3.1.3) or HASMC66 (Section 3.1.5) were maintained in calcification medium (CM) comprising M199 base medium adjusted to 4.3 mM total calcium and 3.0 mM total phosphate. The cells were cultured in CM for five days, with one medium exchange performed on day three.

For extended live staining experiments, VSMC (Section 3.1.4) calcification was triggered by switching the base medium to a serum-depleted calcification medium (S-DCM) comprising DMEM (0.5% FBS) with a total calcium content of 3.6 mM. The decreased serum content served to enhance cell calcification, as serum contains proteins and other molecules with an inhibitory effect on calcification. Culture medium was not exchanged during the experiment.

To mimic kidney calcification, the HEK293 medium (Section 3.1.6) was switched to a kidney calcification medium (KCM) consisting of a base culture medium adjusted to 4.3 mM total calcium and 3.0 mM total phosphate. To generate a calcification-reporting system, HEK293 cells were transiently transfected with a TOPO3.4 vector encoding *mFA-mRuby3* gene 4 h prior to triggering calcification. TransIT-293™ (Mirus Bio, Madison, USA, Cat. # 2700) transfection reagent was used according to the manufacturer's instructions to deliver plasmid DNA into cells. To support protein expression, the culture medium was

supplemented with 1% non-essential amino acids solution (NEAA) (Life Technologies, Grand Island, USA, Cat. # 11140050).

Formulations of media used in these experiments are summarized in Table 2.

Table 2. Media formulations.

Medium	***Base***	***Cells***	***Additives***		***Mineralization***
OM	DMEM (low-gluc.)	MSC	FBS	10%	physiological
			penicillin	100 U/ml	
			streptomycin	100 µg/ml	
			L-glutamine	2 mM	
			DEX	100 nM	
			β-GP	10 mM	
			LAA2P	50 µM	
CM	M199	HASMC66 iVSMC	FBS	10%	pathological
			penicillin	100 U/ml	
			streptomycin	100 µg/ml	
			L-glutamine	2 mM	
			$CaCl_2$	2.5 mM	
			H_2NaPO_4	0.38 mM	
			HNa_2PO_4	1.62 mM	
S-DCM	DMEM	VSMC	FBS	0.5%	pathological
			penicillin	100 U/ml	
			streptomycin	100 µg/ml	
			L-glutamine	2 mM	
			$CaCl_2$	1.8 mM	
KCM	DMEM	HEK293	FBS	2%	pathological
			penicillin	100 U/ml	
			streptomycin	100 µg/ml	
			L-glutamine	2 mM	
			NEAA	1%	
			$CaCl_2$	2.5 mM	
			H_2NaPO_4	0.38 mM	
			HNa_2PO_4	1.62 mM	

3.9 Assessment of osteoclast differentiation and function

Osteoclasts are classically defined as tartrate-resistant acid phosphatase-positive ($TRAP^+$) giant multinucleated cells of monocyte/macrophage origin capable of resorbing bone. However, this definition is not fully accurate due to several reasons. Although TRAP is historically considered a histochemical marker of osteoclasts, its expression is not unique to these cells [164]. Next, the occurrence of mononucleated osteoclasts was reported [165]. Whether such cells can resorb bone remains debatable [166]. Finally, osteoclast size is highly variable and depends on their maturation state, motility, surface parameters etc. Thus, the only defining feature of osteoclasts is the ability to resorb bone. The assessment of bone resorption requires special materials such as bone slices or precoated culture vessels. As neither the size nor the count of osteoclasts can be considered sufficient to evaluate osteoclast formation on plastic, I propose the osteoclast differentiation index (ODI) as a more accurate method to assess osteoclast induction.

3.9.1 Osteoclast differentiation assay

To generate osteoclasts, RAW 264.7 cells were plated in a 24-well plate at a density of 0.5×10^4 cells/cm^2. Osteoclast induction was triggered on day 3 upon the addition of a fetuin-A-RANKL fusion protein. Precursors stimulated with the recombinant sRANKL from institute stocks served as the positive control [167]. On day 14, cells were stained with a cytosolic tracer CellTracker™ Green CMFDA (Thermo Scientific, Eugene, USA, Cat. # C7025) and a nuclear counterstain Hoechst 33342 (Thermo Scientific, Rockford, USA, Cat. # 62249), and ODI was calculated according to the formula below:

$$ODI = \frac{\mathrm{NMuC}}{(\mathrm{NMuC+MoC})},$$

where NMuC is the total number of nuclei in multinucleated (n≥3) cells, and MoC is the number of mononucleated cells per field of view. Only the nuclei of the cells that were completely within the field of view were counted. As can be seen from the formula, binucleate cells are excluded from the calculations as they may represent dividing cells. Thus, ODI is more practical for evaluating osteoclast induction compared to mere cell counting.

Both cytoplasmatic tracer and nuclear stain used in this method can be replaced with the more cost-effective dyes fluorescein diacetate (FDA) and 4′,6-diamidino-2-phenylindole (DAPI).

3.9.2 Resorption assay

Osteoclastic resorption was studied using Corning® Osteo Assay Surface 24-well plates (Corning, New York, USA, Cat. # 1611746). The bottoms of such plates represent a uniform inorganic bone biomimetic surface that can be degraded upon osteoclast activation. Prior to cell plating, some wells were preincubated with DMEM containing varying concentrations of the fetuin-A-sRANKL fusion protein or sRANKL. The plate was then washed with plain DMEM, and RAW 264.7 cells were seeded in wells at a density of 1×10^4 cells/cm. All cells were cultured in DMEM containing 10% FBS until day 3. Starting from day 3, culture medium in wells that were not initially preincubated with cytokines was supplemented with varying concentrations of the fetuin-A-sRANKL fusion protein upon medium exchange which took place every 3-4 days. The experiment was terminated on day 10, and the cells were removed by incubation with cell lysis buffer (0.1 M NaOH, 1% SDS) for 1 h at room temperature upon constant agitation. The wells were then stained according to the method of von Kossa. Briefly, the wells were washed with PBS and incubated with 5% aqueous silver nitrate for 30 min under direct light from a desk lamp. Next, the wells were washed twice with ddH_2O and incubated with 2.5% aqueous sodium thiosulfate for 5 min. The wells were again washed with ddH_2O and immediately imaged using Canon EOS 1000D digital camera. Figure 5 provides a schematic of the experiment.

To evaluate osteoclastogenesis on a natural surface, RAW 264.7 cells were plated on bovine bone discs (Boneslices.com, Jelling, Denmark) placed in the wells of a 96-well plate filled with 100 µl DMEM as above at a density of 5×10^4 cells/well. After 2 h of incubation at 37 °C and 5% CO_2, the non-adherent cells were removed by washing the discs with plain DMEM. The bone slices with cells facing upward were then transferred to a 24-well plate, 3 discs per well, and maintained in DMEM containing 10% FBS. Starting from day 3, osteoclast precursors were additionally treated with either 100 ng/ml sRANKL or an equimolar amount of fetuin-A-sRANKL fusion protein variant. Medium was exchanged every 3-4 days. The experiment was terminated on days 7 and 14, and the bone discs were processed for subsequent electron microscopy.

3.9.3 Quantification of bone biomimetic surface resorption

The area of bone-mimetic surface resorption was quantified using Adobe® Photoshop® software. The RAW photographs of individual wells were converted to grayscale

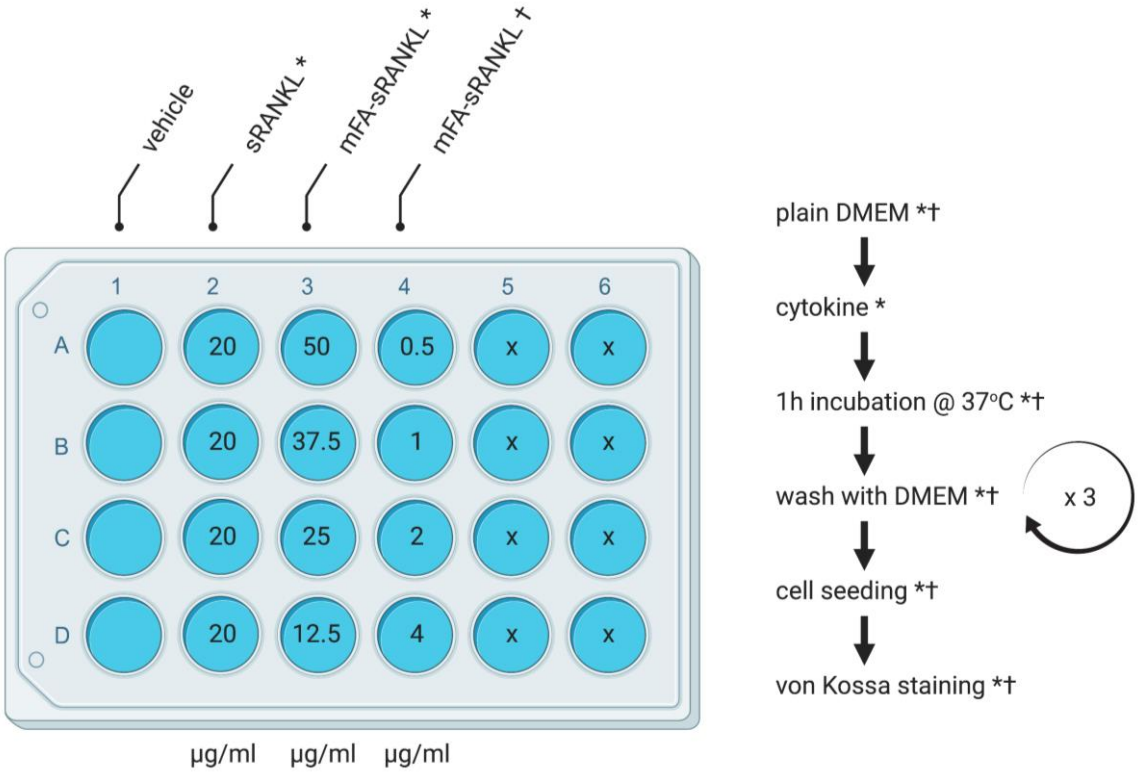

Figure 5. Schematic representation of the resorption assay. Wells in columns marked with an asterisk were preincubated with cytokines prior to cell seeding. Cells in these columns received no additional cytokine supplementation during the experiment. Wells in the column marked with a dagger were preincubated with cytokine-free medium before the cell seeding was performed. In this column, precursors were treated with the cytokine upon medium exchange starting from day 3. Concentrations of the corresponding cytokines are given inside the wells.5

images. The bottom part of each well was selected and copied to a new layer. The Threshold filter was applied to the image so that the intact areas appeared black, and the resorptions pits turned white. All non-transparent areas of the layer were selected, and the percentage of white pixels (intensity level 255), representing the area of resorption, was taken from the histogram panel.

3.10 Cell staining and microscopy

Several staining techniques and imaging modalities were used to examine cell calcification and osteoclast formation. Unless otherwise stated, staining was performed on

living cells. During live imaging, cells were maintained at 37 °C in a humidified atmosphere of 5% CO_2.

3.10.1 Imaging of calcifying cultures

To visualize calcifications in MSC and iVSMC cultures by short-term live staining, fetuin-A-based fluorescent probes, or fluorescein derivative calcein (Sigma Aldrich, Germany, Cat # C0875-5G) were added to the cells at a final concentration of 6 µM or 0.2 mM, respectively. Following staining for 1.5 h at 37 °C and 5% CO_2, the cells were rinsed with PBS to remove unbound probes. Counterstaining was performed with 1 µg/mL Hoechst 33342 (Thermo Scientific, Rockford, USA, Cat. # 62249) and either 5 µg/mL CellTracker™ Green CMFDA (Thermo Scientific, Eugene, USA, Cat. # C7025) or 10µg/mL CellTracker™ CM-DiI (Thermo Scientific, Eugene, USA, Cat. # C7000). Following 15 min incubation at 37 °C, the medium was exchanged, and cells were visualized using a Zeiss LSM 710 confocal laser scanning microscope. After fluorescence imaging, cells were rinsed with PBS, fixed with 4% paraformaldehyde (PFA) and post-stained with Alizarin Red S. Identification of calcified areas in Alizarin-stained cultures was performed using a Leica DMRX microscope (Leica Microsystems GmbH, Wetzlar, Germany).

For extended live staining of VSMC, culture medium (S-DCM) was supplemented with 0.24 µM (corresponding to 20 µg/mL) mFA-mRuby3 as described [47]. Imaging was performed on days 1, 3, and 7 using a Cytation 3 automated cell imaging system (BioSPX, Abcoude, The Netherlands).

To access calcification in a HEK293 culture, fluorescence imaging using a Leica DMI6000 B microscope was performed on day 3 after the cells were transfected with a plasmid encoding fetuin-A-mRuby3 fusion protein. The culture medium was exchanged shortly before microscopy to reduce the background signal caused by the release of a fluorescent protein.

For intracellular vesicle tracking, MSC cultured in basal low-glucose DMEM supplemented with 10% FBS were stained with mFA-mRuby3 at a final concentration of 6 µM for 1.5 h at 37 °C and 5% CO_2. Next, the culture medium was exchanged, and the cells were visualized using a Corrsight spinning disk microscope (FEI, Eindhoven NL) spinning disc microscope. Microphotographs were taken at 0.3 s intervals for 100 s and exported as a time-lapse video file.

3.10.2 Imaging of osteoclasts

Nuclear stain Hoechst 33342 (Thermo Scientific, Rockford, USA, Cat. # 62249) and cytoplasmatic dye CellTracker™ Green CMFDA (Thermo Scientific, Eugene, USA, Cat. # C7025) were used to stain mature osteoclasts and their precursors. To stain osteoclastic actin rings, cells were fixed with 4% PFA for 15 min at room temperature, and cell membrane permeabilization was performed by treating cells with 0.1% Triton X-100 solution (Sigma, Taufkirchen, Germany, Cat. # 93443) for additional 15 min at room temperature. Next, cells were washed with PBS and incubated with TRITC-conjugated phalloidin (Sigma, Taufkirchen, Germany, Cat. # P1951) for 2 h at room temperature following the manufacturer's instructions. Cell nuclei were counterstained using Hoechst 33342. Fluorescence imaging of osteoclasts was performed using a Leica DMI6000 B microscope.

Bone discs with osteoclasts were fixed using a 2% glutaraldehyde solution, critical-point dried and coated with gold/palladium. Scanning electron microscopy (SEM) was performed to visualize osteoclastic bone resorption, and energy-dispersive X-ray spectroscopy (EDX) was carried out to analyze the elemental composition of the samples using a FEI/Philips XL30 ESEM FEG system.

3.10.3 Image analysis

Analysis of micrographs obtained during extended live imaging of VSMC was performed using ImageJ software (v. 1.53a) [168]. Quantification of calcified areas in HEK293 cells and co-localization analysis of signals generated by calcein and a fluorescent protein in MSC and iVSMC cultures were carried out using Fiji software (v. 2.1.0/1.53c) [169]. Particle tracking analysis in MSC was performed using the TrackMate plugin of the Fiji image processing package [170].

3.11 Histology

The hearts, livers, and kidneys of euthanized mice were harvested through a midline laparotomy and rinsed with PBS. Hearts were additionally perfused with ice-cold PBS to remove blood. The samples were then frozen in the Tissue-Tek™ O.C.T. compound (Sakura

Finetek, Torrance, USA, Cat. # 4583), and 5-µm cryosections were made. Tissue sections were placed on glass slides and circled with a paraffin pen. Sections were incubated with 1µM fluorescent protein solution (~50 µg/mL bFA-AF488, ~97 µg/mL bOPN-mRuby3, ~85 µg/mL pm-mFA-mEmerald or mFA-mRuby3) for 4 h at 37 °C and rinsed with PBS three times afterwards. Fluorescence images were recorded using a Leica DMI 6000 microscope. The fluorescent probe was removed by rinsing the slides in phosphate-buffered saline supplemented with 0.05% Tween 20™. Post-staining was carried out using Alizarin Red S (5% in water adjusted to pH 4.2 with HCl).

3.12 Statistics and illustrations

Statistical analysis was performed using GraphPad Prism 9. Protein toxicity was analyzed on triplicates using one-way ANOVA. Fluorescence of calcifying VSMC was analyzed on five replicates each using one-way ANOVA with Tukey correction for multiple comparisons. Osteoclast differentiation was assessed using the Mann-Whitney U test.

Figures 1, 2, 3, 5 were created with BioRender.com.

4. RESULTS

4.1 Production of recombinant proteins

Fetuin-A-based recombinant fusion proteins were expressed in transiently transfected ExpiCHO-S™ cells. Although each protein expression run was carried out following the same protocol, the final protein yield depended largely on the nature of the protein. Figure 6A demonstrates a light chartreuse appearance of the mFA-mEmerald-producing cell culture (left) and a saturated red color of the mFA-mRuby3-expressing cell culture (right) on day 8 post-transfection. Simultaneous brightfield (not shown) and fluorescence imaging (Figures 6B, C) of samples retrieved from the protein-expressing cultures revealed that on day 3 after transfection, 19% of cells transfected with the mFA-mEmerald-encoding plasmid (Figure 6B) and 31% of the cells into which the *mFA-mruby3* gene was introduced (Figure 6C), produced a fluorescent signal. Dot blotting of culture supernatant samples obtained starting from day 1 post-transfection shows a gradual increase in the signals derived from polyhistidine-tagged proteins mFA-mEmerald (Figure 6D, left) and mFA-mRuby3 (Figure 6D, right). Fusion fluorescent proteins purified by IMAC on day 8 were subjected to SDS-PAGE. Coomassie blue staining of the gel revealed bands at about 85 kDa corresponding to mFA-mEmerald (Figure 6E, left) and mFA-mRuby3 (Figure 6E, right). The apparent molecular weight of the proteins was higher than the theoretical (~64 kDa) calculated using the ExPASy ProtParam tool [171], indicating the presence of post-translational modifications.

Of the three fetuin-A-sRANKL fusion variants, only CY1_mFA-sRANKL could be expressed, as evidenced by western blot analysis of the samples taken on days 10-12 post-transfection (Figure 6F). Protein harvesting took place on day 12 post-transfection. The first expression attempt yielded an impure product, as indicated by multiple minor bands detected upon SDS-PAGE (Figure 6G, *), which was likely caused by a low amount of the target protein in the medium. To improve the product quality, I increased the culture volume from 25 ml to 100 ml and performed another expression run that resulted in a product with a higher content of the target fusion protein, distinguishable as a prominent band at about 40 kDa (Figure 6G, **). However, the product still contained a significant amount of impurities.

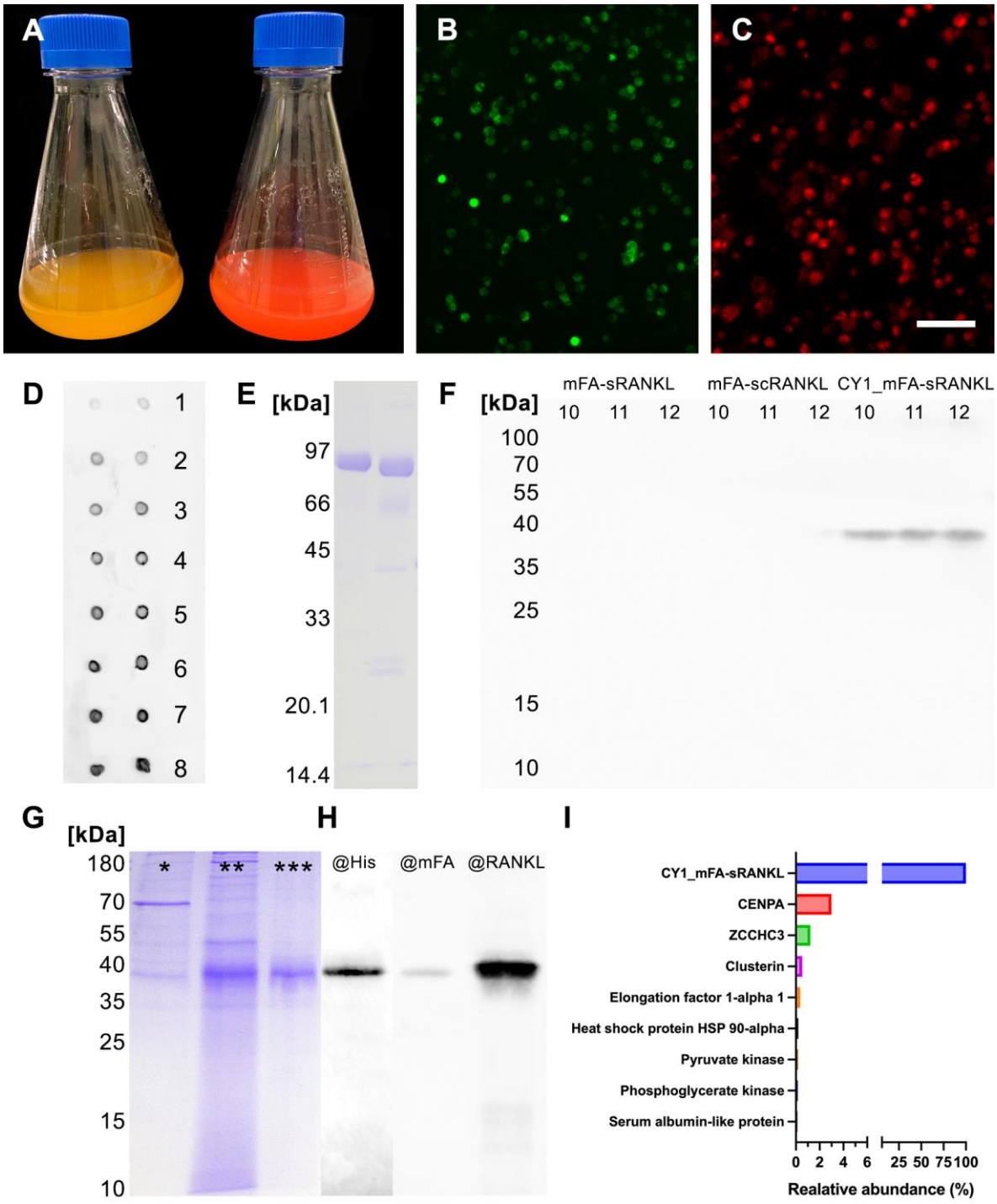

Figure 6. Expression of fetuin-A-based fusion proteins. **(A)** Erlenmeyer flasks with ExpiCHO-S cells expressing mFA-mEmerald (left) and mFA-mRuby3 (right). **(B, C)** Fluorescence imaging of cells expressing mFA-mEmerald (B) and mFA-mRuby3 (C). Scale bar 75 µm. **(D)** Dot blot analysis of mFA-mEmerald (left column) and mFA-mRuby3 (right column) expression. Numbers indicate days post-transfection. Fusion proteins were detected with a HisProbe™-HRP conjugate. **(E)** Coomassie blue-stained gel with protein bands corresponding to mFA-mEmerald (left lane) and mFA-mRuby3 (right lane) after IMAC. **(F)** Western blot analysis of samples from cultures transfected with plasmids encoding mFA-sRANKL, mFA-scRANKL, and CY1_mFA-sRANKL. Numbers in the second row indicate days post-transfection. **(G)** SDS-PAGE and western blot of the purified fusion protein CY1_mFA-sRANKL. **(I)** Mass-spectrometric analysis of the protein band shown in **G**.

To eliminate these impurities, I performed the third expression run that was terminated on day 8 post-transfection. This resulted in a single-band product (Figure 6G, ***) migrating at ~40 kDa, with a small divergence from the theoretical molecular weight of 34.2 kDa. Western blotting of the protein performed using the HisProbe™-HRP conjugate, polyclonal anti-mouse fetuin-A antiserum, and anti-RANKL antibody detected, in each case, the target protein of an expected molecular weight (Figure 6H). The rather weak signal revealed by anti-mFA antiserum can be explained by the absence of certain epitopes, as the CY1_mFA-sRANKL variant contained only a portion of the full-size mFA used to generate the antibodies. To further confirm the purity of the product, the protein band was cut out from the gel and subjected to MALDI-TOF mass spectrometry (Figure 6I).

The final protein yield was 4.5 mg mFA-mEmerald and 5 mg mFA-mRuby3 from 25-ml cultures and 0.66 mg CY1_mFA-sRANKL from a 100-ml culture, as measured spectrophotometrically at 280 nm. The modest yield of the CY1_mFA-sRANKL was predictable, for the physiological plasma concentrations of hormones and cytokines are many orders of magnitude lower than those of liver-derived serum proteins.

4.2 Precipitation inhibition assay

Fetuin-A was shown to effectively inhibit the growth of crystals, thus stabilizing nascent mineral and preventing its precipitation. To test whether the recombinant (chimeric) proteins remained functionally intact in terms of calcium phosphate binding, the calcification precipitation assay was employed. To this end, increasing amounts of proteins to be tested were added to a supersaturated calcium phosphate solution and calcium content in the supernatant, and the precipitate was analyzed in each case. Recombinant mFA bearing a C-terminal polyhistidine tag starts to inhibit calcium phosphate precipitation at ~10 µM (Figure 7A). To mimic the physiological post-translational phosphorylation of mFA, threonine and serine residues at positions 135, 138, 305, 309, 312, and 314 were replaced with glutamic acid, resulting in improved inhibition of calcium phosphate precipitation with an IC_{50} value of 0.5 µM (Figure 7B). Figures 7C and D demonstrate that both the chimeric protein mFA-mRuby3 and its phosphomimetic modification pm-mFA-mRuby3 were effectively inhibiting calcium phosphate precipitation with IC_{50} values of 1 µM and 0.7 µM, respectively. On the contrary, mFA-mEmerald failed to inhibit precipitation at concentrations up to 10 µM (Figure 7E), whereas its phosphomimetic counterpart pm-mFA-mEmerald appeared to have

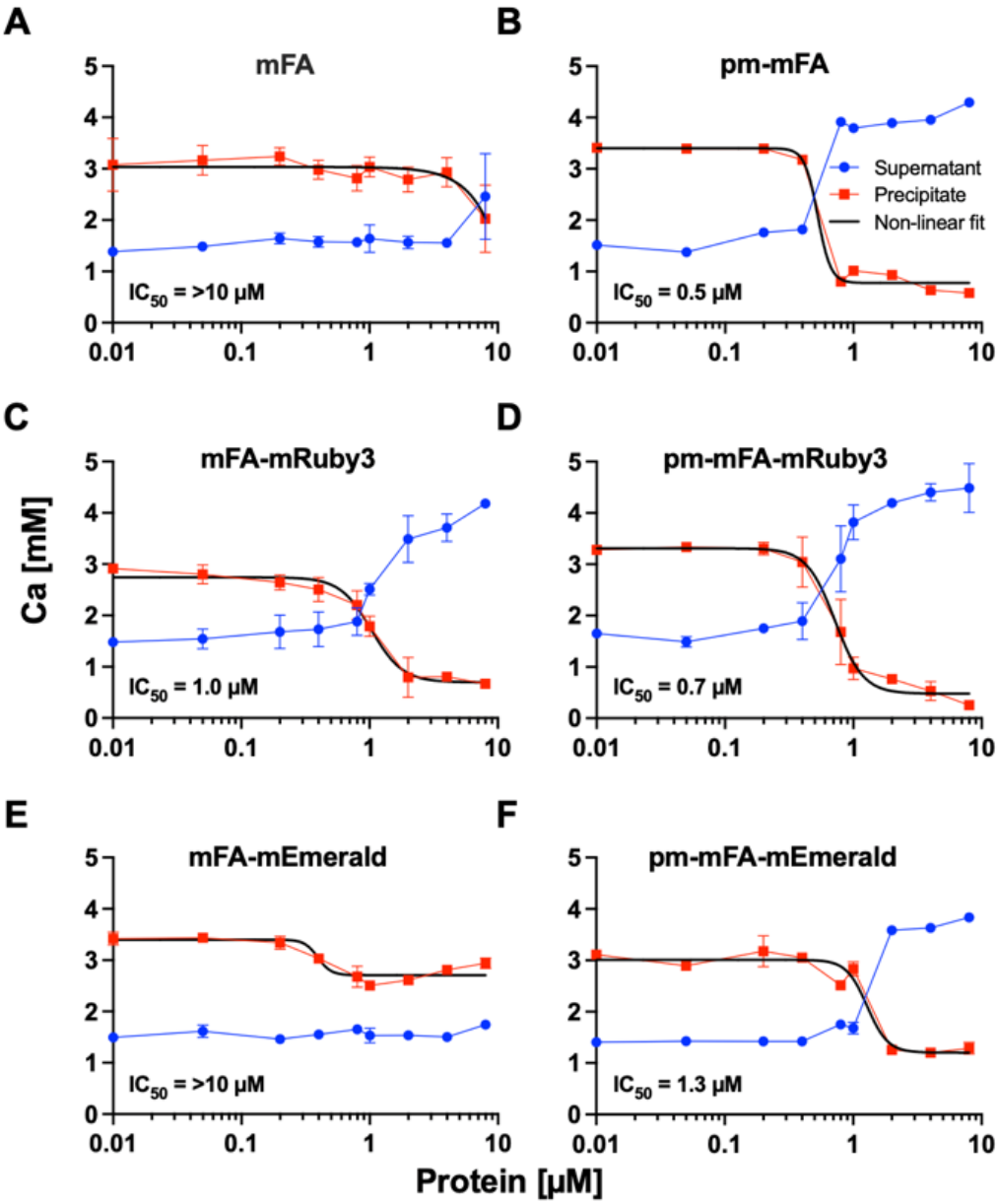

Figure 7. Calcium phosphate precipitation inhibition assay. Red squares show calcium in the precipitate, blue dots show calcium in the supernatant. **(A)** Recombinant mFA with a C-terminal polyhistidine tag did not affect calcium phosphate precipitation at concentrations below 10 µM. **(B)** Replacement of native phosphorylation sites with glutamic acid in pm-mFA increased the inhibitory potential of the protein to IC_{50} 0.5 µM. **(C)** Unmodified mFA-mRuby3 inhibited calcium phosphate precipitation with IC_{50} 1 µM. **(D)** Phosphomimetic substitutions decreased the IC_{50} value of pm-mFA-mRuby3 to 0.7 µM. **(E)** mFA-mEmerald was ineffective in inhibiting calcium phosphate precipitation. **(F)** pm-mFA-mEmerald had a strong inhibitory action on calcium phosphate precipitation with IC_{50} 1.3 µM. Individual data points represent mean ± SD.

an enhanced inhibiting capacity with an IC_{50} value of 1.3 µM (Figure 7F). Taken together, these results indicate that the phosphorylation of murine fetuin-A regulates mineral binding.

4.3 Assessment of toxicity

As fluorescent fetuin-A-based fusion proteins were envisioned as probes to visualize calcification in living cells, checking their toxicity was an important step for the method validation.

With a physiological plasma concentration of about 0.6 mg/ml, fetuin-A is one of the major serum proteins and, therefore, nontoxic. Less is known about the toxicity of fluorescent proteins. Although various fluorescent proteins originate from the endogenous proteins of aquatic invertebrates, they are not native to mammals, which does not allow direct conclusions regarding their non-toxicity for the cell cultures in question.

Figure 8 demonstrates the results of the MSC viability assessment performed 72 h post-incubation with chemically or genetically labeled fluorescent probes. No significant differences were observed between the control and experimental groups, indicating the absence of toxicity in each case. Furthermore, large amounts of recombinant mFA-based fluorescent fusion proteins were expressed in CHO cells, indirectly confirming the non-toxicity of the genetically labeled probes.

CY1_mFA-sRANKL was excluded from the toxicity assessment, as the intended working concentrations of the novel cytokine were within the nanomolar range, and it was unlikely that the protein would exhibit toxicity.

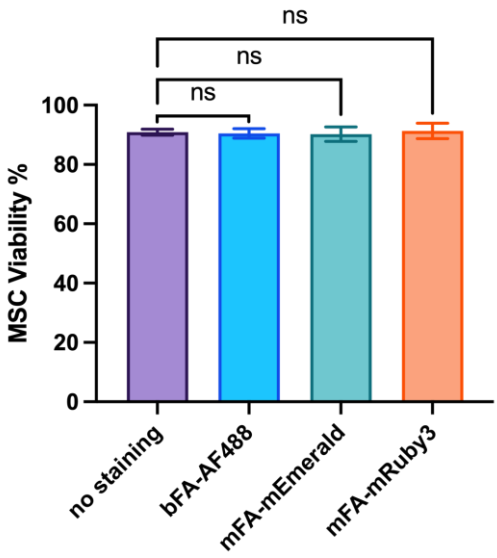

Figure 8. Toxicity assessment of fetuin-A-based fluorescent proteins. MSC viability was evaluated by Trypan Blue exclusion assay 72 h after a 2-hour incubation with the indicated fluorescent probes. Experiments were carried out in triplicates, with a minimum of 400 cells counted in each case. Values represent mean ± SE, n=3.

Detection of calcification

4.4 Identification of candidate probes for calcification imaging

Several candidate molecules were tested for their ability to detect calcium deposits in living cells and body tissues. Along with proteins with known mineral-binding function such as bovine fetuin-A (bFA) and osteopontin (bOPN), as well as the milk fat globule membrane protein (MFGM) and serum albumin (BSA) were studied. HASMC66 cells cultured in CM (Table 2) represented a model of vascular calcification, and myocardial sections from DBA/2 fetuin-A-knockout mice served as a model of heart calcification. Of the substances studied, only chemically labeled bovine fetuin-A and osteopontin were found effective in detecting calcifications both in cell cultures (Figure 9, panel A) and heart tissue (Figure 9, panel B). Differential interference contrast (DIC) microscopy confirmed myocardial calcified lesions (Figure 9, panel C). Staining with fluorescent MFGM-AF488 resulted in dim fluorescence, which, however, was insufficient to delineate areas of calcification (Figure 9, panels A and B). Similarly, no specific fluorescence was detected in calcified cells and tissue sections stained with fluorescent BSA-AF488. Given the imaging results, only chemically or genetically labeled fetuin-A and OPN along with established histological calcification stains agents were used in subsequent experiments.

4.5 Live imaging of cell-mediated mineralization

Osteogenic differentiation of human MSC (Section 3.8) was selected as a model of physiological bone mineralization. Alizarin Red S staining of MSC cultured in OM (Table 2) for two weeks revealed significant matrix mineralization (Figure 10A), whereas MSC cultured in basal DMEM remained alizarin-negative (Figure 10B). MSC-derived osteoblasts were stained with either bFA-AF488 or one of the fetuin-A-based fusion fluorescent probes pm-mFA-mEmerald or mFA-mRuby3 and imaged using high-resolution confocal laser scanning microscopy. In each case, osteoblastic mineralization was observed as sub-micrometer-sized cell contour-associated mineralization foci (Figures 10C, E, G). The high specificity of fetuin-A-based fluorescent probes was verified by the absence of fetuin-A-derived signal in non-mineralizing MSC cultured in basal medium (Figures 10D, F, H). The observed features of MSC mineralization were further confirmed using the fusion fluorescent

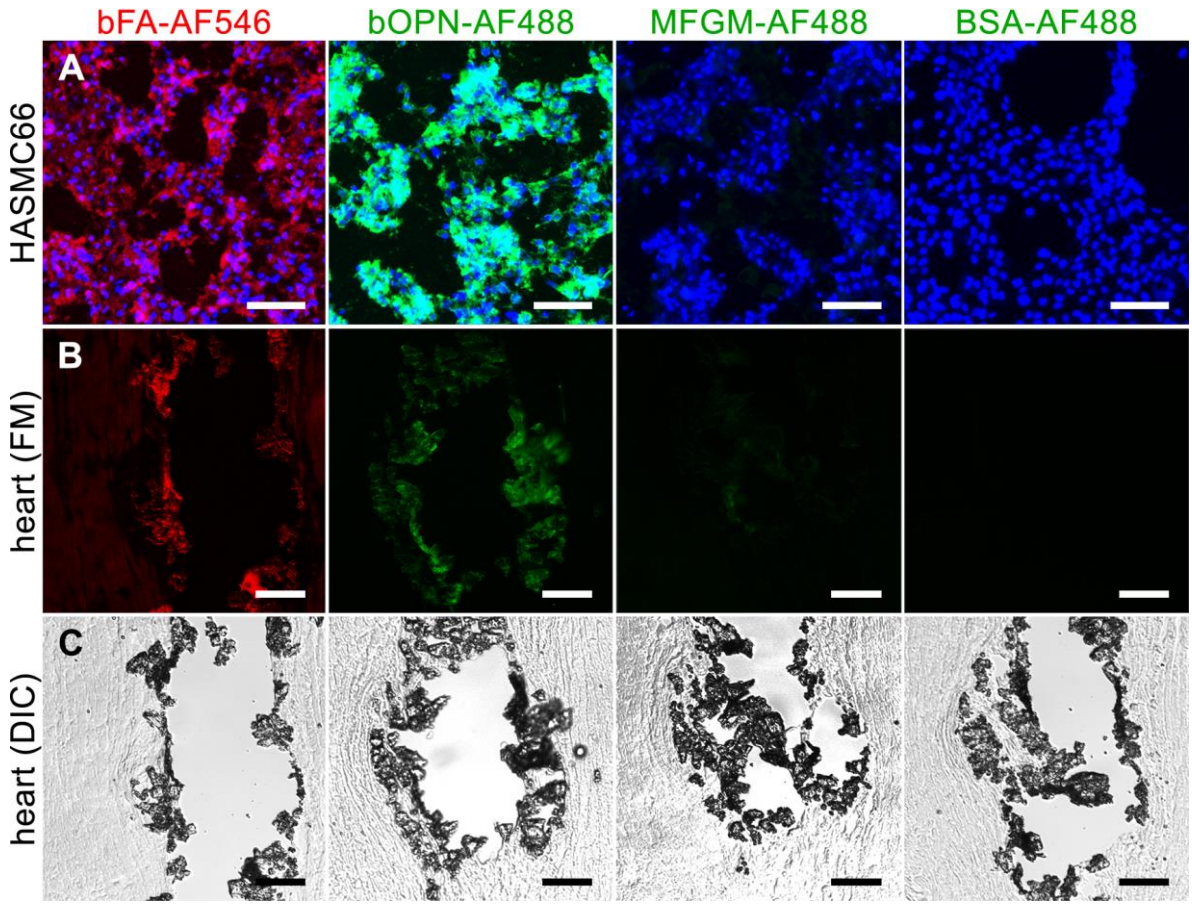

Figure 9. Detection of calcification in cell culture and myocardium. **(Panel A)** Fluorescence microscopy of calcifying HASMC66 cultures. Large coalescing calcification foci can be identified with bFA-AF546 and bOPN-AF488 but not with MFGM-AF488 or BSA-AF488. Cell nuclei were counterstained using Hoechst 33342. **(Panel B)** Fluorescence microscopy of myocardium retrieved from a fetuin-A-knockout mouse. Tissue staining with bFA-AF546 or bOPN-AF488 enables the detection of calcified lesions, whereas the application of Alexa Fluor®- 488-labeled MFGM or bovine serum albumin does not. **(Panel C)** DIC microscopy of calcified lesions shown in panel **B**. Intact tissue is light gray, while calcified lesions appear dark gray to black. Scale bars 100 µm.

protein bOPN-mRuby3 (Figure 11A, white arrowheads). Similar to fetuin-A-based probes, bOPN-mRuby3 produced no unspecific signal as showed by the absence of fluorescence in undifferentiated MSC (Figure 11B).

4.5 Live imaging of cell-mediated calcification

The vasculature is commonly affected by ectopic calcification. To investigate the potential of the designed fluorescent probes to detect pathological mineral deposits, calcified iVSMC (Section 3.8) representing a model of vascular calcification were subjected to live staining and imaging. Alizarin Red S staining of iVSMC maintained in CM showed irregular

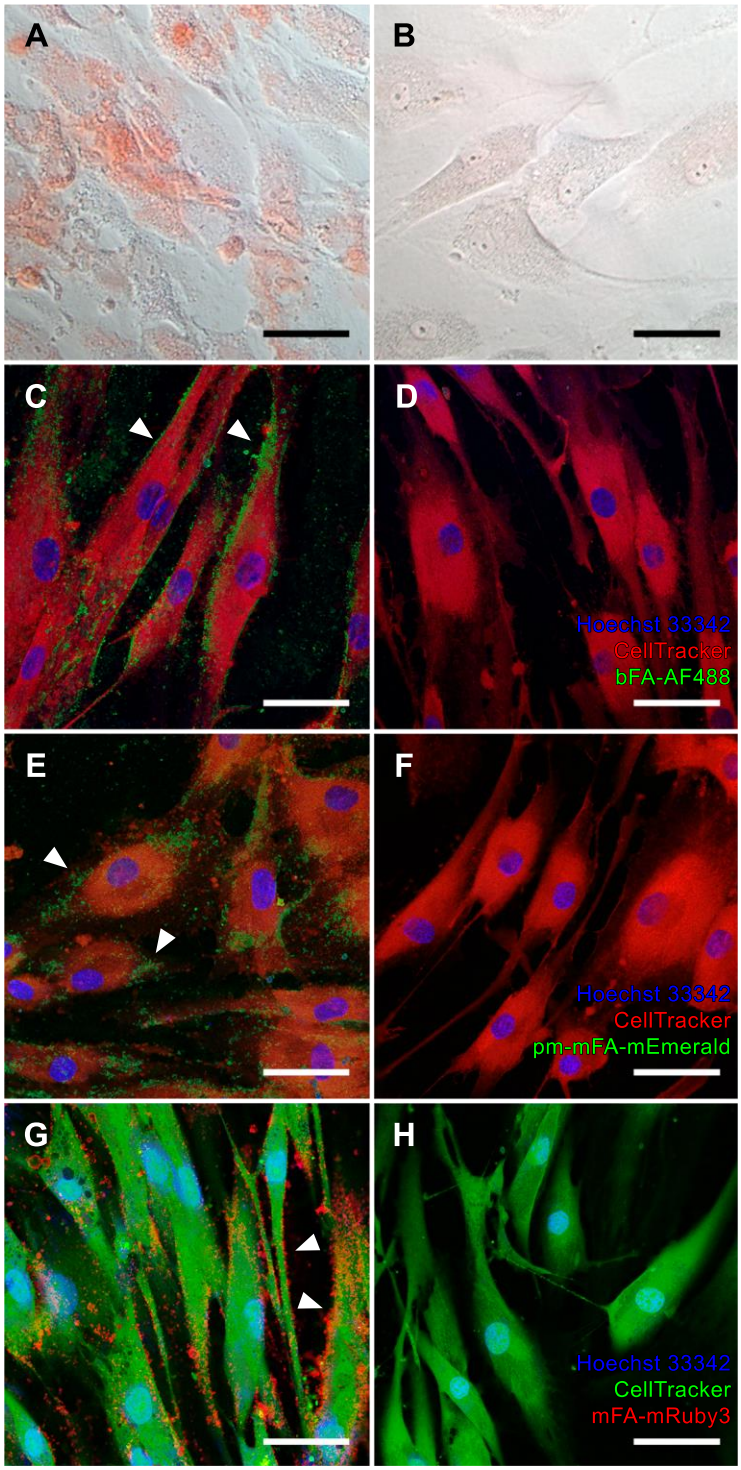

Figure 10. Mineralization of MSC. **(A, B)** Brightfield microscopy, Alizarin Red S staining. **(C-H)** Confocal laser scanning microscopy of MSC stained with bFA-AF488 **(C, D, green)**, pm-mFA-mEmerald **(E, F, green)** or mFA-mRuby3 **(G, H, red)**. **(A, C, E, G)** MSC maintained in OM. **(B, D, F, H)** MSC cultured in basal medium. MSC maintained in OM develop sub-micrometer mineralization outlining cell contours (white arrowheads), whereas cells cultured in basal medium show no signs of mineralization as indicated by staining with fluorescent fetuin-A probes. Cytoplasms were stained with CellTracker™ CM-DiI **(C-F, red)** or CellTracker™ CMFDA **(G-H, green)**, and cell nuclei were counterstained with Hoechst 33342. Scale bars 50 µm.

patches of calcification (Figure 12A), and iVSMC cultured in basal medium lacked staining (Figure 12B). Similar to Alizarin Red staining, live fluorescence staining of calcifying iVSMC using bFA-AF488 (Figure 12C), pm-mFA-mEmerald (Figure 12E) or mFA-mRuby3 (Figure 12G) revealed areas of dystrophic calcification.

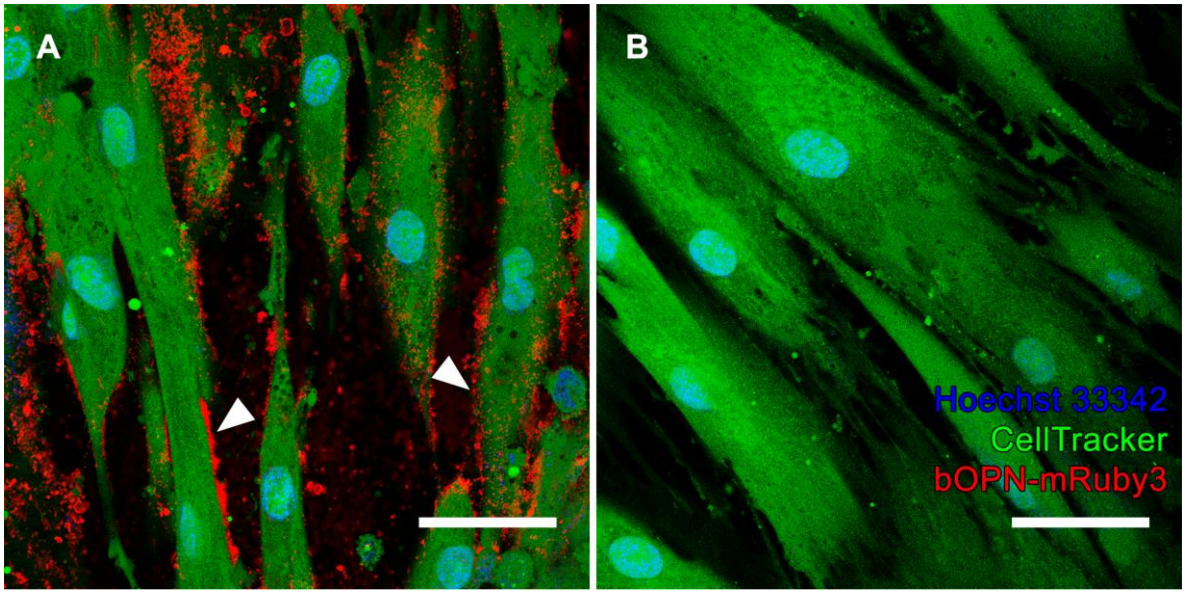

Figure 11. Detection of MSC mineralization using bOPN-mRuby3. **(A)** The fluorescent protein stains membranes of MSC-derived osteoblasts (white arrowheads). **(B)** No bOPN-mRuby3-derived signal is observed in MSC cultured in basal medium. Scale bars 50 µm.

Unlike physiological mineralization of MSC demarcating cell membranes (Figures 10C, E, G, white arrowheads), mineral deposition was also observed in zones free of viable cells (Figures 12C, E, G, white arrowheads), indicating calcification of cell debris. The high selectivity of mineral staining was confirmed by the absence of calcification-related fluorescence in iVSMC kept in basal medium (Figures 12D, F, H).

4.6 Co-localization analysis

Application of fetuin-A-based fluorescent probes revealed clear differences in staining patterns of mineralizing MSC and calcifying iVSMC. To test whether the observed distinctive features can be detected using an established staining method, MSC-derived osteoblasts and iVSMC cultured in CM were simultaneously stained with commercially available fluorescein derivative calcein and mFA-mRuby3. Co-localization analysis of

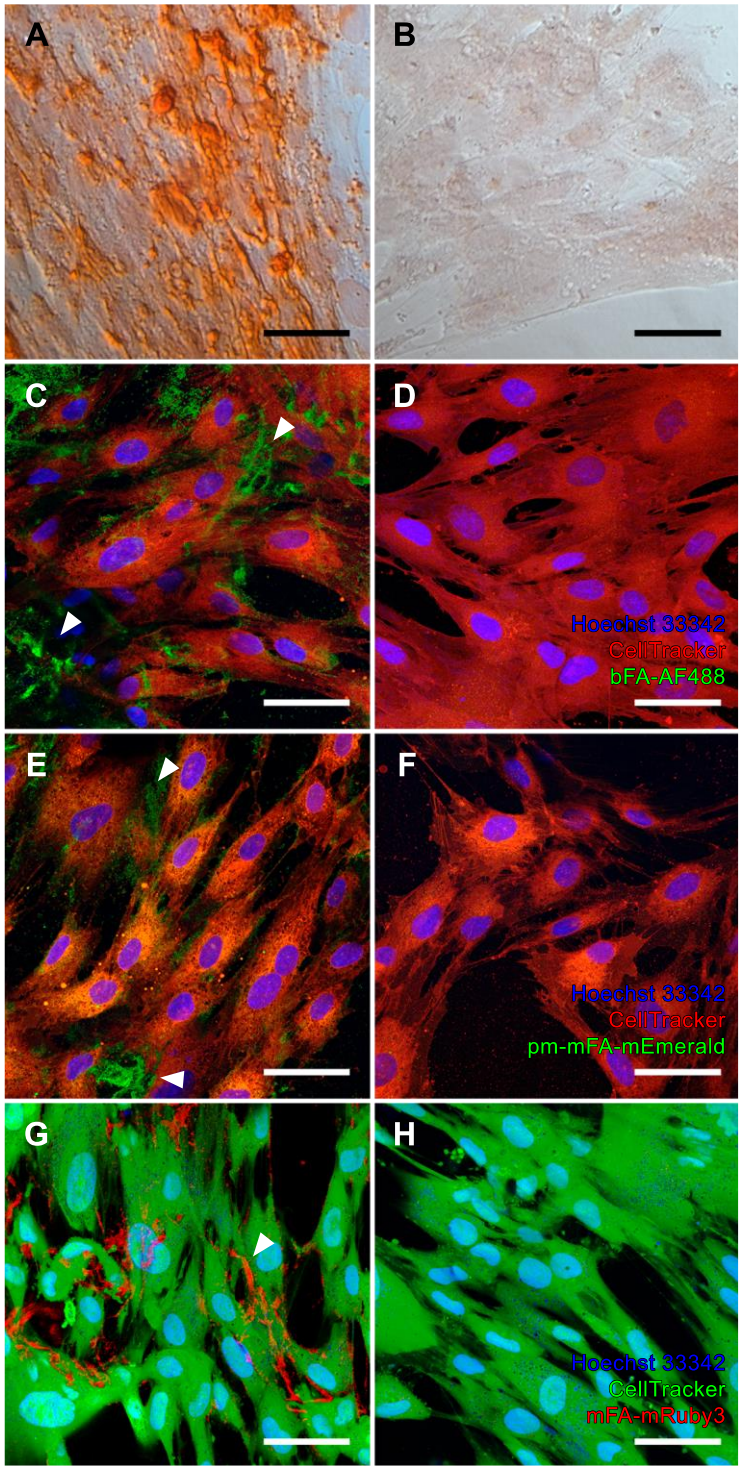

Figure 12. Calcification of iVSMC. **(A, B)** Brightfield microscopy, Alizarin Red S staining. **(C-H)** Confocal laser scanning microscopy of cells stained with bFA-AF488 **(C, D, green)**, pm-mFA-mEmerald **(E, F, green)** or mFA-mRuby3 **(G, H, red)**. **(A, C, E, G)** Calcifying iVSMC. **(B, D, F, H)** iVSMC cultured in basal medium. Multiple patchy areas of enhanced fetuin-A-derived signal reflecting the irregular pattern of dystrophic calcification (white arrowheads) were detected in iVSMC maintained in CM. No fetuin-A-derived fluorescence was observed in cells cultured in basal medium. Cytoplasms were stained with CellTracker™ CM-DiI **(C-F, red)** or CellTracker™ CMFDA **(G-H, green)**, and cell nuclei were contrasted with Hoechst 33342. Scale bars 50 µm.

fluorescent signals performed using the Pearson correlation coefficient revealed a partial overlap in mineralized MSC (Figure 13A, r = 0.42) and a strong correlation in calcifying iVSMC (Figure 13B, r = 0.9). This finding indicates that fetuin-A-based fluorescent proteins are more sensitive probes than the conventionally used calcein, which failed to detect fine features of matrix mineralization in MSC.

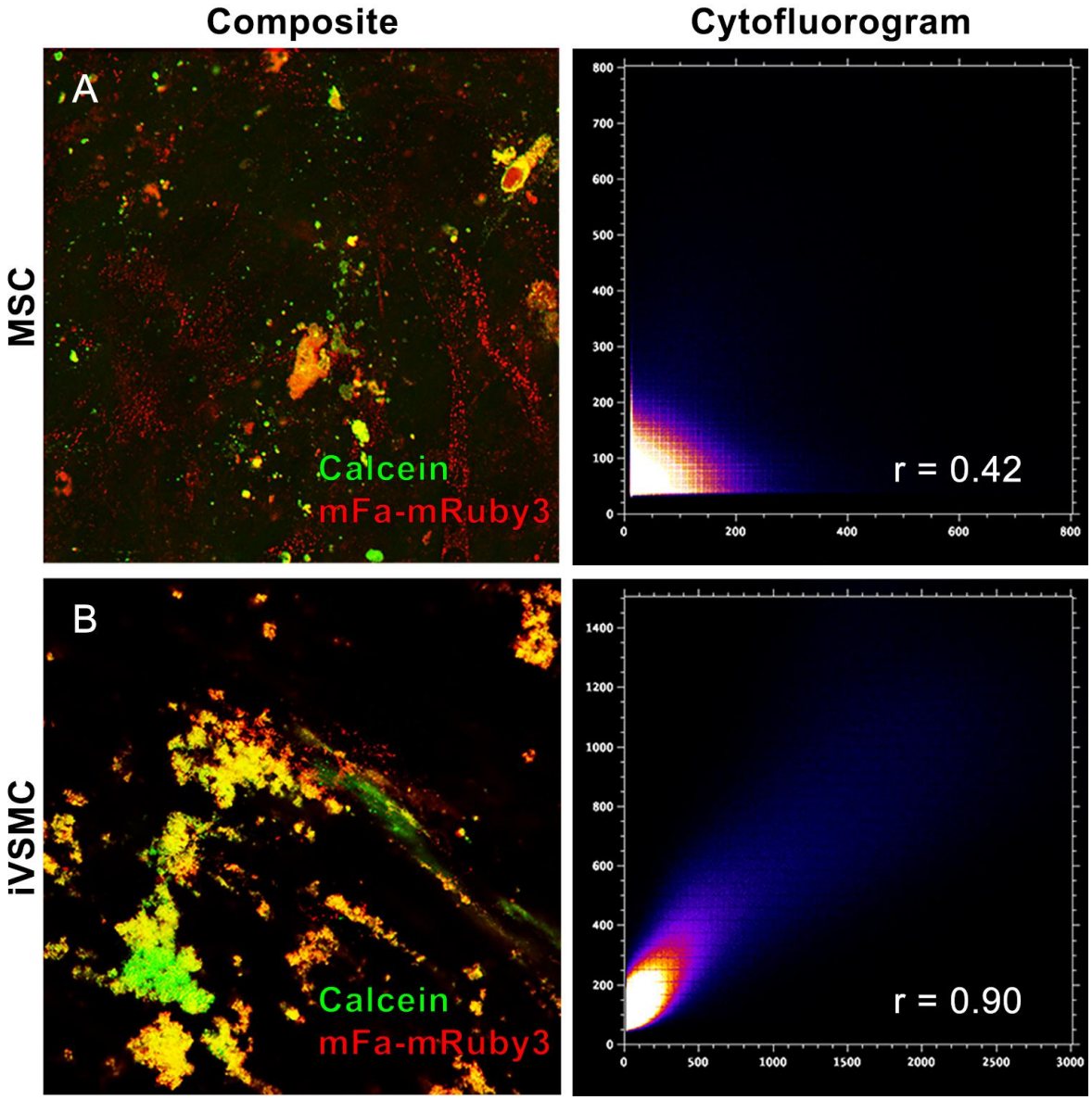

Figure 13. Co-localization analysis of calcein- and mFA-mRuby3-derived signals. **(A)** Composite image of mineralizing MSC and a corresponding scatter plot indicating a partial overlap between channels. **(B)** Composite image of calcifying iVSMC and a corresponding scatter plot demonstrating a strong overlap between channels. The intensity of pixel fluorescence increase is shown using a heatmap. r-value: the Pearson correlation coefficient.

4.7 Continuous live imaging of calcification

As fetuin-A-based probes were shown to be non-toxic and effective in detecting mineralized matter in cell cultures down to the micrometer scale, I asked whether they can be used to study temporal development of calcification in cell culture. To this end, VSMC were maintained in S-DCM (Table 2) supplemented with 0.24 µM mFA-mRuby3, and image acquisition was performed on days 1, 3, and 7. Culture medium was specifically formulated to stunt cell proliferation and promote calcification. Fluorescence imaging showed a constant increase in the number of cells stained with mFA-mRuby3, indicating the progression of calcification (Figure 14A). This observation was in line with a quantitative assessment of fluorescence signal normalized to the number of cells (Figure 14B). Measurements were performed in five fields of view on each day.

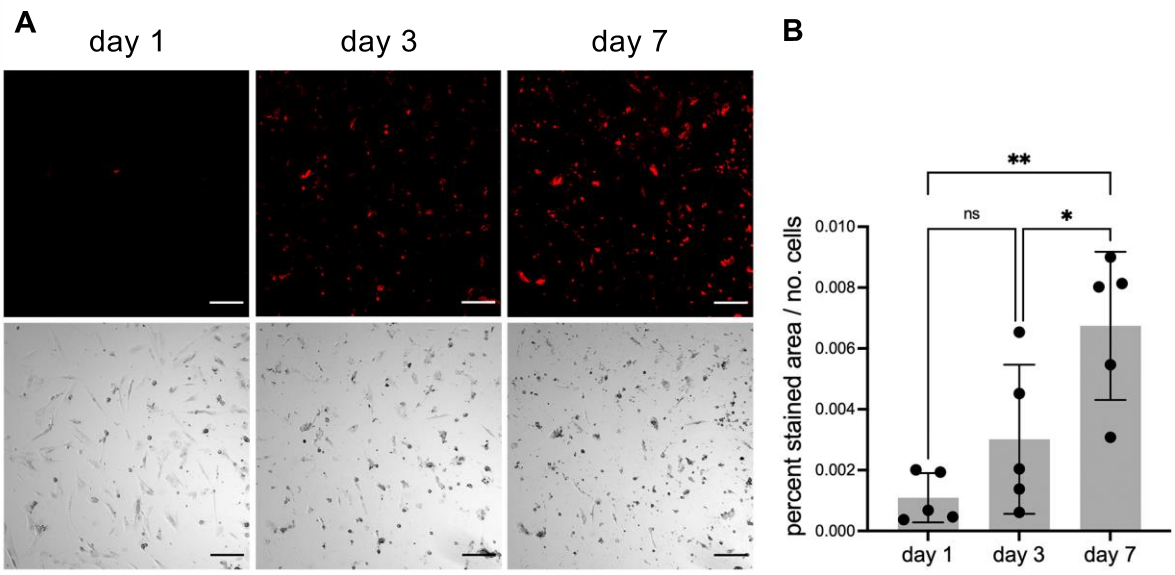

Figure 14. Continuous live imaging of calcifying VSMC. Cells were maintained in S-DCM containing 20 µg/mL mFA-mRuby3. **(A)** Fluorescence (upper panel) and brightfield micrographs (lower panel) of calcifying cells. Scale bars 200 µm. **(B)** Quantification of fluorescent signal in calcifying VSMC culture. Data represent the ratio of fluorescence area (%) to the number of cells (ns, not significant; * – P value <0.05, ** – P value < 0.01). Mean ± SD, n = 5.

4.8 Cell-based system for calcification screening

Routine methods for detecting calcifications in cell cultures or tissue samples rely on the use of dyes that are either extracted from natural sources or produced by means of chemical synthesis. In contrast, fetuin-A-based fusion proteins mFA-mEmerald and mFA-

mRuby3 (along with their phosphomimetic variants) are inherently fluorescent, i.e., once secreted by a cell, they require no further processing to become functionally active. To test whether the fusion fluorescent protein can be employed to generate calcification-reporting cell culture, HEK293 cells were transiently transfected with a plasmid encoding mFA-mRuby3 and maintained in KCM (Table 2). No specific signal could be detected in untransfected calcifying cells stained for 24 h using supernatant from transfected cells collected on day 3 (Figure 15A), and protein-expressing cells cultured in basal medium were visible as bright red spots on day 3 post-transfection (Figure 15B, white arrowheads). Culture supernatant of mFA-mRuby3-expressing cells contained sufficient fluorescent protein to stain untransfected calcifying cells upon 24-h incubation (Figure 15C). Figure 15D shows transfected cells cultured under procalcifying conditions. In addition to mFA-mRuby3-expressing cells (white arrowheads), multiple coalescing areas of the fluorescent signal representing calcified lesions were detectable (white arrows). To quantify fluorescent imaging, micrographs shown in Figures 15B, D were subjected to grayscale conversion, and particle analysis was performed to measure fluorescent areas (Figures 15E, F). The total area of fluorescence increased from 2.5% in non-calcifying cells to 20.3% in cells cultured in calcification medium, and the number of fluorescent areas representing protein-expressing cells or coalesced calcified lesions increased from 151 to 377, respectively (Figure 15G). Furthermore, maintaining cells under procalcifying conditions increased the average size of the fluorescent areas from 78 μm^2 to 142 μm^2, respectively. Collectively, these findings indicate that endogenous expression of mFA-mRuby3 in calcifying HEK293 cells enabled the detection of calcification in real time with high specificity and sensitivity. Thus, fetuin-A-based fusion fluorescent proteins can be used to generate calcification-reporting cell lines for ex vivo continuous screening of calcification.

4.9 Intracellular particle tracking analysis

Application of the novel fusion fluorescent proteins pm-mFA-mEmerald and mFA-mRuby3 for imaging mineralization and calcification in living cells revealed very little to no protein-derived fluorescent signal in cells cultured in basal medium, confirming high specificity and sensitivity of the probes. However, immediately after staining, isolated spots of fluorescence, resolvable at the highest magnification of the confocal microscope, were

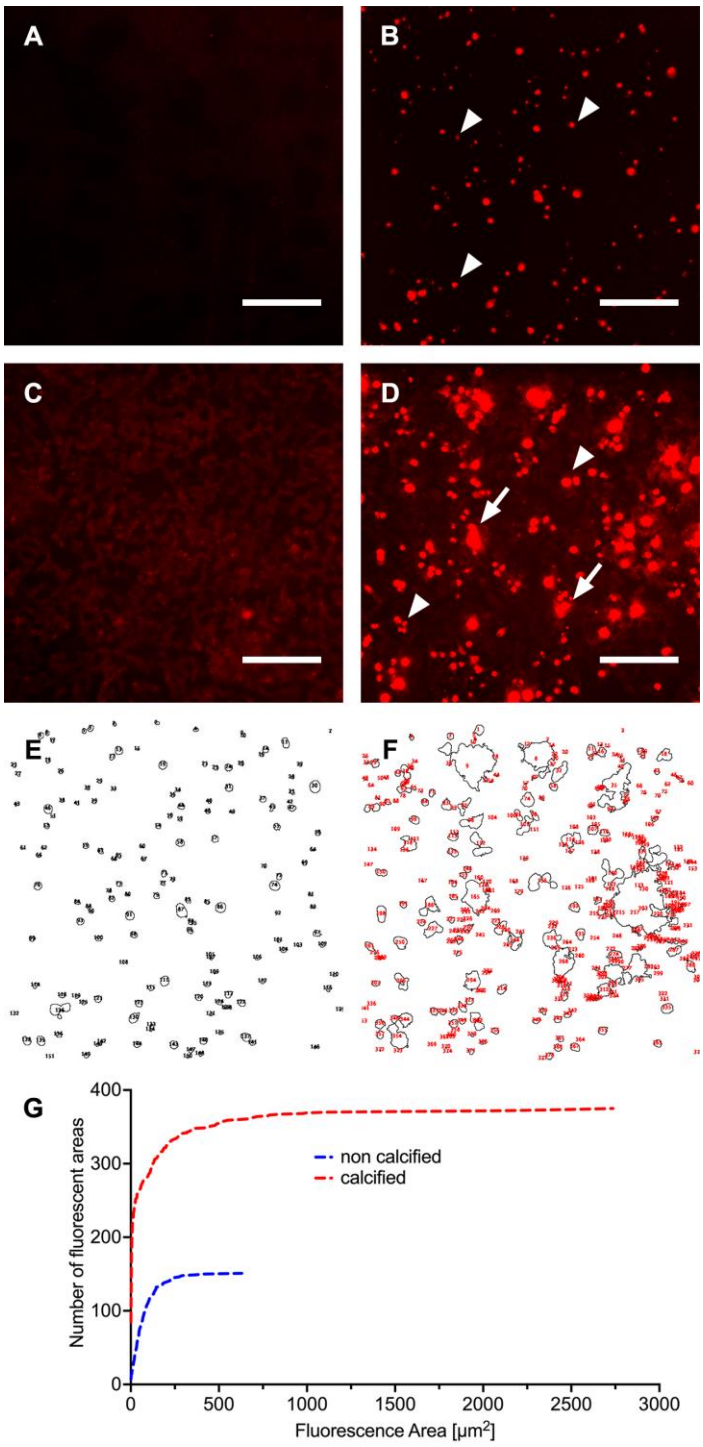

Figure 15. Calcification-reporting cell culture. **(A)** Absence of fluorescence in untransfected HEK293 cells cultured in DMEM and post-stained for 1 day using culture supernatant from mFA-mRuby3-expressing cells. **(B)** mFA-mRuby3-expressing HEK293 cells cultured in basal DMEM present as bright red dots (arrowheads) on day 3 post-transfection. **(C)** Untransfected HEK293 cells cultured in calcification medium show dim fluorescence after post-staining with culture supernatant from mFA-mRuby3-transfected cells. **(D)** Calcifying HEK293 cells transfected with mFA-mRuby3-encoding plasmid are visible as bright red dots (arrowheads) on day 3 post-transfection. Large coalescing fluorescent areas indicate calcified cells (arrows). **(E, F)** Particle analysis of micrographs shown in **B, D**. **(G)** Accumulate frequency distribution of fluorescent areas identified in micrographs shown in **B, D**. Scale bars 150 µm.

detectable inside the cells. These intracellular signals were temporary and quickly faded in contrast to the extracellular fluorescence highlighting mineralized matrix or calcified cells. To identify the source of the intracellular signal, MSC cultured in basal medium were stained with mFA-mRuby3 as described (Section 3.10.1) and subjected to spinning disc time-lapse

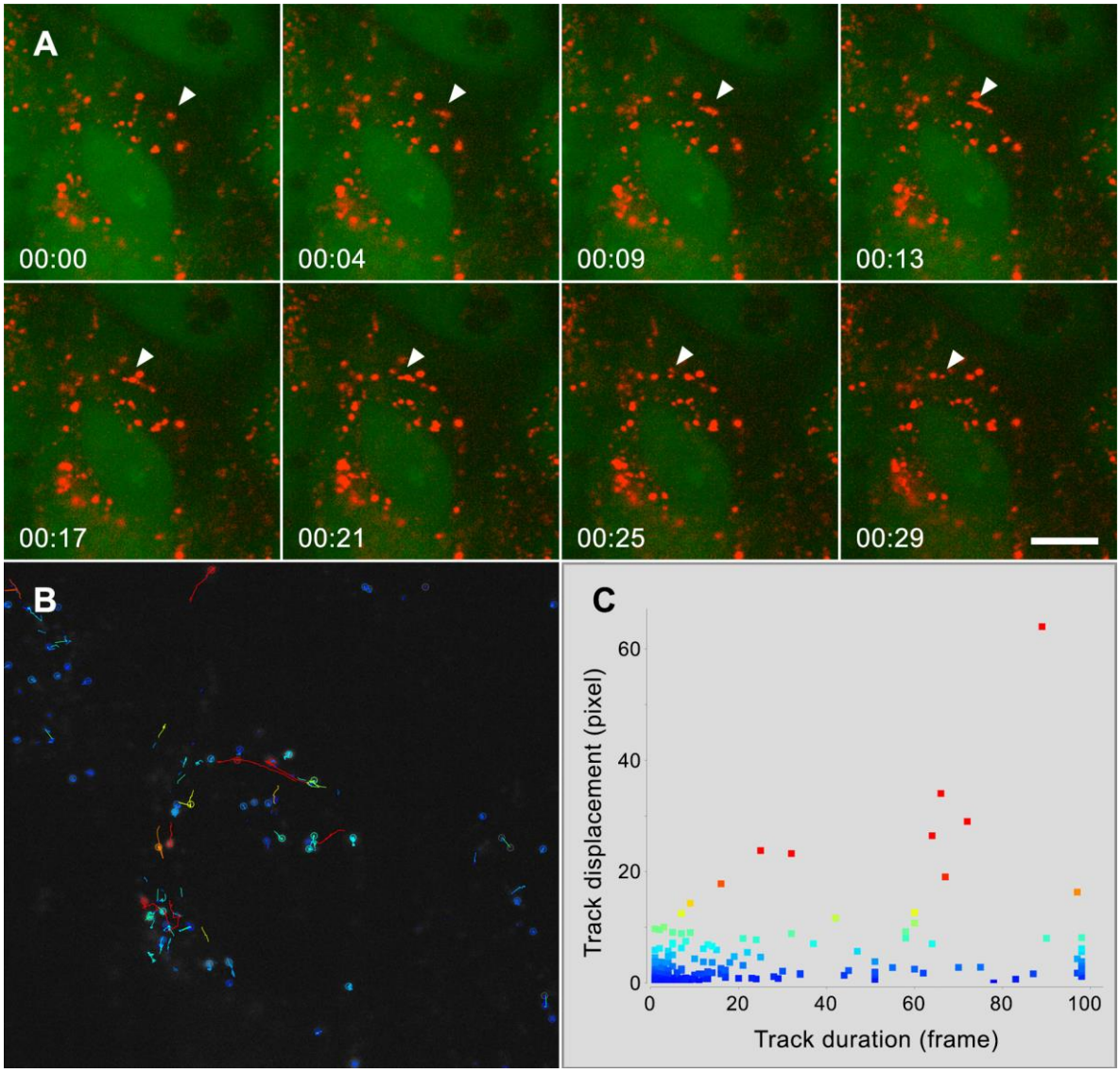

Figure 16. Visualization and movement analysis of intracellular vesicles. **(A)** Spinning disc confocal microscopy. Multiple mFA-mRuby3-laden vesicles (red) are observed in a perinuclear zone of MSC counterstained with CellTracker™ CMFDA (green). White arrowheads indicate the position of an individual vesicle in the course of imaging. Timestamp format mm:ss. Scale bar 10 µm. **(B)** Single-particle tracking in the time-lapse shown in panel A using the TrackMate plugin. Individual tracks are color coded on a rainbow scale, with blue indicating the shortest and red the longest tracks. **(C)** Particle tracking analysis shows the distribution of vesicles by track displacement over time, revealing a larger fraction of slow-moving vesicles (blue, cyan) and a smaller fraction of fast-moving vesicles (orange, red).

microscopy, which revealed that the observed bright dots represented fluorescent fetuin-loaded vesicles involved in intracellular transport (Figure 16A). Visualization of individual particle tracks color coded by track lengths (Figure 16B) showed that a significant fraction of the particles was mobile, with a maximum track displacement of approximately 10 μm (Figure 16C). This observation indicated that a certain amount of fluorescent protein was endocytosed by live unfixed cells. However, the transient signal generated by the endocytosed probe was much weaker than the ECM-associated signal and did not distort the imaging results shown in Figures 10 and 12. The rapid fading of the intracellular fluorescence was apparently due to enzymatic degradation of the protein probe. In contrast, the ECM-associated extracellular mFA-mRuby3-derived fluorescence persisted for at least one week after the live staining of mineralized/calcified cells.

4.10 Histology

Having confirmed that fetuin-A-based fusion fluorescent proteins can be used for live detection of mineralization and calcification in cell cultures, I asked if the same probes stain calcified lesions in tissue sections. Freshly harvested hearts, livers, and kidneys of DBA/2 fetuin-A-knockout mice were embedded in the Tissue-Tek™ O.C.T. compound, and 5-μm cryosections were made. Tissue sections were then placed on glass slides and stained using one of the fluorescent fetuin-A probes. Fluorescence microscopy revealed that both chemically and genetically labeled fluorescent fetuin-A proteins effectively detected microcalcifications in the myocardium (Figure 17, panel A), liver (Figure 17, panel B), and kidney (Figure 17, panel C). Moreover, fetuin-A-based probes detected more calcified lesions (Figure 17C, white arrowheads) than traditional staining with Alizarin Red S (Figure 17D, black arrowheads), as indicated by confirmatory staining of kidney sections shown in Figure 17C (Figure 17, panel D). The application of a fetuin-A-based probe enabled the identification of calcified matter in the renal tubules (Figure 17C, boxed area) consistent with intraluminal nephrocalcinosis, whereas upon staining with Alizarin Red S, these tubules appeared completely intact (Figure 17D, boxed area). Likewise, simultaneous staining of renal calcifications with mFA-mRuby3 and calcein showed the inability of the latter to detect smaller lesions, while mature calcifications were clearly distinguishable (Figure 18). These findings agreed with the previous observations that Alizarin Red S and calcein had not been sufficiently sensitive toward incipient calcified lesions.

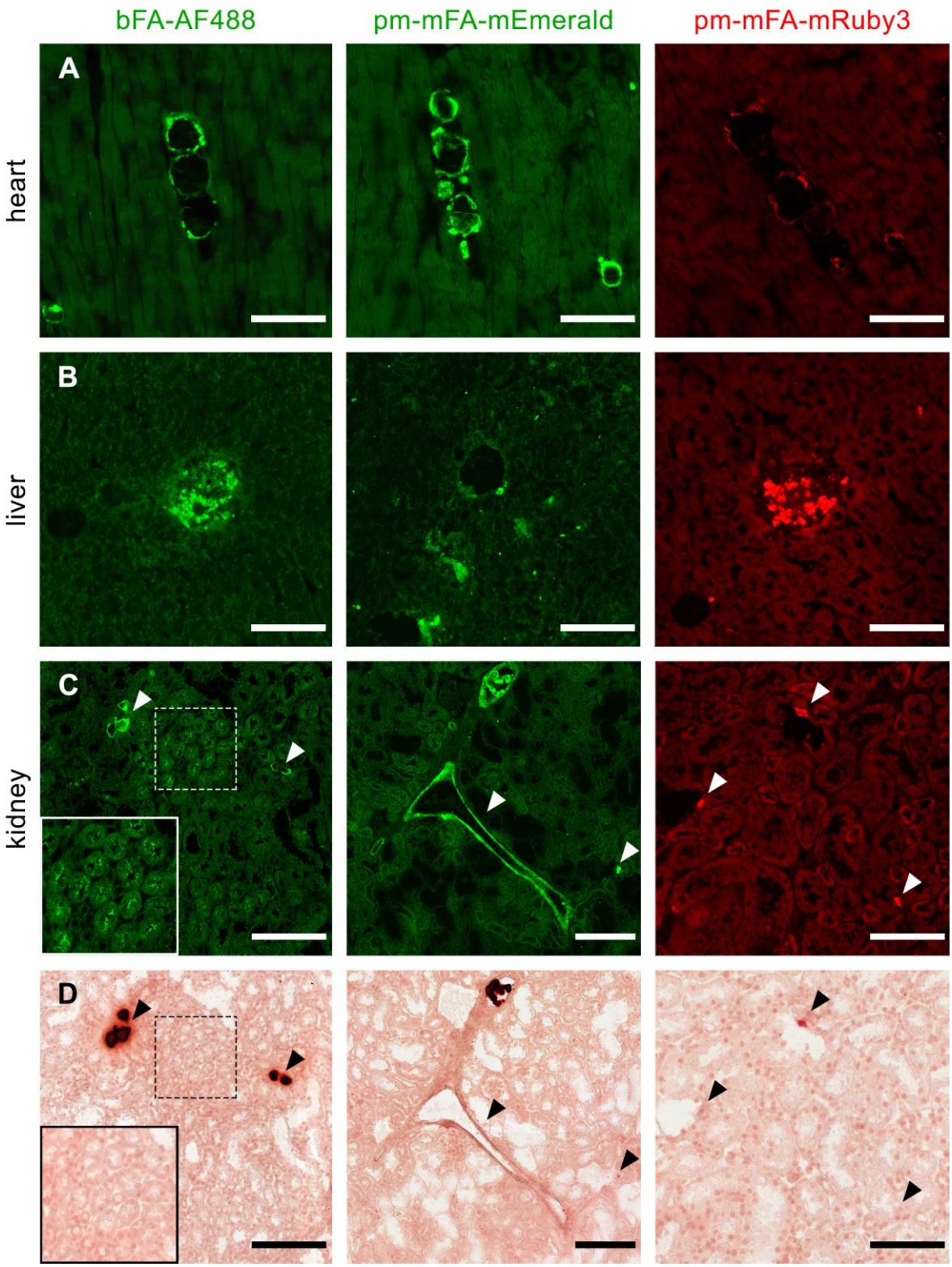

Figure 17. Detection of calcifications in tissue sections. **(A-B)** Small calcified lesions in the myocardium and liver. **(C)** Large and small renal calcifications (white arrowheads) stained with bFA-AF488, pm-mFA-mEmerald, and mRuby3, and an area of tubular calcification (white box) stained with bFA-AF488. **(D)** Post-staining of the sections shown in panel **C** (Alizarin Red S). Black arrowheads copy the positions of white arrowheads in panel **C**. Scale bars 200 µm (left and central images in panels **C, D**), 100 µm (panel **A,** right images in panels **C, D**), and 70 µm (images in panel **B**).

Staining of the myocardium with hydroxyapatite-binding protein bovine osteopontin coupled to mRuby3 (bOPN-mRuby3) also revealed areas of calcification similar to those detected using the fetuin-A probes (Figure 19).

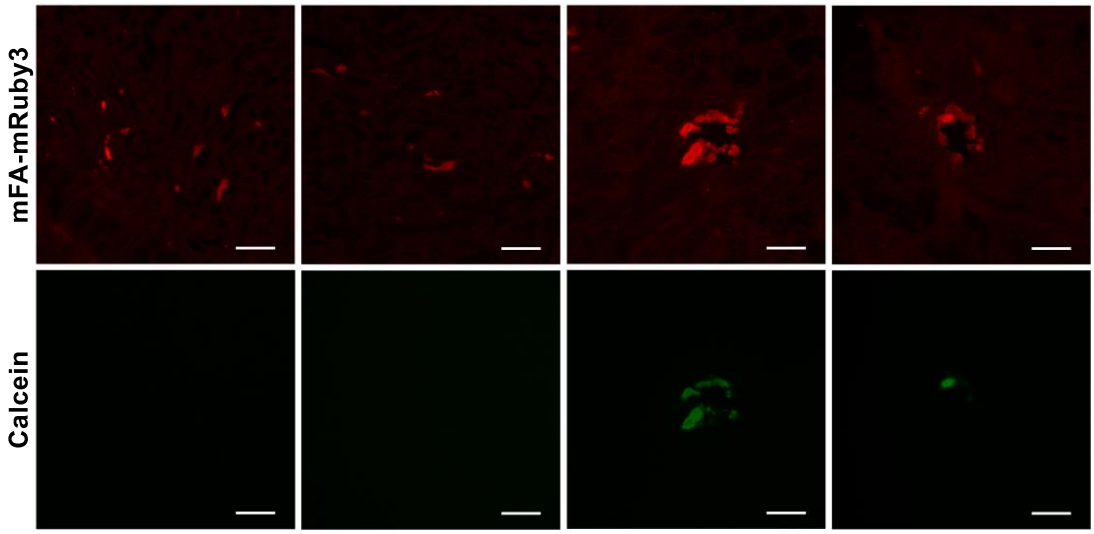

Figure 18. Simultaneous staining of kidney calcifications with mFA-mRuby3 and calcein. **(Upper panel)** mFA-mRuby3 (red) enabled the detection of small and large calcified lesions. **(Lower panel)** Calcein (green) stained larger mineral deposits but failed to detect microcalcifications. Scale bars 100 µm.

4.11 Application of radiolabeled fetuin-A for intravital imaging

Fetuin-A-knockout mice on a DBA/2 genetic background represent a robust model of ectopic calcification, as they develop spontaneous soft-tissue calcifications as seen on a CT scan (Figure 20A, upper image). The presence of at least one functional fetuin-A allele, on the other hand, completely corrects the calcification phenotype, which is demonstrated by the lack of extraosseous calcification in heterozygous animals (Figure 20A, lower image). In order to perform intravital detection of ectopic mineral deposits using radiolabeled fetuin-A, a mouse was placed under anesthesia and injected with ^{99m}Tc-labeled recombinant mFA via the tail vein. Two hours after injection, the anesthetized animal was placed in a SPECT imager and the scan was performed with correction for the total acquisition time. Maximum signal intensity was observed in the livers and bladders of both animals, indicating active hepatic uptake and renal clearance of the tracer (Figure 20B). Furthermore, radioactive mFA accumulated in the skeleton of the knockout but not the heterozygous animal. In fact, the

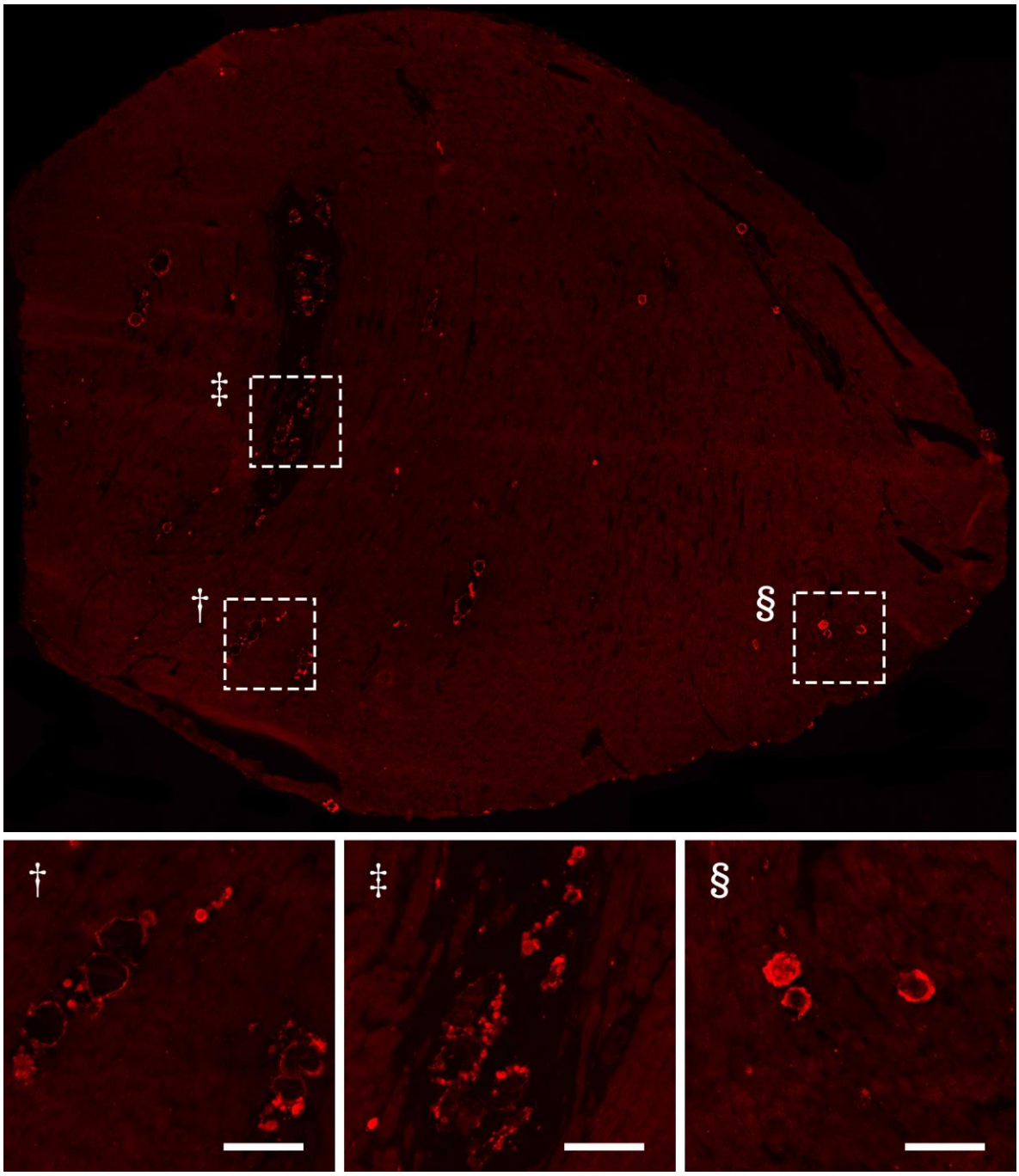

Figure 19. Detection of calcifications in the myocardium using bOPN-mRuby3. **(Upper panel)** Tile scan micrograph of a stained heart cross-section. **(Lower panel)** Enlarged images of the boxed regions marked with the dagger, double dagger, and paragraph sign in the upper panel. Scale bars 100 µm.

tracer outlined the animal's bones in such detail that it was possible to visualize the finest anatomical structures down to individual vertebrae. However, it was not possible to distinguish between signals derived from bone or calcification-bound ^{99m}Tc-mFA.

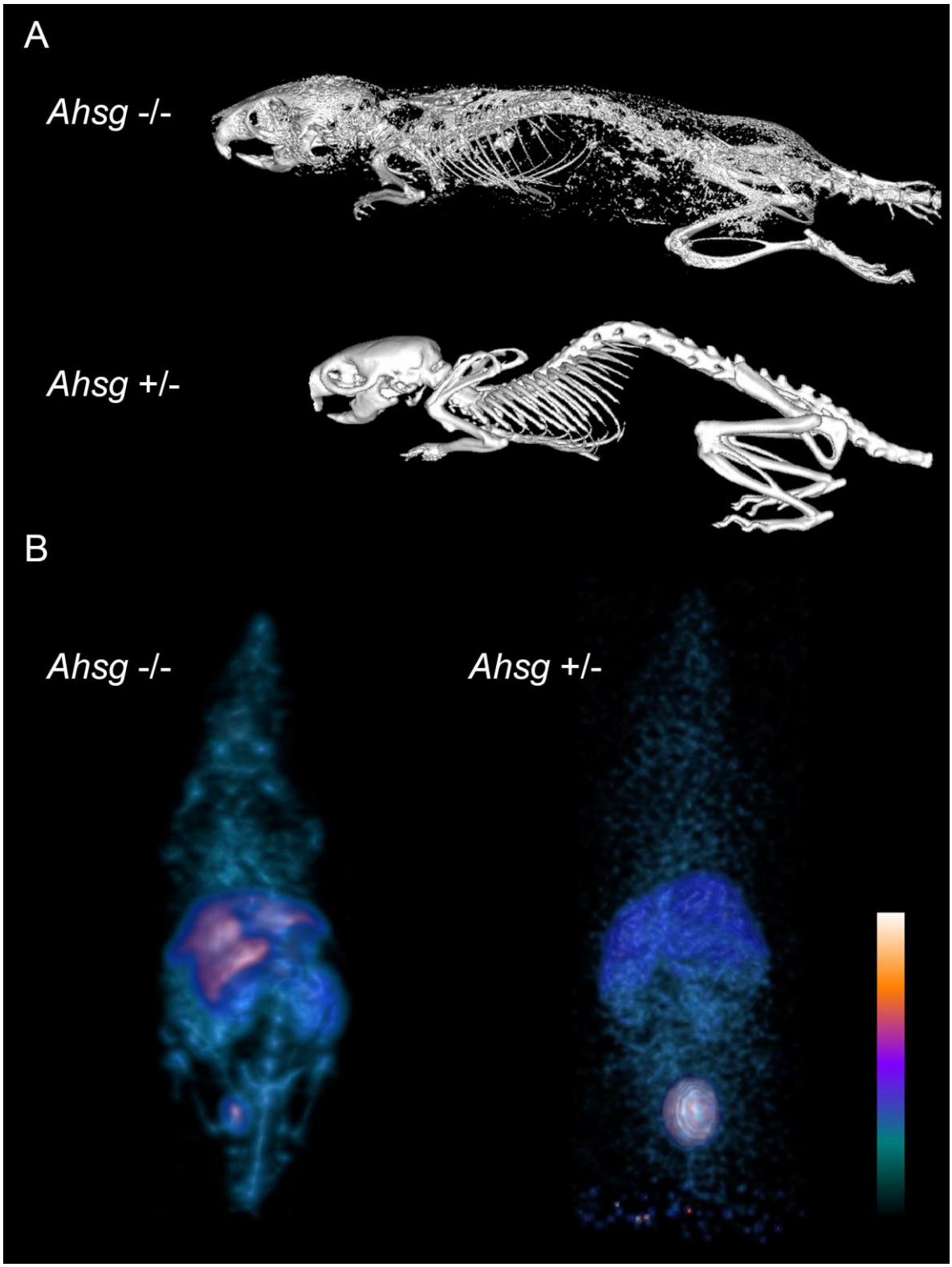

Figure 20. Intravital imaging. **(A)** CT scan of a fetuin-A-deficient animal (upper image) reveals the presence of pronounced soft tissue calcification, while a heterozygous mouse has a normal phenotype (lower image). **(B)** SPECT imaging performed 2 h after radiotracer injection shows an accumulation of ^{99m}Tc-mFA in the liver and bladder as well as in the skeleton of a knockout mouse (left image), whereas no bone-associated areas of signal enhancement were registered in the heterozygous littermate.

Development of cell-based treatment for ectopic calcification

4.10 Osteoclast differentiation assay

Osteoclasts are highly specialized multinucleate cells that are capable of resorbing bone. Induction and maturation of osteoclasts are complex processes regulated by the RANK/RANKL/OPG axis. Osteoclast differentiation was induced in a RAW 264.7 cell line using either recombinant sRANKL or CY1_sRANKL fusion protein, both produced in ExpiCHO-S cells. For a more accurate assessment of osteoclast differentiation, I introduced a new value, the osteoclast differentiation index (ODI), which is described in detail in Section 3.9. Figures 21A, B show typical micrographs of osteoclasts taken on day 14 after inducing osteoclast differentiation, and Figure 21C demonstrates the results of the Mann-Whitney U test used to analyze differences in ODI values between the two groups. According to the statistical analysis, both cytokines showed similar activity, indicating that coupling sRANKL to CY1_mFA did not interfere with sRANKL-RANK interaction. In contrast, the mere counting of giant multinucleated cells in the same set of micrographs gives the false impression that one cytokine is superior to another in its ability to induce osteoclast differentiation (Figure 21D), and should therefore be avoided.

Polymerization of actin filaments is known to be essential for bone resorption by osteoclasts. Extended stimulation of cells with CY1_mFA-sRANKL resulted in the formation of typical actin rings in osteoclasts, as showed by phalloidin staining performed on day 21 after culture initiation (Figure 21E). As the culture matured, the osteoclasts increased in size and became more rounded, and their nuclei moved from the center to the periphery. Concomitantly, the ODI doubled in mature cultures, reaching values of 0.8-0.9, mainly due to the extensive fusion of RANKL-sensitive precursors and perishing mononuclear cells that were not responsive to stimulation with the cytokine (Figure 21F).

Although ODI is a sensitive measure of osteoclast differentiation, this parameter does not reflect the functional activity of osteoclasts, which can only be evaluated by osteoclast resorption assays.

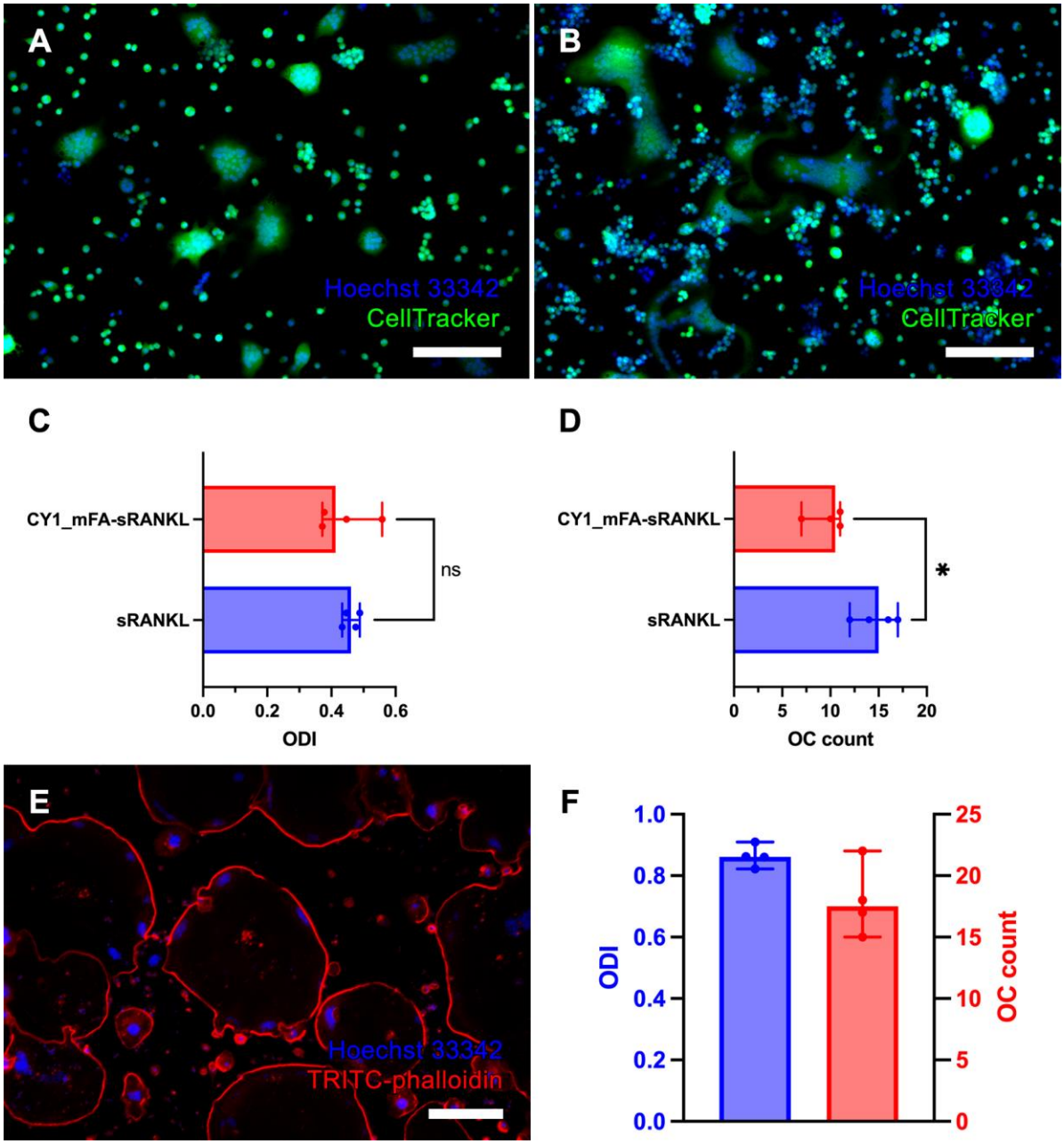

Figure 21. Osteoclast differentiation. **(A, B)** Multiple giant multinucleated can be observed in cultures treated for 14 days with recombinant murine sRANKL **(A)** or CY1_mFA-sRANKL **(B)**. **(C)** Statistical analysis revealed no significant differences between the two groups with regard to the ODI value (P value 0.69) on day 14. **(D)** The mere counting of giant multinucleated cells leads to a false conclusion that recombinant sRANKL is a stronger activator of osteoclastogenesis than CY1_mFA-sRANKL. * – P value < 0.05. **(E)** Phalloidin staining detects ring-like organization of actin filaments in mature osteoclasts on day 21. **(F)** ODI value increases in osteoclast cultures treated with CY1_mFA-sRANKL on day 21, whereas the number of giant multinucleated cells changes insignificantly. Scale bars 150 µm **(A, B)** and 250 µm **(E)**. Data presented as median with range.

4.11 Resorption assay

The ability to resorb bone tissue is a characteristic feature of mature osteoclasts. Biological materials, such as dentin or cortical bone slices, are most frequently used to study bone resorption. Typical bone resorption assays are based on visualization and measurement of resorption pits and lacunae on the surface of the biomaterial (Figure 22A, asterisks) created by osteoclasts (Figure 22A, arrowheads), in this case stimulated with CY1_mFA-sRANKL equimolar to 100 ng/ml sRANKL for 21 days. Figure 22B demonstrates a high-magnification SEM micrograph of an early osteoclast (treated with CY1_mFA-sRANKL for 3 days) on cortical bone. Although no resorption pits were present on the bone surface, EDX analysis of the sample revealed peaks of calcium, phosphorus, and oxygen in dense vesicle-like

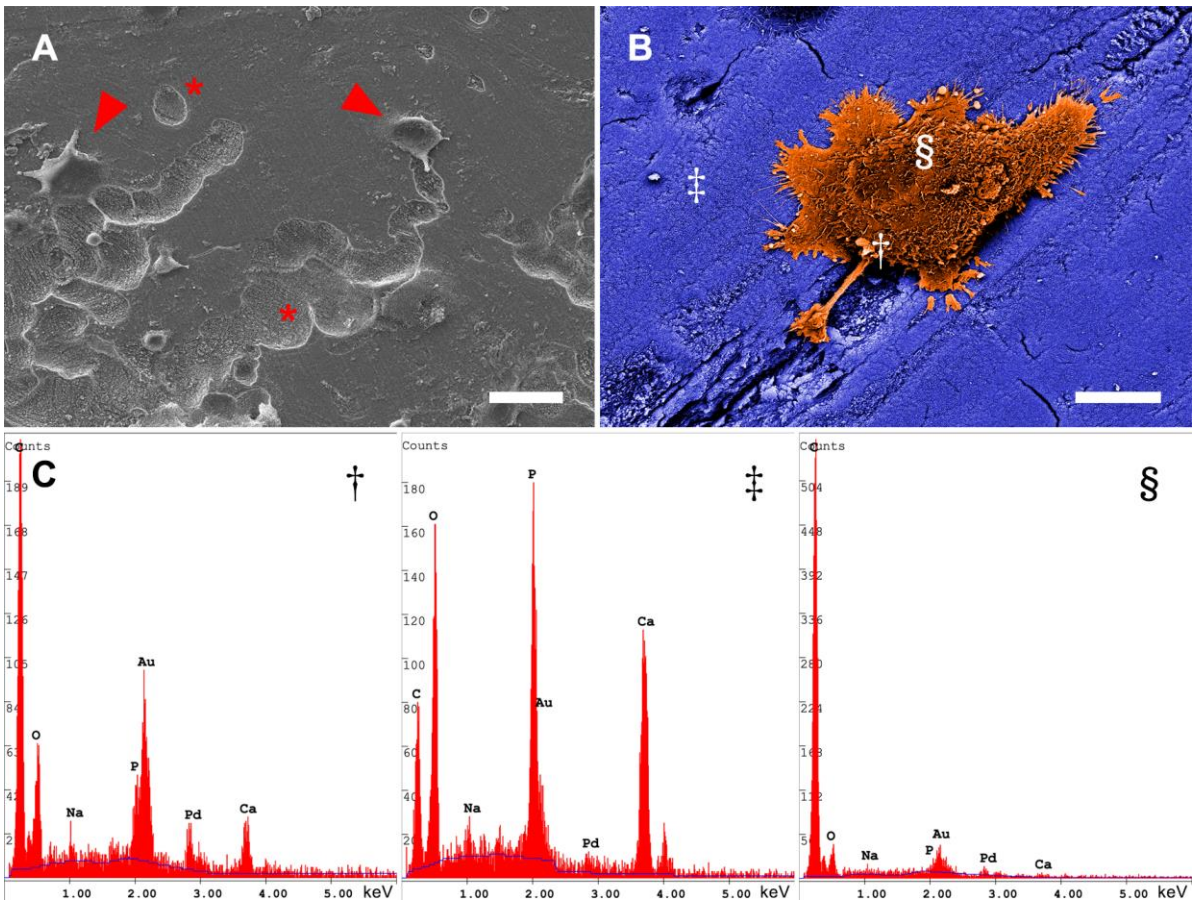

Figure 22. Bone resorption by osteoclasts. **(A)** SEM micrograph of bone-resorbing osteoclasts on day 21 after culture initiation. Red arrowheads indicate osteoclasts, and red asterisks mark resorption lacunae. **(B)** False-colored SEM image of an early osteoclast (orange) attached to the bone surface (blue). The dagger, double dagger and section sign mark areas where EDX spectra were taken. **(C)** EDX spectra recorded at the positions marked in **B**. Vesicles on the cell surface (dagger) are abundant in hydroxyapatite, indicating active bone resorption. Analysis of bone surface (double dagger) reveals high calcium, phosphorus and oxygen content. The cell surface (section sign) contains trace amounts of the mineral. Scale bars 50 µm **(A)** and 15 µm **(B)**.

structures on the cell surface (Figure 22C, left plot). Similar but more prominent peaks were detected on the bone surface (Figure 22C, central plot) but not outside of the vesicles on the cell surface (Figure 22C, right plot), suggesting that vesicles contained hydroxyapatite-rich products of bone resorption. This finding is consistent with the current understanding of transcellular trafficking in actively resorbing osteoclasts.

Although both dentin and bone are physiological targets for osteoclasts, these materials are naturally occurring and, therefore, not perfectly homogeneous, which negatively affects the reproducibility of measurements. To address this issue, I induced osteoclast differentiation in a 24-well plate precoated with an inorganic material mimicking

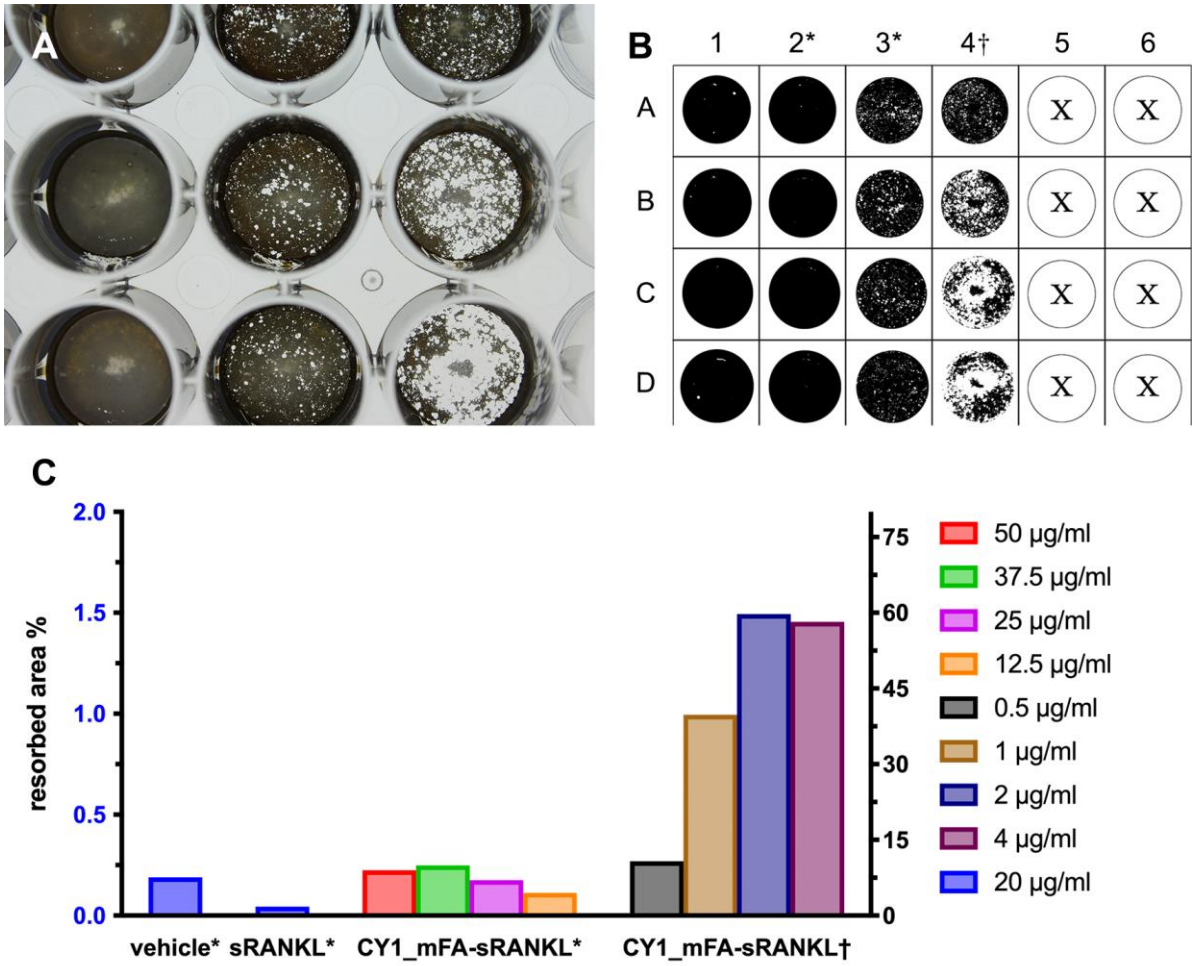

Figure 23. Resorption assay. **(A)** Precoated culture plate stained according to the method of von Kossa on day 10 after culture initiation. The dark areas represent the intact biomimetic surface, and the white areas indicate zones of resorption. **(B)** Processed images of individual wells arranged according to their original positions in the plate. **(C)** Quantification of the resorption area. The mineral surface remains intact in the wells preincubated with vehicle or sRANKL. Moderate resorption is observed in the wells preincubated with CY1_mFA-sRANKL. Vigorous dose-dependent resorption is evident in the wells where cells were continuously supplied with the cytokine. Asterisks indicate columns in which the corresponding cytokine was added prior to cell seeding and washing step. Dagger indicates the column in which the cytokine was added upon each medium exchange.

the bone surface (Section 3.9.2). On day 10, the cultures were terminated, and the wells were stained according to the procedure described by von Kossa. Figure 23A shows a macroscopic view of the plate after staining, and Figure 23B demonstrates processed images of stained wells arranged according to their original positions in the plate. The intact material was stained black, and the resorption pits appeared white as they contained no hydroxyapatite. Image analysis reveals that no resorption took place in wells preincubated with vehicle or sRANKL (Figure 23C), indicating that the cytokine did not bind to the calcium-rich surface and was washed away. On the contrary, considerable resorption of about 10% of total surface area was observed in wells preincubated with varying amounts of CY1_mFA-sRANKL. Interestingly, the extent of resorption did not depend upon the amount of fusion protein with which the wells were preincubated prior to cell seeding, suggesting that the plate surface was saturated with the bound CY1_mFA-sRANKL. This assumption is indirectly supported by the observation that cell cultures treated with increasing amounts of the osteoclastogenic fusion protein exhibit exuberant dose-dependent resorption approaching 60% of total surface area in the high-dose groups. Collectively, these findings indicate that CY1_mFA-sRANKL retained the properties of its constituent proteins both in terms of binding to calcium-rich materials and in terms of its ability to trigger osteoclast differentiation.

5. DISCUSSION

Ectopic calcification is a common disturbance of mineral metabolism that can aggravate underlying conditions and cause lethal complications. The vasculature is constantly exposed to high serum calcium concentrations and is therefore prone to calcification. Pathological mineralization of blood vessels can cause various complications, including plaque instability due to atherosclerotic intimal microcalcification. The small size and lack of a defined crystalline structure hinder the diagnosis of the disorder. Moreover, regardless of the size of the developed lesions, soft tissue calcification is irreversible, and there are currently no pharmacological approaches to its treatment. Fluorescence molecular tomography and similar imaging techniques based on the use of specific fluorescent probes were reported to be advantageous in detecting early stages of ectopic calcification.

Extraosseous precipitation of calcium salts is actively prevented by a number of local and circulating inhibitors of calcification. Hepatic glycoprotein fetuin-A is one of the principal serum components that stabilizes excess calcium phosphate. Negatively charged amino acids incorporated in the protein's backbone, alongside its unique spatial organization, determine the ability of fetuin-A to prevent the growth of crystallization nuclei by forming colloidal complexes termed calciprotein particles. Chemically labeled fluorescent fetuin-A was established as a sensitive probe for the detection of calcifications. To further increase the diagnostic value of the probe, I sought to design and produce a set of chimeric proteins consisting of murine fetuin-A coupled to either a green or red fluorescent protein variant, mEmerald or mRuby3, respectively. All recombinant proteins were expressed in a suspension-adapted ExpiCHO-S mammalian cell line optimized for high-yield protein production.

Major modifications of the protein structure caused by protein fusion can negatively affect nearly all stages of protein biosynthesis, including protein folding, its intra- and extracellular trafficking, and post-translational modifications. Consequently, such changes can arrest protein expression or result in nonfunctional proteins. Although both fusion proteins retained strong fluorescence (Figure 6A), one of them, mFA-mEmerald, had an impaired ability to inhibit calcium phosphate precipitation (Figure 7E). To address this problem, natural phosphorylation sites of mFA, represented by threonine and serine residues at positions 135, 138, 305, 309, 312, and 314, were replaced with glutamic acid,

reconstituting the negative charge of phosphorylated residues. This phosphomimetic modification fully restored the function of the protein (Figure 7F). After the fetuin-A-based fusion fluorescent probes were confirmed to be non-toxic (Figure 8), they were successfully used to image the physiological mineralization of MSC-derived osteoblasts (Figure 10) and pathological calcification of iVSMC (Figure 12). To further expand the palette of calcification probes, hydroxyapatite-binding protein osteopontin was fused to mRuby3 and successfully used for imaging of MSC mineralization, with sensitivity comparable to that of fluorescent fetuin-A (Figure 11). Overall, application of fluorescent probes based on mFA or bOPN allowed the identification of micrometer-sized features, confirming the high selectivity of these probes to incipient mineral deposits. Importantly, despite their protein nature, the fusion fluorescent probes produced only minor uptake-associated intracellular fluorescence in cultures maintained in a basal medium (Figure 16), which was, however, temporary and by no means impaired the quality of imaging (the negative controls in Figures 10-12). On the other hand, the use of standard staining methods had significant drawbacks, related both to the requirement for cell fixation and to the quality of detection. Although routine Alizarin Red S staining allowed the distinction between non-mineralizing MSC and osteoblasts and also revealed larger calcified lesions in iVSMC, it failed to identify the typical grain-like mineralization delineating the contours of osteoblasts. The above was also true for the commercially available fluorescent dye calcein. Co-localization analysis of mFA-mRuby3- and calcein-derived signals in double-stained mineralizing MSC and calcifying iVSMC revealed a moderate overlap in the case of MSC, which were sparsely stained with calcein, and a strong correlation in the case of iVSMC, which developed larger lesions detected by both probes (Figure 13). Thus, standard probes can detect mature crystalline material but lack sensitivity toward micrometer-sized calcifications. The observation that the smallest calcifications are recognized as pro-inflammatory and deleterious fundamentally justifies the use of microcalcification-sensitive fluorescent probes in the clinical setting. Collectively, these findings indicate that the designed fusion fluorescent proteins can detect both physiological and pathological patterns of calcium deposition in living cells with high specificity and sensitivity.

High cell compatibility due to lack of toxicity is another major advantage of protein probes over chemical dyes used to detect minerals. To test whether fetuin-A-based fusion fluorescent proteins can be used for extended live staining of calcifying cells, patient-isolated VSMC were maintained for one week in serum-depleted calcification medium supplemented

with mFA-mRuby3. Fluorescence imaging revealed a gradual increase in the number of cells stained with the probe over the course of the experiment, indicating continuous calcification of VSMC (Figure 14). Starting from day 1, the high signal-to-noise ratio enabled precise automated quantification of calcification at individual time points. Remarkably, the amount of added mFA-mRuby3 was insufficient to suppress calcification, thus altering the experiment, as shown by the calcium phosphate precipitation inhibition assay (Figure 7C). The stability and high cytocompatibility of fetuin-A-based fusion fluorescent probes create a prerequisite for their inclusion in calcification media for continuous monitoring of calcification in cell cultures. In addition, low susceptibility to bleaching makes the engineered probes ideal candidates for use in long-term experiments employing automated cell imaging systems. Reflecting on the clinical significance of such assays, it should be kept in mind that ectopic calcification has long been established as an actively regulated process [35], and the predisposition to pathological mineralization is embedded at the cellular and tissue levels. Thus, the assessment of calcification propensity in the cells isolated from patients seems to be a promising diagnostic and prognostic method for conditions associated with the development of ectopic calcification. In addition, testing of anti-calcification therapeutic candidates in the patient-derived material might soon become an essential part of personalized medicine in the field of mineral metabolism disorders, so that the development of sensitive and non-toxic probes for imaging of early stages of calcification is more than justified.

In contrast to conventional probes, fetuin-A-based fusion proteins are inherently fluorescent and fully functional upon secretion. Their ability to emit light upon excitation relies primarily on the proper folding of the corresponding fluorescent β-barrels, which, in turn, depends on the presence of the required molecular machinery. Fortunately, mammalian cells possess a wide range of chaperones and other folding-assisting molecules. To test whether functional fluorescent fusion proteins can be expressed in a calcifying cell line, thus constituting a calcification screening system, epithelial kidney cells HEK293 were transfected with a plasmid encoding mFA-mRuby3, and calcification was triggered shortly thereafter. Given that both transfection and induction of calcification can launch cellular stress response mechanisms, the main concern was whether these treatments performed simultaneously would negatively affect cell viability. Calcifying and non-calcifying transfected HEK293 cells assumed a spherical shape (Figures 15B, D) but remained viable for at least 4 days post-transfection. The amount of fluorescent protein released in culture

medium by transfected cells was sufficient to stain calcified untransfected cells (Figure 15C), indicating the expression of a functional fusion protein. HEK293 cells subjected to both transfection and calcification stained the irregular calcified areas, and the protein-expressing cells appeared as bright red dots, like their counterparts cultured in basal medium. Explicit morphological differences between calcified lesions and protein-producing cells allowed their clear distinction and quantitative analysis. Modern techniques for introducing genetic material into cells enable further development of such cell-based reporter systems. For instance, stable transfection of a cell line with a fluorescent probe would reduce the cost of live calcification screening many times over. Furthermore, a fusion fluorescent protein sequence cloned into an inducible expression vector would grant spatial and temporal control of probe production, providing new insights into calcification dynamics in living cells. Finally, the expression of fluorescent proteins with different emission wavelengths in response to various external stimuli seems to be a potent tool for multichannel imaging, enabling the study of the intricate relationship between calcification, inflammation, and cell death.

Although fetuin-A-based fusion fluorescent proteins were shown to have strong potential as novel probes for the live imaging of ectopic calcification due to their high sensitivity and good safety profile, in the clinical setting, the final diagnosis of ectopic calcification depends largely on the histopathological examination to date. To study the application of fusion fluorescent probes as histological calcification dyes, hearts, livers, and kidneys harvested from calcification-prone mice were subjected to cryosectioning and stained using pm-mFA-mEmerald or pm-mFA-mRuby3 alongside their chemically labelled counterpart bFA-AF488, and conventional Alizarin Red S staining was used as a positive control. All fetuin-A-based probes were able to detect micrometer-sized calcifications in tissue samples (Figure 17). Additionally, these probes produced dim fluorescence in intact areas that accurately highlighted the morphology of examined tissues and thus obviated the need to use counterstain. The most striking observations were made upon examination of the kidney sections. Not only did routine Alizarin Red S staining fail to detect a significant number of microcalcifications, but it also failed to identify quite large, apparently fresh lesions measuring about 500 µm. Furthermore, multiple foci of intratubular calcification consistent with nephrocalcinosis, which were clearly detectable with fetuin-A, appeared intact when stained with Alizarin Red S (boxed areas in Figures 17C, D). Tissue staining with calcein could only detect mature large, calcified lesions, providing even less sensitivity

than Alizarin Red S (Figure 18). Given that renal pathology is one of the few clinical areas that does require the use of electron microscopy, e.g., to diagnose minimal change disease, the development of sensitive probes can be a valid option to provide novel, cost-effective solutions in the field. The concept of a calcium-detecting molecule fused to a fluorescent protein was further extended to generate OPN-based probes. Like fetuin-A fusion fluorescent proteins, bOPN-mRuby3 was found to be a sensitive tool for staining microcalcifications in the myocardium (Figure 19). It is known that extensive phosphorylation and intrinsically disordered structure of both mFA and bOPN allow these proteins to bind calcium-rich minerals [148]. Here, I showed that the binding is preserved in chimeric forms of the proteins.

Intravital imaging is another promising application of calcification probes. Incorporating a short hexahistidine tag into the amino acid sequences of the recombinant proteins for purification purposes made it possible to further exploit the chemical properties of this tag for its rapid and site-specific labeling with gamma-emitting radionuclide ^{99m}Tc. Upon injection, radiolabeled murine fetuin-A demonstrated significant hepatic uptake in both fetuin-A-deficient and heterozygous mice, most likely due to its glycosylation profile not fully corresponding to the physiological (Figure 20B). Another reason for such biodistribution could be the histidine label itself, as some other authors have already observed increased accumulation of hexahistidine-labeled proteins in the liver [172]. This challenge can be addressed by replacing the hexahistidine tag with similar sequences that result in reduced hepatic uptake of the labeled proteins. Interestingly, fetuin-A-based radiotracer precisely outlined the skeleton of the fetuin-A-knockout but not the heterozygous animal. Given that fetuin-A accounts for a quarter of noncollagenous bone proteins [173], this observation can be explained by the complete occupancy of the fetuin-A-binding sites in the bones of the heterozygous animal and their availability in the skeleton of the knockout littermate. In fact, the high bone uptake of ^{99m}Tc-mFA did not allow extraction of the signal produced by the probe bound to microcalcifications. Overall, more research is required to establish reliable fetuin-A-based intravital radiotracers for the imaging of microcalcifications.

Having established that fluorescent fetuin-A probes are potent tools for calcification imaging suitable for histological verification of diagnosis, I asked whether a bioengineering approach can be further employed to design and produce fusion proteins with therapeutic potential in ectopic calcification, as there is no conservative treatment for the condition to date. Although dissolving calcium phosphate is not challenging per se, it requires lowering

the pH well below the physiological range (7.35-7.45), which is impossible in a living organism. However, degradation of biological hydroxyapatite constantly occurs in bones and teeth in a process known as bone resorption. This process is inherently targeted and precisely regulated, as it can only take place when a highly specialized cell, the osteoclast, attaches to the bone surface and creates a sealed acidifying microenvironment under the portion of its membrane opposed to the bone surface. Such a microenvironment mobilizes the mineral while not disturbing the overall acid-base homeostasis. As skeletal hydroxyapatite and the mineral found in soft tissue calcium deposits are substantially the same matter, I hypothesized that bone-resorbing osteoclasts can be generated locally at the sites of ectopic calcification in order to dissolve the pathological foci. To test this hypothesis, a set of fusion proteins consisting of N-terminal murine fetuin-A (or parts thereof) coupled to the osteoclast-activating cytokine RANKL was designed. The idea was to create RANKL-saturated interfaces in calcified lesions that would induce osteoclast differentiation from precursors upon contact. RANKL is functional in its membrane and soluble forms so that contact induction of osteoclasts represents one of its physiological mechanisms of action. Two of the three initially designed fusion proteins, mFA-sRANKL and mFA-scRANKL, could not be expressed in ExpiCHO-S cells, most likely due to folding issues. CY1_mFA-sRANKL, consisting of the first cystatin-like domain CY1 of fetuin-A and soluble RANKL, was successfully expressed, although several process optimization steps were required to obtain a pure product. The comparatively low final yield of the fusion protein is explained by the fact that cytokines act at nano- and picomolar concentrations, which distinguishes them from serum and structural proteins, which are physiologically produced in large amounts.

To test the activity of the osteoclastogenic fusion protein, osteoclast precursor cells (RAW 264.7) were treated with the engineered protein, and the cells stimulated with recombinant sRANKL served as the positive control. Multiple giant multinucleated cells were apparent in both cultures on day 14 of the experiment (Figures 21 A, B). However, the exact assessment of osteoclastogenesis was challenging, as conventional counting of multinucleated cells alone does not characterize osteoclast differentiation. For instance, a cell culture with ten osteoclasts, each containing three nuclei, would be considered to have a higher degree of differentiation than a culture with two larger osteoclasts, each having fifty nuclei. In an attempt to eliminate this obvious inconsistency, I introduced a new measure of osteoclast differentiation, the osteoclast differentiation index. This new approach to evaluating osteoclast development takes into account the number of nuclei in multinucleated ($n \geq 3$) cells,

providing more accurate data on osteoclast fate commitment. Indeed, mere cell counting showed that more osteoclasts developed in a culture treated with recombinant sRANKL compared to the study group (Figure 21D, P value < 0.05), but the comparison of ODI values of the two cultures revealed no statistically significant difference between the groups (Figure 21C), indicating that both cytokines were similarly active regarding their ability to induce osteoclastogenesis. While useful for the quick assessment of osteoclast differentiation, the ODI value, however, does not provide information on the functional activity of developed osteoclasts.

Osteoclast-mediated resorption was studied using bone biomimetic plates. To test whether the osteoclastogenic fusion protein retained the fetuin's characteristic ability to bind calcium-rich minerals, the culture plate wells were preincubated with CY1_mFA-sRANKL and washed with plain culture medium prior to cell seeding. As expected, the fusion protein but not the recombinant sRANKL was able to drive osteoclastogenesis, as indicated by the considerable surface resorption observed on day 10 after culture initiation (Figures 23B, C). This observation suggests that the cystatin-like domain CY1 of fetuin-A is sufficient to provide mineral binding, but further research is required for a more accurate assessment. Interestingly, maintaining osteoclast precursors in the wells precoated with varying concentrations of CY1_mFA-sRANKL (12.5 – 50 µg/ml) resulted in a similar resorption response of about 10% of total surface area in each case, whereas the continuous supplementation of progenitor cells with much lower amounts of the cytokine (0.5 – 4 µg/ml) occasioned extensive dose-dependent resorption. This finding indicates that preincubation with the cytokine fully saturated the surface with the fusion protein, which triggered homogenous osteoclast development in the study groups. In contrast, constant exposure to the cytokine in the groups where it was added to the cells each time alongside medium exchange resulted in a sustained stimulation of osteoclasts that were able to resorb up to 60% of total surface area in high-dose groups.

Taken together, the findings of this study intimate that the bioengineering of fusion proteins with desired properties might provide the basis for novel approaches to the management of ectopic calcification. The hepatic glycoprotein fetuin-A was shown to be an efficient mineral-binding protein capable of directing fluorescent molecules or effector agents to sites of ectopic calcification. In a set of experiments, fetuin-A-based fusion fluorescent proteins were demonstrated to be specific and sensitive probes that enable the imaging of calcification in living cells. The introduction of the inherently fluorescent fusion

proteins into calcifying cells provided a cell-based platform for the real-time screening of calcification. Furthermore, the novel fluorescent probes used for histological evaluation of ectopic calcification were able to resolve micrometer-sized lesions that appeared intact when stained using conventional techniques. The attempt to use physiological mechanisms to treat ectopic calcification led to the concept of a fetuin-A-based osteoclastogenic fusion protein. The therapeutic potential of the designed protein was validated in resorption assays.

6. ZUSAMMENFASSUNG

Kalzium ist ein wesentlicher Bestandteil des menschlichen Körpers, der etwa 2 % des Körpergewichts ausmacht. Aufgrund seiner direkten Beteiligung an einer Vielzahl von physiologischen Prozessen ist sein Stoffwechsel genau geregelt. Die Biomineralisierung ist der Prozess, bei dem Kalzium in die Körpergewebe eingebaut wird, um sie zu härten und ihre physiologischen Funktionen zu gewährleisten. Beim Menschen ist die Biomineralisierung auf Knochen und Zähne beschränkt und wird in anderen Geweben aktiv durch ein Netz von zirkulierenden und lokalen Kalzifizierungshemmern verhindert. Endokrine Störungen, entzündliche und altersbedingte Erkrankungen können dieses Netzwerk stören, was zur Ablagerung von Kalziumphosphat in Weichteilgeweben führt, die man als ektopische Kalzifizierung bezeichnet. Solche abnormen Ablagerungen von Kalziumsalzen können die Blutgefäße versteifen oder den Verlauf der Atherosklerose verschlimmern und zu schweren und sogar tödlichen Komplikationen wie Herzinfarkt oder Schlaganfall führen. Während es möglich ist, große verkalkte Läsionen zu visualisieren, sind entzündungsfördernde mikrometergroße Kalziumablagerungen mit herkömmlichen bildgebenden Verfahren nur schwer zu erkennen. Unabhängig von der Größe der Verkalkungen gibt es derzeit keine konservativen Behandlungen zur Beseitigung bestehender Kalksalzablagerungen. Ziel der aktuellen Arbeit war es, Ansätze zur Bildgebung und Behandlung von ektopischen Verkalkungen zu entwickeln.

Fetuin-A ist ein aus der Leber stammender, zirkulierender Verkalkungshemmer, der die Ausfällung von Kalziumphosphat verhindert. Seine hohe Affinität zu kalziumreichen Mineralien erklärt sich durch seine einzigartigen strukturellen Eigenschaften sowie durch seine molekulare Ladungsverteilung. Durch Anhängen von fluoreszierenden Proteinen an ein Molekül des murinen Fetuin-A wurde eine Reihe von fluoreszierenden Kalzifizierungssonden hergestellt. Die neuartigen Sonden erwiesen sich als ungiftig und geeignet für die Visualisierung von Verkalkungen an lebenden Zellen und übertrafen die herkömmlichen Färbetechniken. Darüber hinaus erwiesen sich die auf Fetuin-A basierenden Sonden als viel empfindlicher gegenüber Mikroverkalkungen als die chemischen Farbstoffe, die oft die kleinsten verkalkten Läsionen ungefärbt ließen. Schließlich wurden die neuen, mit einem Radionuklid markierten Sonden für die intravitale Bildgebung verwendet.

Die Knochenresorption durch Osteoklasten ist der einzige natürliche Prozess, bei dem ansonsten unlösliches Kalziumsalz abgebaut wird. Die Differenzierung und Aktivierung der knochenresorbierenden Osteoklasten hängt im Wesentlichen von einem Zytokin namens RANKL ab. Durch die Fusion von RANKL mit Fetuin-A habe ich ein wirksames Instrument zur gezielten Aktivierung von Osteoklasten an Verkalkungsstellen erhalten. Insgesamt zeigen Fetuin-A-basierte Fusionsproteine ein vielversprechendes theranostisches Potenzial für ektopische Verkalkung.

7. SOCIETAL IMPACT

Ectopic calcification is defined as a pathological deposition of calcium salts in soft tissues. It accompanies a multitude of systemic diseases, with cardiovascular calcification in atherosclerosis and CKD being the most salient examples of the detrimental effects associated with this condition. Vascular calcification is strongly associated with all-cause mortality and long recognized as an independent risk factor for acute cardiovascular events, as it directly contributes to plaque instability in case of intimal calcification and arterial stiffness with subsequent left ventricular hypertrophy, MI and heart failure in medial calcification linked to end-stage renal disease [29, 174]. In fact, distinct forms of cardiovascular calcification are observed in 60-70% of individuals aged 41 to 80 years [175], and the prevalence increases up to 81% in patients with T2DM [176] and to a striking 100% in end-stage renal disease patients on hemodialysis [177]. As ectopic calcification is a feature of numerous diseases, it is difficult to assess its real burden. However, the very fact that conditions traditionally linked to extraosseous mineralization, such as IHD, stroke, diabetes, and CKD, are among the leading causes of global disability-adjusted life-years [178], clearly indicates the great impact of this health problem. Despite decades of research, there are no pharmacological treatments to completely stop progression of ectopic calcification, and the reversal of the process is considered the holy grail in the field of mineral pathophysiology. Moreover, the lack of sensitive and non-toxic imaging agents capable of detecting micrometer-sized calcified lesions creates additional obstacles in the management of the disease.

In this dissertation, I sought to develop a new approach to imaging and potential treatment of vascular calcification by establishing a novel theranostic platform based on mineral-binding protein fetuin-A. Firstly, I demonstrated that the chimeric proteins created upon fusion of fetuin-A and fluorescent protein variants were fully functional and could be used to detect mineralization and calcification in living cell cultures. Next, it was shown that fetuin-A-based probes surpass existing methods for detecting calcifications in both sensitivity and specificity. Application of novel imaging agents enabled identification of microcalcifications in seemingly intact tissues, significantly enhancing the diagnostic potential of optical microscopy in histological confirmation of soft tissue calcification, while eliminating the need for high-cost electron microscopy for early diagnosis of this pathology.

Further, radiolabeled fetuin-A was successfully used to visualize mineralized tissues in mice, demonstrating the potential of the molecule as a tomographic imaging agent. Finally, I proposed a new cell-based approach to the treatment of ectopic calcification based on the use of a chimeric cytokine that provides targeted activation of osteoclasts capable of resolving calcium salt deposits.

Taken together, the findings of this dissertation shed light on the application of bioengineered proteins to diagnose and treat mineral metabolism disorders. While some of the developed agents, such as fusion fluorescent proteins, do not require substantial optimization and can find immediate application in pathology departments, contributing to improved diagnosis of the condition, others might need further validation to advance the current management of ectopic calcification.

ACKNOWLEDGEMENTS

It is with profound gratitude that I pen these acknowledgements, for the realization of this doctoral thesis represents a culmination of years of collaborative work with a number of brilliant scientists whose collective contributions have been instrumental in making this work possible.

First and foremost, I would like to thank my supervisor, **Prof. Dr. Willi Jahnen-Dechent**, whose guidance, discerning insights, and constructive critique have inspired me to strive for excellence, and for that, I am immensely grateful. I would also like to extend my heartfelt appreciation to my supervisor **Prof. Dr. Leon Schurgers**, for welcoming me during my secondment in Maastricht and for valuable insights, constructive feedback, and critical evaluation of my work. Your contributions have helped me to improve the quality of my research and broaden my perspective on mineralization biology. My sincere gratitude also goes to **Prof. Dr. Felix Mottaghy**, whose professional expertise added much to the clinical aspect of this dissertation. Further, I am deeply indebted to **Prof. Dr. Catherine Shanahan** and **Dr. Nina Petrova**, whose input, thoughtful suggestions, and rigorous scrutiny have sharpened my thinking and fostered my intellectual growth. Your generous mentorship during my time in London has greatly strengthened my knowledge of bone biology and allowed me to develop several new concepts that constituted a significant part of my research.

I want to thank the entire Biointerface group, especially **Dr. Carlo Schmitz**, **Dr. Michaela Bienert**, **Dr. Andrea Gorgels**, **Hanna Malyaran**, **Chloé Radermacher**, and **Christian Hasberg** for supporting me throughout this academic endeavor. To my fellow INTRICARE students, I offer my sincere thanks for your friendship and collaboration, you guys (I refuse to refer to you as Drs, although many of you already are) are fun! I had the privilege of working closely with some of you, and I am happy to share that producing scholarly efforts together with **Anouk Gentier**, **Cengiz Akbulut**, **Till Seime**, and **Nikolaos Skenteris** was a truly rewarding experience! But regardless of shared publications, through the highs and lows, challenges and triumphs, we have grown together, laughed together, and supported each other every step of the way. As we go our separate ways and embark on new adventures, I will always cherish the memories we created together and hold dear the lessons we learned from each other. Thank you for being such an integral part of my life, and for helping me become the best version of myself. I want to thank **Dr. Armand**

Jaminon for the collaboration and many interesting discussions arising over a cup of afternoon tea during my time in Maastricht. My further thanks go to the rest of the INTRICARE consortium for the opportunity to work in such an exceptional academic environment.

This work entailed extensive use of sophisticated instrumentation and cutting-edge technologies, and I would like to thank the staff who helped me with various experiments: **Dr. Sabrina Ernst**, **Dr. Kèvin Knoops**, and **Stephan Rütten** for the many and lengthy microscopy sessions; **Dr. Alexandru Florea** and **Sabri Sahnoun** for the help with the SPECT imaging; **Dr. Christian Preisinger** for mass spectrometry and **Steffen Gräber** for protein labeling.

Finally, I am very grateful to my family and friends, whose enduring love, encouragement, and unwavering support have sustained me through the ups and downs of working on this dissertation. Your steadfast faith in my abilities and your belief in my potential have been a constant source of motivation, and for that, I am forever grateful.

REFERENCES

1. Goldstein DA. Serum Calcium. In: Walker HK, Hall WD, Hurst JW, editors. Clinical Methods: The History, Physical, and Laboratory Examinations. Boston: Butterworths Copyright © 1990, Butterworth Publishers, a division of Reed Publishing.; 1990.
2. Wills MR, Lewin MR. Plasma calcium fractions and the protein-binding of calcium in normal subjects and in patients with hypercalcaemia and hypocalcaemia. J Clin Pathol. 1971; 24: 856-66.
3. Clapham DE. Calcium signaling. Cell. 2007; 131: 1047-58.
4. Green JR. On certain points connected with the Coagulation of the Blood. J Physiol. 1887; 8: 354-71.
5. Homa ST, Carroll J, Swann K. The role of calcium in mammalian oocyte maturation and egg activation. Hum Reprod. 1993; 8: 1274-81.
6. Szent-Györgyi AG. Calcium regulation of muscle contraction. Biophys J. 1975; 15: 707-23.
7. Wakabayashi T. Mechanism of the calcium-regulation of muscle contraction--in pursuit of its structural basis. Proc Jpn Acad Ser B Phys Biol Sci. 2015; 91: 321-50.
8. EFSA Panel on Dietetic Products N, Allergies. Scientific Opinion on Dietary Reference Values for calcium. EFSA Journal. 2015; 13: 4101.
9. Pettifor JM. Nutritional rickets: deficiency of vitamin D, calcium, or both? Am J Clin Nutr. 2004; 80: 1725s-9s.
10. Bronner F. Mechanisms of intestinal calcium absorption. J Cell Biochem. 2003; 88: 387-93.
11. Bronner F. Intestinal calcium transport: the cellular pathway. Miner Electrolyte Metab. 1990; 16: 94-100.
12. Christakos S, Barletta F, Huening M, Dhawan P, Liu Y, Porta A, et al. Vitamin D target proteins: function and regulation. J Cell Biochem. 2003; 88: 238-44.
13. Brenza HL, Kimmel-Jehan C, Jehan F, Shinki T, Wakino S, Anazawa H, et al. Parathyroid hormone activation of the 25-hydroxyvitamin D3-1alpha-hydroxylase gene promoter. Proc Natl Acad Sci U S A. 1998; 95: 1387-91.
14. Zhong Y, Armbrecht HJ, Christakos S. Calcitonin, a regulator of the 25-hydroxyvitamin D3 1alpha-hydroxylase gene. J Biol Chem. 2009; 284: 11059-69.
15. Bacchetta J, Sea JL, Chun RF, Lisse TS, Wesseling-Perry K, Gales B, et al. Fibroblast growth factor 23 inhibits extrarenal synthesis of 1,25-dihydroxyvitamin D in human monocytes. J Bone Miner Res. 2013; 28: 46-55.
16. Silva BC, Bilezikian JP. Parathyroid hormone: anabolic and catabolic actions on the skeleton. Curr Opin Pharmacol. 2015; 22: 41-50.
17. Moor MB, Bonny O. Ways of calcium reabsorption in the kidney. Am J Physiol Renal Physiol. 2016; 310: F1337-50.
18. Cochran M, Peacock M, Sachs G, Nordin BE. Renal effects of calcitonin. Br Med J. 1970; 1: 135-7.
19. Keller J, Catala-Lehnen P, Huebner AK, Jeschke A, Heckt T, Lueth A, et al. Calcitonin controls bone formation by inhibiting the release of sphingosine 1-phosphate from osteoclasts. Nat Commun. 2014; 5: 5215.
20. Knoll AH. Biomineralization and Evolutionary History. Reviews in Mineralogy and Geochemistry. 2003; 54: 329-56.

21. Reznikov N, Hoac B, Buss DJ, Addison WN, Barros NMT, McKee MD. Biological stenciling of mineralization in the skeleton: Local enzymatic removal of inhibitors in the extracellular matrix. Bone. 2020; 138: 115447.
22. Fukumoto S. [Ectopic calcification]. Clin Calcium. 2014; 24: 185-9.
23. Babler A, Schmitz C, Buescher A, Herrmann M, Gremse F, Gorgels T, et al. Microvasculopathy and soft tissue calcification in mice are governed by fetuin-A, magnesium and pyrophosphate. PLoS One. 2020; 15: e0228938.
24. Luo G, Ducy P, McKee MD, Pinero GJ, Loyer E, Behringer RR, et al. Spontaneous calcification of arteries and cartilage in mice lacking matrix GLA protein. Nature. 1997; 386: 78-81.
25. Schurgers LJ. Vitamin K: key vitamin in controlling vascular calcification in chronic kidney disease. Kidney Int. 2013; 83: 782-4.
26. Hutcheson JD, Maldonado N, Aikawa E. Small entities with large impact: microcalcifications and atherosclerotic plaque vulnerability. Curr Opin Lipidol. 2014; 25: 327-32.
27. Jono S, Shioi A, Ikari Y, Nishizawa Y. Vascular calcification in chronic kidney disease. J Bone Miner Metab. 2006; 24: 176-81.
28. Pugliese G, Iacobini C, Blasetti Fantauzzi C, Menini S. The dark and bright side of atherosclerotic calcification. Atherosclerosis. 2015; 238: 220-30.
29. Abedin M, Tintut Y, Demer LL. Vascular calcification: mechanisms and clinical ramifications. Arterioscler Thromb Vasc Biol. 2004; 24: 1161-70.
30. Cardoso L, Weinbaum S. Microcalcifications, Their Genesis, Growth, and Biomechanical Stability in Fibrous Cap Rupture. Adv Exp Med Biol. 2018; 1097: 129-55.
31. Murphy WA, Jr., Nedden Dz D, Gostner P, Knapp R, Recheis W, Seidler H. The iceman: discovery and imaging. Radiology. 2003; 226: 614-29.
32. Floege J. When man turns to stone: Extraosseous calcification in uremic patients. Kidney International. 2004; 65: 2447-62.
33. Ketteler M, Schlieper G, Floege Jr. Calcification and Cardiovascular Health. Hypertension. 2006; 47: 1027-34.
34. Thompson B, Towler DA. Arterial calcification and bone physiology: role of the bone-vascular axis. Nat Rev Endocrinol. 2012; 8: 529-43.
35. Giachelli CM, Speer MY, Li X, Rajachar RM, Yang H. Regulation of vascular calcification: roles of phosphate and osteopontin. Circ Res. 2005; 96: 717-22.
36. Sage AP, Tintut Y, Demer LL. Regulatory mechanisms in vascular calcification. Nat Rev Cardiol. 2010; 7: 528-36.
37. Boström K, Watson KE, Horn S, Wortham C, Herman IM, Demer LL. Bone morphogenetic protein expression in human atherosclerotic lesions. J Clin Invest. 1993; 91: 1800-9.
38. Herrmann M, Babler A, Moshkova I, Gremse F, Kiessling F, Kusebauch U, et al. Lumenal calcification and microvasculopathy in fetuin-A-deficient mice lead to multiple organ morbidity. PLoS One. 2020; 15: e0228503.
39. Mc G-RS. Histochemical methods for calcium. J Histochem Cytochem. 1958; 6: 22-42.
40. Cameron GR, Scholar G. The staining of calcium. The Journal of Pathology and Bacteriology. 1930; 33: 929-55.
41. Smith ER, Hewitson TD, Holt SG. Diagnostic Tests for Vascular Calcification. Adv Chronic Kidney Dis. 2019; 26: 445-63.
42. Puchtler H, Meloan SN, Terry MS. On the history and mechanism of alizarin and alizarin red S stains for calcium. J Histochem Cytochem. 1969; 17: 110-24.

43. Hale LV, Ma YF, Santerre RF. Semi-quantitative fluorescence analysis of calcein binding as a measurement of in vitro mineralization. Calcif Tissue Int. 2000; 67: 80-4.
44. Gremse F, Doleschel D, Zafarnia S, Babler A, Jahnen-Dechent W, Lammers T, et al. Hybrid μCT-FMT imaging and image analysis. J Vis Exp. 2015: e52770.
45. Pouliquen H, Algoet M, Buchet V, Le Bris H. Acute toxicity of fluorescein to turbot (Scophthalmus maximus). Vet Hum Toxicol. 1995; 37: 527-9.
46. Adami S, Zamberlan N. Adverse effects of bisphosphonates. A comparative review. Drug Saf. 1996; 14: 158-70.
47. Jaminon AMG, Akbulut AC, Rapp N, Kramann R, Biessen EAL, Temmerman L, et al. Development of the BioHybrid Assay: Combining Primary Human Vascular Smooth Muscle Cells and Blood to Measure Vascular Calcification Propensity. Cells. 2021; 10.
48. Greenland P, Blaha MJ, Budoff MJ, Erbel R, Watson KE. Coronary Calcium Score and Cardiovascular Risk. J Am Coll Cardiol. 2018; 72: 434-47.
49. Agatston AS, Janowitz WR, Hildner FJ, Zusmer NR, Viamonte M, Jr., Detrano R. Quantification of coronary artery calcium using ultrafast computed tomography. J Am Coll Cardiol. 1990; 15: 827-32.
50. Demer LL, Tintut Y, Nguyen KL, Hsiai T, Lee JT. Rigor and Reproducibility in Analysis of Vascular Calcification. Circ Res. 2017; 120: 1240-2.
51. Sigrist MK, Taal MW, Bungay P, McIntyre CW. Progressive vascular calcification over 2 years is associated with arterial stiffening and increased mortality in patients with stages 4 and 5 chronic kidney disease. Clin J Am Soc Nephrol. 2007; 2: 1241-8.
52. Baldwin P. Breast calcification imaging. Radiol Technol. 2013; 84: 383M-404M; quiz 5M-8M.
53. Ferreira Botelho MP, Koktzoglou I, Collins JD, Giri S, Carr JC, Gupta N, et al. MR imaging of iliofemoral peripheral vascular calcifications using proton density-weighted, in-phase three-dimensional stack-of-stars gradient echo. Magn Reson Med. 2017; 77: 2146-52.
54. Wang Y, Osborne MT, Tung B, Li M, Li Y. Imaging Cardiovascular Calcification. J Am Heart Assoc. 2018; 7.
55. Disthabanchong S, Boongird S. Role of different imaging modalities of vascular calcification in predicting outcomes in chronic kidney disease. World J Nephrol. 2017; 6: 100-10.
56. Lucas VS, Burk RS, Creehan S, Grap MJ. Utility of high-frequency ultrasound: moving beyond the surface to detect changes in skin integrity. Plast Surg Nurs. 2014; 34: 34-8.
57. Mintz GS. Intravascular imaging of coronary calcification and its clinical implications. JACC Cardiovasc Imaging. 2015; 8: 461-71.
58. Zysk AM, Nguyen FT, Oldenburg AL, Marks DL, Boppart SA. Optical coherence tomography: a review of clinical development from bench to bedside. J Biomed Opt. 2007; 12: 051403.
59. Nakajima A, Araki M, Kurihara O, Minami Y, Soeda T, Yonetsu T, et al. Predictors for Rapid Progression of Coronary Calcification: An Optical Coherence Tomography Study. J Am Heart Assoc. 2021; 10: e019235.
60. Irkle A, Vesey AT, Lewis DY, Skepper JN, Bird JL, Dweck MR, et al. Identifying active vascular microcalcification by (18)F-sodium fluoride positron emission tomography. Nat Commun. 2015; 6: 7495.
61. Florea A, Sigl JP, Morgenroth A, Vogg A, Sahnoun S, Winz OH, et al. Sodium [18F]Fluoride PET Can Efficiently Monitor In Vivo Atherosclerotic Plaque Calcification Progression and Treatment. Cells. 2021; 10: 275.

62. Fiz F, Morbelli S, Piccardo A, Bauckneht M, Ferrarazzo G, Pestarino E, et al. ^{18}F-NaF Uptake by Atherosclerotic Plaque on PET/CT Imaging: Inverse Correlation Between Calcification Density and Mineral Metabolic Activity. J Nucl Med. 2015; 56: 1019-23.
63. Sorci O, Batzdorf AS, Mayer M, Rhodes S, Peng M, Jankelovits AR, et al. (18)F-sodium fluoride PET/CT provides prognostic clarity compared to calcium and Framingham risk scoring when addressing whole-heart arterial calcification. Eur J Nucl Med Mol Imaging. 2020; 47: 1678-87.
64. Bastawrous S, Bhargava P, Behnia F, Djang DS, Haseley DR. Newer PET application with an old tracer: role of 18F-NaF skeletal PET/CT in oncologic practice. Radiographics. 2014; 34: 1295-316.
65. Oudkerk SF, de Jong PA, Blomberg BA, Scholtens AM, Mali WP, Spiering W. Whole-Body Visualization of Ectopic Bone Formation of Arteries and Skin in Pseudoxanthoma Elasticum. JACC Cardiovasc Imaging. 2016; 9: 755-6.
66. Hardcastle N, Hofman MS, Lee CY, Callahan J, Selbie L, Foroudi F, et al. NaF PET/CT for response assessment of prostate cancer bone metastases treated with single fraction stereotactic ablative body radiotherapy. Radiat Oncol. 2019; 14: 164.
67. Evrard S, Delanaye P, Kamel S, Cristol JP, Cavalier E. Vascular calcification: from pathophysiology to biomarkers. Clin Chim Acta. 2015; 438: 401-14.
68. Shanahan CM, Crouthamel MH, Kapustin A, Giachelli CM. Arterial calcification in chronic kidney disease: key roles for calcium and phosphate. Circ Res. 2011; 109: 697-711.
69. Shantouf R, Ahmadi N, Flores F, Tiano J, Gopal A, Kalantar-Zadeh K, et al. Impact of phosphate binder type on coronary artery calcification in hemodialysis patients. Clin Nephrol. 2010; 74: 12-8.
70. Toussaint ND, Lau KK, Polkinghorne KR, Kerr PG. Attenuation of aortic calcification with lanthanum carbonate versus calcium-based phosphate binders in haemodialysis: A pilot randomized controlled trial. Nephrology (Carlton). 2011; 16: 290-8.
71. Chan S, Au K, Francis RS, Mudge DW, Johnson DW, Pillans PI. Phosphate binders in patients with chronic kidney disease. Aust Prescr. 2017; 40: 10-4.
72. Massy ZA, Drüeke TB. Magnesium and outcomes in patients with chronic kidney disease: focus on vascular calcification, atherosclerosis and survival. Clin Kidney J. 2012; 5: i52-i61.
73. KDIGO 2017 Clinical Practice Guideline Update for the Diagnosis, Evaluation, Prevention, and Treatment of Chronic Kidney Disease-Mineral and Bone Disorder (CKD-MBD). Kidney Int Suppl (2011). 2017; 7: 1-59.
74. Chertow GM, Burke SK, Raggi P. Sevelamer attenuates the progression of coronary and aortic calcification in hemodialysis patients. Kidney Int. 2002; 62: 245-52.
75. Wright IS. The Conservative Treatment of Occlusive Arterial Disease. New Engl J Medicine. 1941; 225: 805-11.
76. Wood AJJ, Hiatt WR. Medical Treatment of Peripheral Arterial Disease and Claudication. New Engl J Medicine. 2001; 344: 1608-21.
77. Fernandes JFe, Fernandes RFe, Garrido P, Melo RG, Rodrigues A, Sousa P. Peripheral arterial disease - indications for intervention: from open surgery to endovascular and hybrid repair. e-J Cardiol Practice. 2021; 20.
78. Ernst E. Chelation therapy for peripheral arterial occlusive disease: a systematic review. Circulation. 1997; 96: 1031 3.
79. Schaar JVd, R TBP, E B-B. The Effects of Magnesium-EDTA Chelation Therapy on Arterial Stiffness. Health. 2014; 06: 2848-53.
80. Lei Y, Grover A, Sinha A, Vyavahare N. Efficacy of reversal of aortic calcification by chelating agents. Calcif Tissue Int. 2013; 93: 426-35.

81. Guldager B, Brixen KT, Jørgensen SJ, Nielsen HK, Mosekilde L, Jelnes R. Effects of intravenous EDTA treatment on serum parathyroid hormone (1-84) and biochemical markers of bone turnover. Dan Med Bull. 1993; 40: 627-30.
82. Holland JF, Danielson E, Sahagian-Edwards A. Use of ethylene diamine tetra acetic acid in hypercalcemic patients. Proc Soc Exp Biol Med. 1953; 84: 359-64.
83. Lei Y, Nosoudi N, Vyavahare N. Targeted chelation therapy with EDTA-loaded albumin nanoparticles regresses arterial calcification without causing systemic side effects. J Control Release. 2014; 196: 79-86.
84. Karamched SR, Nosoudi N, Moreland HE, Chowdhury A, Vyavahare NR. Site-specific chelation therapy with EDTA-loaded albumin nanoparticles reverses arterial calcification in a rat model of chronic kidney disease. Sci Rep. 2019; 9: 2629.
85. Fihn SD, Blankenship JC, Alexander KP, Bittl JA, Byrne JG, Fletcher BJ, et al. 2014 ACC/AHA/AATS/PCNA/SCAI/STS focused update of the guideline for the diagnosis and management of patients with stable ischemic heart disease: a report of the American College of Cardiology/American Heart Association Task Force on Practice Guidelines, and the American Association for Thoracic Surgery, Preventive Cardiovascular Nurses Association, Society for Cardiovascular Angiography and Interventions, and Society of Thoracic Surgeons. J Am Coll Cardiol. 2014; 64: 1929-49.
86. Ravalli F, Vela Parada X, Ujueta F, Pinotti R, Anstrom KJ, Lamas GA, et al. Chelation Therapy in Patients With Cardiovascular Disease: A Systematic Review. J Am Heart Assoc. 2022; 11: e024648.
87. Villarruz MV, Dans A, Tan F. Chelation therapy for atherosclerotic cardiovascular disease. Cochrane Db Syst Rev. 2002: CD002785.
88. Alam MU, Kirton JP, Wilkinson FL, Towers E, Sinha S, Rouhi M, et al. Calcification is associated with loss of functional calcium-sensing receptor in vascular smooth muscle cells. Cardiovasc Res. 2009; 81: 260-8.
89. Ureña P, Frazão JM. Calcimimetic agents: review and perspectives. Kidney Int Suppl. 2003: S91-6.
90. Jung S, Querfeld U, Müller D, Rudolph B, Peters H, Krämer S. Submaximal suppression of parathyroid hormone ameliorates calcitriol-induced aortic calcification and remodeling and myocardial fibrosis in uremic rats. J Hypertens. 2012; 30: 2182-91.
91. Ter Braake AD, Tinnemans PT, Shanahan CM, Hoenderop JGJ, de Baaij JHF. Magnesium prevents vascular calcification in vitro by inhibition of hydroxyapatite crystal formation. Sci Rep. 2018; 8: 2069.
92. O'Donovan R, Baldwin D, Hammer M, Moniz C, Parsons V. Substitution of aluminium salts by magnesium salts in control of dialysis hyperphosphataemia. Lancet. 1986; 1: 880-2.
93. Termine JD, Peckauskas RA, Posner AS. Calcium phosphate formation in vitro. II. Effects of environment on amorphous-crystalline transformation. Arch Biochem Biophys. 1970; 140: 318-25.
94. Pasch A, Farese S, Gräber S, Wald J, Richtering W, Floege J, et al. Nanoparticle-based test measures overall propensity for calcification in serum. J Am Soc Nephrol. 2012; 23: 1744-52.
95. Sakaguchi Y, Hamano T, Obi Y, Monden C, Oka T, Yamaguchi S, et al. A Randomized Trial of Magnesium Oxide and Oral Carbon Adsorbent for Coronary Artery Calcification in Predialysis CKD. J Am Soc Nephrol. 2019; 30: 1073-85.
96. Mori H, Tack J, Suzuki H. Magnesium Oxide in Constipation. Nutrients. 2021; 13.

97. Perelló J, Ferrer MD, Del Mar Pérez M, Kaesler N, Brandenburg VM, Behets GJ, et al. Mechanism of action of SNF472, a novel calcification inhibitor to treat vascular calcification and calciphylaxis. Br J Pharmacol. 2020; 177: 4400-15.
98. Raggi P, Bellasi A, Bushinsky D, Bover J, Rodriguez M, Ketteler M, et al. Slowing Progression of Cardiovascular Calcification With SNF472 in Patients on Hemodialysis: Results of a Randomized Phase 2b Study. Circulation. 2020; 141: 728-39.
99. Sietsema WK, Ebetino FH, Salvagno AM, Bevan JA. Antiresorptive dose-response relationships across three generations of bisphosphonates. Drugs Exp Clin Res. 1989; 15: 389-96.
100. Fleisch HA, Russell RG, Bisaz S, Mühlbauer RC, Williams DA. The inhibitory effect of phosphonates on the formation of calcium phosphate crystals in vitro and on aortic and kidney calcification in vivo. Eur J Clin Invest. 1970; 1: 12-8.
101. Nitta K, Akiba T, Suzuki K, Uchida K, Watanabe R, Majima K, et al. Effects of cyclic intermittent etidronate therapy on coronary artery calcification in patients receiving long-term hemodialysis. Am J Kidney Dis. 2004; 44: 680-8.
102. Russell RG, Smith R, Bishop MC, Price DA. Treatment of myositis ossificans progressiva with a diphosphonate. Lancet. 1972; 1: 10-1.
103. Bartolomeo K, Tan XY, Fatica R. Extraosseous calcification in kidney disease. Cleve Clin J Med. 2022; 89: 81-90.
104. Boström KI. DNA Damage Response, Runx2 (Runt-Related Transcription Factor 2), and Vascular Calcification. Arterioscler Thromb Vasc Biol. 2021; 41: 1358-9.
105. Ghadially FN. As you like it, Part 3: A critique and historical review of calcification as seen with the electron microscope. Ultrastruct Pathol. 2001; 25: 243-67.
106. Jaminon AMG, Dai L, Qureshi AR, Evenepoel P, Ripsweden J, Söderberg M, et al. Matrix Gla protein is an independent predictor of both intimal and medial vascular calcification in chronic kidney disease. Sci Rep. 2020; 10: 6586.
107. McCabe KM, Booth SL, Fu X, Shobeiri N, Pang JJ, Adams MA, et al. Dietary vitamin K and therapeutic warfarin alter the susceptibility to vascular calcification in experimental chronic kidney disease. Kidney Int. 2013; 83: 835-44.
108. Ansell J, Hirsh J, Hylek E, Jacobson A, Crowther M, Palareti G. Pharmacology and management of the vitamin K antagonists: American College of Chest Physicians Evidence-Based Clinical Practice Guidelines (8th Edition). Chest. 2008; 133: 160s-98s.
109. Poterucha TJ, Goldhaber SZ. Warfarin and Vascular Calcification. Am J Med. 2016; 129: 635.e1-4.
110. Price PA, Faus SA, Williamson MK. Warfarin causes rapid calcification of the elastic lamellae in rat arteries and heart valves. Arterioscler Thromb Vasc Biol. 1998; 18: 1400-7.
111. Dai L, Li L, Erlandsson H, Jaminon AMG, Qureshi AR, Ripsweden J, et al. Functional vitamin K insufficiency, vascular calcification and mortality in advanced chronic kidney disease: A cohort study. PLoS One. 2021; 16: e0247623.
112. Levy DS, Grewal R, Le TH. Vitamin K deficiency: an emerging player in the pathogenesis of vascular calcification and an iatrogenic consequence of therapies in advanced renal disease. Am J Physiol Renal Physiol. 2020; 319: F618-f23.
113. Westenfeld R, Krueger T, Schlieper G, Cranenburg EC, Magdeleyns EJ, Heidenreich S, et al. Effect of vitamin K2 supplementation on functional vitamin K deficiency in hemodialysis patients: a randomized trial. Am J Kidney Dis. 2012; 59: 186-95.
114. Suzuki S, Suzuki M, Hanafusa N, Tsuchiya K, Nitta K. Denosumab Recovers Aortic Arch Calcification During Long-Term Hemodialysis. Kidney Int Rep. 2021; 6: 605-12.

115. Chen CL, Chen NC, Wu FZ, Wu MT. Impact of denosumab on cardiovascular calcification in patients with secondary hyperparathyroidism undergoing dialysis: a pilot study. Osteoporos Int. 2020; 31: 1507-16.
116. Iseri K, Watanabe M, Yoshikawa H, Mitsui H, Endo T, Yamamoto Y, et al. Effects of Denosumab and Alendronate on Bone Health and Vascular Function in Hemodialysis Patients: A Randomized, Controlled Trial. J Bone Miner Res. 2019; 34: 1014-24.
117. Samelson EJ, Miller PD, Christiansen C, Daizadeh NS, Grazette L, Anthony MS, et al. RANKL inhibition with denosumab does not influence 3-year progression of aortic calcification or incidence of adverse cardiovascular events in postmenopausal women with osteoporosis and high cardiovascular risk. J Bone Miner Res. 2014; 29: 450-7.
118. Blair HC. How the osteoclast degrades bone. Bioessays. 1998; 20: 837-46.
119. Harada S, Rodan GA. Control of osteoblast function and regulation of bone mass. Nature. 2003; 423: 349-55.
120. Blair HC, Teitelbaum SL, Ghiselli R, Gluck S. Osteoclastic bone resorption by a polarized vacuolar proton pump. Science. 1989; 245: 855-7.
121. Teitelbaum SL. Bone resorption by osteoclasts. Science. 2000; 289: 1504-8.
122. Nakamura I, Pilkington MF, Lakkakorpi PT, Lipfert L, Sims SM, Dixon SJ, et al. Role of alpha(v)beta(3) integrin in osteoclast migration and formation of the sealing zone. J Cell Sci. 1999; 112 (Pt 22): 3985-93.
123. Väänänen HK, Horton M. The osteoclast clear zone is a specialized cell-extracellular matrix adhesion structure. J Cell Sci. 1995; 108 (Pt 8): 2729-32.
124. Coxon FP, Taylor A. Vesicular trafficking in osteoclasts. Semin Cell Dev Biol. 2008; 19: 424-33.
125. Sasaki T, Hong MH, Udagawa N, Moriyama Y. Expression of vacuolar H(+)-ATPase in osteoclasts and its role in resorption. Cell Tissue Res. 1994; 278: 265-71.
126. Salo J, Lehenkari P, Mulari M, Metsikkö K, Väänänen HK. Removal of osteoclast bone resorption products by transcytosis. Science. 1997; 276: 270-3.
127. Lacey DL, Timms E, Tan HL, Kelley MJ, Dunstan CR, Burgess T, et al. Osteoprotegerin ligand is a cytokine that regulates osteoclast differentiation and activation. Cell. 1998; 93: 165-76.
128. Udagawa N, Takahashi N, Akatsu T, Tanaka H, Sasaki T, Nishihara T, et al. Origin of osteoclasts: mature monocytes and macrophages are capable of differentiating into osteoclasts under a suitable microenvironment prepared by bone marrow-derived stromal cells. Proc Natl Acad Sci U S A. 1990; 87: 7260-4.
129. Arai F, Miyamoto T, Ohneda O, Inada T, Sudo T, Brasel K, et al. Commitment and differentiation of osteoclast precursor cells by the sequential expression of c-Fms and receptor activator of nuclear factor kappaB (RANK) receptors. J Exp Med. 1999; 190: 1741-54.
130. Asagiri M, Takayanagi H. The molecular understanding of osteoclast differentiation. Bone. 2007; 40: 251-64.
131. Lum L, Wong BR, Josien R, Becherer JD, Erdjument-Bromage H, Schlöndorff J, et al. Evidence for a role of a tumor necrosis factor-alpha (TNF-alpha)-converting enzyme-like protease in shedding of TRANCE, a TNF family member involved in osteoclastogenesis and dendritic cell survival. J Biol Chem. 1999; 274: 13613-8.
132. Sabbota AL, Kim HR, Zhe X, Fridman R, Bonfil RD, Cher ML. Shedding of RANKL by tumor-associated MT1-MMP activates Src-dependent prostate cancer cell migration. Cancer Res. 2010; 70: 5558-66.

133. Xiong J, Cawley K, Piemontese M, Fujiwara Y, Zhao H, Goellner JJ, et al. Soluble RANKL contributes to osteoclast formation in adult mice but not ovariectomy-induced bone loss. Nat Commun. 2018; 9: 2909.
134. Lam J, Nelson CA, Ross FP, Teitelbaum SL, Fremont DH. Crystal structure of the TRANCE/RANKL cytokine reveals determinants of receptor-ligand specificity. J Clin Invest. 2001; 108: 971-9.
135. Warren JT, Nelson CA, Decker CE, Zou W, Fremont DH, Teitelbaum SL. Manipulation of receptor oligomerization as a strategy to inhibit signaling by TNF superfamily members. Sci Signal. 2014; 7: ra80.
136. Simonet WS, Lacey DL, Dunstan CR, Kelley M, Chang MS, Lüthy R, et al. Osteoprotegerin: a novel secreted protein involved in the regulation of bone density. Cell. 1997; 89: 309-19.
137. Chambers TJ, McSheehy PM, Thomson BM, Fuller K. The effect of calcium-regulating hormones and prostaglandins on bone resorption by osteoclasts disaggregated from neonatal rabbit bones. Endocrinology. 1985; 116: 234-9.
138. Huang JC, Sakata T, Pfleger LL, Bencsik M, Halloran BP, Bikle DD, et al. PTH differentially regulates expression of RANKL and OPG. J Bone Miner Res. 2004; 19: 235-44.
139. Takahashi N, Udagawa N, Suda T. Vitamin D endocrine system and osteoclasts. Bonekey Rep. 2014; 3: 495.
140. Jahnen-Dechent W, Heiss A, Schäfer C, Ketteler M. Fetuin-A regulation of calcified matrix metabolism. Circ Res. 2011; 108: 1494-509.
141. Schafer C, Heiss A, Schwarz A, Westenfeld R, Ketteler M, Floege J, et al. The serum protein alpha 2-Heremans-Schmid glycoprotein/fetuin-A is a systemically acting inhibitor of ectopic calcification. J Clin Invest. 2003; 112: 357-66.
142. Heiss A, DuChesne A, Denecke B, Grötzinger J, Yamamoto K, Renné T, et al. Structural basis of calcification inhibition by alpha 2-HS glycoprotein/fetuin-A. Formation of colloidal calciprotein particles. J Biol Chem. 2003; 278: 13333-41.
143. Boskey AL, Villarreal-Ramirez E. Intrinsically disordered proteins and biomineralization. Matrix Biol. 2016; 52-54: 43-59.
144. Newcombe EA, Fernandes CB, Lundsgaard JE, Brakti I, Lindorff-Larsen K, Langkilde AE, et al. Insight into Calcium-Binding Motifs of Intrinsically Disordered Proteins. Biomolecules. 2021; 11.
145. Rudloff S, Jahnen-Dechent W, Huynh-Do U. Tissue chaperoning-the expanded functions of fetuin-A beyond inhibition of systemic calcification. Pflugers Arch. 2022; 474: 949-62.
146. Yoshikawa M, Sasaki R, Chiba H. Effects of Chemical Phosphorylation of Bovine Casein Components on the Properties Related to Casein Micelle Formation. Agricultural and Biological Chemistry. 1981; 45: 909-14.
147. Jahnen-Dechent W, Schäfer C, Ketteler M, McKee MD. Mineral chaperones: a role for fetuin-A and osteopontin in the inhibition and regression of pathologic calcification. J Mol Med (Berl). 2008; 86: 379-89.
148. Lenton S, Nylander T, Holt C, Sawyer L, Härtlein M, Müller H, et al. Structural studies of hydrated samples of amorphous calcium phosphate and phosphoprotein nanoclusters. Eur Biophys J. 2016; 45: 405-12.
149. Pedersen KO. Binding of calcium to serum albumin. II. Effect of pH via competitive hydrogen and calcium ion binding to the imidazole groups of albumin. Scand J Clin Lab Invest. 1972; 29: 75-83.

150. Mazzali M, Kipari T, Ophascharoensuk V, Wesson JA, Johnson R, Hughes J. Osteopontin--a molecule for all seasons. Qjm. 2002; 95: 3-13.
151. Hunter GK. Role of osteopontin in modulation of hydroxyapatite formation. Calcif Tissue Int. 2013; 93: 348-54.
152. Vegarud GE, Langsrud T, Svenning C. Mineral-binding milk proteins and peptides; occurrence, biochemical and technological characteristics. Br J Nutr. 2000; 84 Suppl 1: S91-8.
153. Lee H, Padhi E, Hasegawa Y, Larke J, Parenti M, Wang A, et al. Compositional Dynamics of the Milk Fat Globule and Its Role in Infant Development. Front Pediatr. 2018; 6: 313.
154. Holt C, Sørensen ES, Clegg RA. Role of calcium phosphate nanoclusters in the control of calcification. Febs j. 2009; 276: 2308-23.
155. Cross KJ, Huq NL, Palamara JE, Perich JW, Reynolds EC. Physicochemical characterization of casein phosphopeptide-amorphous calcium phosphate nanocomplexes. J Biol Chem. 2005; 280: 15362-9.
156. Wurm FM. CHO Quasispecies—Implications for Manufacturing Processes. Processes. 2013; 1: 296-311.
157. Haynesworth SE, Goshima J, Goldberg VM, Caplan AI. Characterization of cells with osteogenic potential from human marrow. Bone. 1992; 13: 81-8.
158. Pittenger MF, Mackay AM, Beck SC, Jaiswal RK, Douglas R, Mosca JD, et al. Multilineage potential of adult human mesenchymal stem cells. Science. 1999; 284: 143-7.
159. Jumper J, Evans R, Pritzel A, Green T, Figurnov M, Ronneberger O, et al. Highly accurate protein structure prediction with AlphaFold. Nature. 2021; 596: 583-9.
160. Matsui I, Hamano T, Mikami S, Fujii N, Takabatake Y, Nagasawa Y, et al. Fully phosphorylated fetuin-A forms a mineral complex in the serum of rats with adenine-induced renal failure. Kidney Int. 2009; 75: 915-28.
161. Tokmakov AA, Kurotani A, Takagi T, Toyama M, Shirouzu M, Fukami Y, et al. Multiple post-translational modifications affect heterologous protein synthesis. J Biol Chem. 2012; 287: 27106-16.
162. Kaufmann H, Mazur X, Fussenegger M, Bailey JE. Influence of low temperature on productivity, proteome and protein phosphorylation of CHO cells. Biotechnol Bioeng. 1999; 63: 573-82.
163. Herrmann M, Schäfer C, Heiss A, Gräber S, Kinkeldey A, Büscher A, et al. Clearance of Fetuin-A–Containing Calciprotein Particles Is Mediated by Scavenger Receptor-A. Circ Res. 2012; 111: 575-84.
164. Hayman AR. Tartrate-resistant acid phosphatase (TRAP) and the osteoclast/immune cell dichotomy. Autoimmunity. 2008; 41: 218-23.
165. Ries WL, Gong JK. A comparative study of osteoclasts: in situ versus smear specimens. Anat Rec. 1982; 203: 221-32.
166. Vignery A. Macrophage fusion: the making of osteoclasts and giant cells. J Exp Med. 2005; 202: 337-40.
167. Dzhanaev R. Rational design and production of recombinant RANK ligand [Doctoral dissertation]. Aachen: RWTH Aachen University; 2020.
168. Rasband WS. ImageJ. U S National Institutes of Health, Bethesda, Maryland, USA. http://rsb.info.nih.gov/ij/: 1997-2009.
169. Schindelin J, Arganda-Carreras I, Frise E, Kaynig V, Longair M, Pietzsch T, et al. Fiji: an open-source platform for biological-image analysis. Nat Methods. 2012; 9: 676-82.

170. Ershov D, Phan MS, Pylvänäinen JW, Rigaud SU, Le Blanc L, Charles-Orszag A, et al. TrackMate 7: integrating state-of-the-art segmentation algorithms into tracking pipelines. Nat Methods. 2022; 19: 829-32.
171. Wilkins MR, Gasteiger E, Bairoch A, Sanchez JC, Williams KL, Appel RD, et al. Protein identification and analysis tools in the ExPASy server. Methods Mol Biol. 1999; 112: 531-52.
172. Tolmachev V, Hofström C, Malmberg J, Ahlgren S, Hosseinimehr SJ, Sandström M, et al. HEHEHE-tagged affibody molecule may be purified by IMAC, is conveniently labeled with [^{99}(m)Tc(CO)$_3$](+), and shows improved biodistribution with reduced hepatic radioactivity accumulation. Bioconjug Chem. 2010; 21: 2013-22.
173. Termine JD, Belcourt AB, Conn KM, Kleinman HK. Mineral and collagen-binding proteins of fetal calf bone. J Biol Chem. 1981; 256: 10403-8.
174. Jablonski KL, Chonchol M. Vascular calcification in end-stage renal disease. Hemodial Int. 2013; 17 Suppl 1: S17-21.
175. Samelson EJ, Cupples LA, Broe KE, Hannan MT, O'Donnell CJ, Kiel DP. Vascular calcification in middle age and long-term risk of hip fracture: the Framingham Study. J Bone Miner Res. 2007; 22: 1449-54.
176. Reaven PD, Sacks J. Coronary artery and abdominal aortic calcification are associated with cardiovascular disease in type 2 diabetes. Diabetologia. 2005; 48: 379-85.
177. Kraus MA, Kalra PA, Hunter J, Menoyo J, Stankus N. The prevalence of vascular calcification in patients with end-stage renal disease on hemodialysis: a cross-sectional observational study. Ther Adv Chronic Dis. 2015; 6: 84-96.
178. Vos T, Lim SS, Abbafati C, Abbas KM, Abbasi M, Abbasifard M, et al. Global burden of 369 diseases and injuries in 204 countries and territories, 1990–2019: a systematic analysis for the Global Burden of Disease Study 2019. The Lancet. 2020; 396: 1204-22.

Erklärung § 5 Abs. 1 zur Datenaufbewahrung

Hiermit erkläre ich, dass die dieser Dissertation zu Grunde liegenden Originaldaten bei meinem Betreuer, Prof. Wilhelm Jahnen-Dechent, Institut für Biomedizinische Technologien - Zell- und Molekularbiologie an Grenzflächen, des Universitätsklinikums Aachen, hinterlegt sind.

Eidesstattliche Erklärung gemäß § 5 Abs. (1) und § 11 Abs. (3) 12. der Promotionsordnung

Hiermit erkläre ich, Robert Dzhanaev an Eides statt, dass ich folgende in der von mir selbstständig erstellten Dissertation „Fetuin-A-based theranostics in ectopic calcification“ dargestellten Ergebnisse erhoben habe:

Bei der Durchführung der Arbeit hatte ich folgende Hilfestellungen, die in der Danksagung angegeben sind:

	Robert Dzhanaev	Christian Hasberg	Anouk Gentiers	Prof. Dr. Felix Mottaghy	Prof. Dr. Leon Schurgers	Dr. Sabrina Ernst	Dr. Kévin Knoops	Stephan Rütten	Sabri Sahnoun	Dr. Alexandru Florea	Steffen Gräber	Dr. Christian Preisinger	Prof. Dr. Willi Jahnen-Dechent	Summe (%)
Studienüberwachung				10	10								80	100
Studiendesign	70				15								15	100
Mikroskopie	50		10			10	10	20						100
Konzeption der nuklearmedizinischen Untersuchungen	50			25									25	100
Datenauswertung	100													100
Durchführung des Präzipitationstests	10	90												100
Produktion der rekombinanten Proteine	100													100
SDS-PAGE, Western Blot	100													100
Zytotoxizitätstest	100													100
Statistische Auswertung	100													100
Chemische Proteinlabeling											100			100
Radiomarkierung									100					100
Injektion von radiomarkiertem Protein										100				100
Massenspektrometrie												100		100
Osteoklasten-Assays	100													100
Histologische Untersuchung	100													100
DNA-Aufreinigung	70	30												100
Interpretation der Datenauswertung	60				20								20	100

_____

Unterschrift des Doktoranden

Als Betreuer der obigen Dissertation bestätige ich die Angaben von Robert Dzhanaev

_____

Unterschrift des Doktorvaters